Università degli Studi di Ferrara

DOTTORATO DI RICERCA IN

"Biochimica, Biologia Molecolare e Biotecnologie"

CICLO XXVIII

COORDINATORE Prof. Francesco Bernardi

Extranuclear promyelocytic leukemia protein (PML) and p53 down regulation promote cancer by subverting multiple tumor suppression pathways

Settore Scientifico Disciplinare **MED/04**

Dottorando:

Dott.ssa Sonia Missiroli

Tutore:

Prof. Paolo Pinton

Cotutore:

Dott.ssa Carlotta Giorgi

Anni 2013/2015

Index

Abbreviations **3**

Abstract **5**

Riassunto **6**

Introduction **8**

The Ca^{2+}-signalling toolkit 9

ER-mitochondria crosstalk 11

Calcium release from cellular store 14

Mitochondria: cell physiology and molecular nature of the mitochondrial Ca^{2+} uptake and release machinery 16

Remodelling ER-mitochondria Ca^{2+} transfer in cell survival and death 21

Mitochondria-associated membranes: role of structural and regulatory proteins in the control of Ca^{2+} transfer between ER and mitochondria 23

Mitochondria-associated membranes and autophagy 26

Mitochondria-associated membranes and inflammation 28

p53 at the endoplasmic reticulum regulates apoptosis in a Ca^{2+}-dependent manner **31**

p53 is a master regulator of cell fate 31

The mitochondrial route of p53 34

Introduction 37

Results 38

Discussion 48

Intravital imaging reveals p53-dependent cancer cell death induced by phototherapy via calcium signaling **49**

Introduction 49

Results 50

Discussion 58

PML at mitochondria-associated membranes is critical for the repression of autophagy and cancer development **60**

PML and cell death 60

PML and autophagy 62

PML Expression in Human Tumors 62

Introduction 65

Results 66

Discussion 78

Future perspectives **80**
Materials and methods **82**
Cell Culture, Transfection, and Detection of Cell Death. 82
Aequorin Measurements 82
Fura-2 Measurements 83
FRET-Based Measurements of ER Ca^{2+}. 83
Subcellular Fractionation 83
Mitochondrial Morphology Analysis 84
Immunolocalization of p53 Protein 84
Western blot 84
Transformation assays and in vivo tumorigenicity 85
Dorsal skinfold chamber and intravital microscopy 85
Autophagy induction and inhibition 85
Analysis of autophagic flux 86
Measurements of mitochondrial membrane potential (Ψm) 86
Cell proliferation and viability assay 86
Cell survival assay 87
Migration assay 87
Mouse treatment studies 87
Detection of cell death in vivo 88
Tissue processing 88
XF bioenergetic analysis 89
References **90**

Abbreviations

AEQ, aequorin;
ANT, adenine nucleotide translocase;
APL, acute promyelocytic leukemia;
ATG, autophagy related genes;
Ca^{2+}, calcium ions;
$[Ca^{2+}]$, Ca^{2+} concentration;
$[Ca^{2+}]_c$, cytosolic Ca^{2+} concentration;
$[Ca^{2+}]_{er}$, endoplasmic reticulum Ca^{2+} concentration;
$[Ca^{2+}]_m$, mitochondrial Ca^{2+} concentration;
CABPs, intraluminal Ca^{2+}-binding proteins;
DAG:diacylglycerol;
ER, endoplasmic reticulum;
FACL4, long-chain fatty acid-CoA ligase type 4;
FRET, fluorescence resonance energy transfer;
GFP, green fluorescent protein;
GPCRs: G protein coupled receptors
grp75, glucose-regulated protein 75;
HK, hexokinase;
IMM, inner mitochondrial membrane;
IMS, intermembrane space;
IP3, inositol 1,4,5-trisphosphate;
IP3R, inositol 1,4,5-trisphosphate receptor;
Letm1, leucine zipper-EF-hand containing transmembrane protein 1;
MAMs, mitochondria-associated membranes;
MAVS, mitochondrial anti-viral signaling;
Mefs: mouse embryonic fibroblasts;
MCU, mitochondrial Ca^{2+} uniporter;
MICU1, mitochondrial calcium uptake 1;
mTOR, mammalian target of rapamycin;
mHCX, mitochondrial H^+/Ca^{2+} exchanger;
mNCX, mitochondrial Na^{2+}/Ca^{2+} exchanger;
MOMP, mitochondrial outer membrane permeabilization;
NCX, Na^{2+}/Ca^{2+} exchanger;
OMM, outer mitochondrial membrane;
PACS-2, phosphofurin acidic cluster sorting protein 2;
PAMs, plasma membrane associated membranes;
PAS, pre-autophagosomal structure;
PI3K, phosphatidylinositol 3-kinase;
PIP2, phosphatidylinositol 4,5-bisphosphate;

PIP3, phosphatidylinositol 3,4,5-trisphosphate;

PLC-β: phospholipase C-β

PMCA, plasma membrane Ca^{2+} ATPase;

PML, promyelocytic leukemia protein;

PP2a, protein phosphatase 2a;

PTEN, phosphatase and tensin homolog deleted on chromosome 10;

PTP, permeability transition pore;

ROCs: receptor operated Ca^{2+} channels:

ROS, reactive oxygen species;

RyR, ryanodine receptor;

SERCA, sarco-endoplasmic reticulum Ca^{2+} ATPase;

Sig-1R, Sigma-1 receptor;

SMOCs: second messenger operated Ca^{2}+ channels;

SOCE, store-operated Ca^{2+} entry;

SR, sarcoplasmic reticulum;

STIM: stromal interaction molecule;

STING, stimulator of IFN genes;

TIM: transporters of the Inner Membrane;

TKR: tyrosine-kinase receptors

TOM (Transporters of the Outer Membrane);

UCP, uncoupling protein;

VDAC, voltage-dependent anion channel;

VOCs: voltage operated Ca^{2+} channels.

Abstract

The endoplasmic reticulum (ER) and mitochondria join together at multiple contact sites to form specific domains, termed mitochondria-ER associated membranes (MAMs), with distinct biochemical properties and a characteristic set of proteins.

There is growing evidence to indicate that contact sites between the mitochondria and ER act as preferential gateways for signal transmission and behave as platforms where components of cytoplasmic and nuclear pathways can modulate the sensitivity to apoptosis, such as by manipulating the rheostat represented by Ca^{2+} transmission.

During my PhD we demonstrated that two master tumor suppressors, p53 and the promyelocytic leukemia protein (PML) localize at the ER/MAM contact sites where they play an important role in modulating Ca^{2+} signaling, cell death and cancer.

We found that p53 becomes enriched at MAM compartments after anticancer treatments enhancing cell death. At these sites, p53 interacts with the C-terminal portion of the sarco/ER Ca^{2+}ATPase (SERCA) pump, changing its oxidative state and, in turn, increasing ER Ca^{2+} loading.

To test the relevance of these findings in an *in vivo* approach of tumor environment, we used a novel technological platform for the intravital microscopy allowing detection of Ca^{2+} signaling in a three dimensional tumor mass. Using this technique we were able to confirm *in vivo* that the tumor suppressor p53 is able to modulate Ca^{2+} homeostasis in response to a photodynamic cancer therapy (PDT) favoring cells sensitivity to apoptosis and thus in turn limiting tumor growth.

These evidences highlighted how the MAMs are important specialized domains where many tumor suppressors exert their pro-apoptotic activities via calcium-mediated pathways.

In the second part of my PhD work, we identified a new extra-nuclear role of PML as a negative regulator of autophagy. It is already known that ER–mitochondria interface also represents the primary platform for autophagosome formation and the function of pro-survival autophagy machinery. We provide evidence that the localization of PML at the ER-mitochondria contact sites is fundamental not only for apoptosis control but also for autophagy regulation, repressing at these sites autophagosome formation and, thus, autophagy induction. We observed in vivo that the absence of PML promotes tumor development associated with resistance to anticancer drugs due to increased autophagy levels in the tumor.

Since autophagy levels promote the secretion of inflammatory cytokines like interleuchin-1β (IL-1β) and the major complex involved in the IL-1β released, the NLRP3 inflammasome, it has been identified at the ER/MAM domains, our future directions will be focused to explore the role of PML in inflammation process.

Riassunto

Il reticolo endoplasmatico (ER) e i mitocondri interagiscono tra di loro in più siti di contatto a formare specifici domini, denominati "membrane associate ai mitocondri" (MAMs), con differenti proprietà biochimiche e un definito set di proteine.

È sempre più evidente come i siti di contatto tra mitocondri e ER rappresentino le vie preferenziali per la trasmissione del segnale e si comportino come piattaforme biologiche in cui vie di segnalazione citoplasmatiche e nucleari possano modulare la sensibilità all'apoptosi, come ad esempio manipolando l'omeostasi del segnale calcio (Ca^{2+}) intracellulare.

Durante il mio dottorato abbiamo dimostrato come due importanti oncosoppressori, p53 e promyelocytic leukemia protein (PML), localizzino nei siti di contatto ER/MAM dove svolgono un ruolo importante nella modulazione del segnale Ca^{2+}, nella morte cellulare e nel tumore.

Abbiamo dimostrato che p53 si arricchisce alle MAMs in seguito a trattamenti antitumorali che portano a morte cellulare. In questi siti, p53 interagisce con la porzione C-terminale della pompa sarco/ER Ca^{2+} ATPasi (SERCA), cambiando il suo stato ossidativo e, di conseguenza, aumentando l'accumulo del Ca^{2+} reticolare.

Per confermare questi risultati in vivo, abbiamo utilizzato una piattaforma tecnologica innovativa per la microscopia che permette il rilevamento del segnale Ca^{2+} in una massa tumorale tridimensionale. Utilizzando questa tecnica siamo stati in grado di confermare in vivo che l'oncosoppressore p53 è in grado di modulare l'omeostasi del Ca^{2+} in risposta alla fototerapia antitumorale (PDT), favorendo la sensibilità delle cellule all'apoptosi e di conseguenza limitando la crescita tumorale.

Queste evidenze sottolineano come le MAMs siano importanti domini specializzati dove molti oncosoppressori esercitano la loro attività pro-apoptotica mediante vie mediate dal Ca^{2+}.

Nella seconda parte del mio dottorato, abbiamo identificato un nuovo ruolo extranucleare di PML come regolatore negativo dell'autofagia. E' già noto come l'interfaccia ER-MAM rappresenti anche la piattaforma biologica primaria per la formazione degli autofagosomi e per il meccanismo di sopravvivenza via autofagia.

Abbiamo dimostrato come la localizzazione di PML ai siti di contatto ER-mitocondri non sia solo fondamentale per il controllo dell'apoptosi, ma anche per la regolazione dell'autofagia, reprimendo a livello di questi siti la formazione degli autofagosomi e, di conseguenza, l'induzione dell'autofagia. Abbiamo osservato in vivo che l'assenza di PML promuove lo sviluppo tumorale causato da alti livelli di autofagia nel tumore che portano a resistenza contro farmaci antitumorali.

Dal momento che alti livelli di autofagia promuovono la secrezione di citochine infiammatorie come l'interleuchina 1-β (IL-1β) e che il maggior complesso coinvolto nel rilascio di IL-1β, il NLRP3 inflammasoma, è stato identificato localizzare nei domini ER/MAMs, studi futuri saranno orientati al ruolo di PML nel processo infiammatorio.

Introduction

Changes in the levels of intracellular calcium ions (Ca^{2+}) provide dynamic and highly versatile signals that regulates several processes as diverse as energy transduction, fertilization, secretions, muscle contraction, chemotaxis and neuronal synaptic plasticity in learning and memory[1]. However, under certain conditions increases in intracellular Ca^{2+} are cytotoxic and lead to apoptosis (programmed cell death). Consequently, Ca^{2+} needs to be used in an appropriate manner to determine cell fate; if this balancing act is compromised, pathology may ensue [2].

Ca^{2+} signalling proteins and organelles are emerging as additional cellular targets of oncogenes and tumour suppressors. The Ca^{2+} signal has major roles in the regulation of processes relevant to tumorigenesis, including migration, invasion, proliferation, and apoptotic sensitivity [3]. Intracellular Ca^{2+} homeostasis has been the focus of researchers characterizing changes in Ca^{2+} signalling in cancer cells. In order for the cancer cells to proliferate at higher rates and still protect themselves from apoptosis, many cancer cells remodel the expression or activity of their Ca^{2+} signalling machinery. Spatially restricted Ca^{2+} signalling within specific cellular compartments or discrete cytosolic domains provides an additional layer of complexity in the regulation of cellular processes important in tumorigenesis. In normal cells, the Ca^{2+} signalling is highly regulated spatially such as between endoplasmic reticulum (ER) and mitochondria, two intracellular organelles which play crucial roles in Ca^{2+} signalling and may decide the ultimate fate of the cell. Indeed, by adjusting the load of Ca^{2+} imposed upon the mitochondrion, the same Ca^{2+} efflux from ER (the main intracellular Ca^{2+} store) that is responsible for regulating processes for maintaining life could also act as a death-inducing signal.

Since ER and mitochondria play significant roles in the regulation of cell proliferation and apoptosis, the remodelling of Ca^{2+} signalling machinery in ER and mitochondria in cancer cells seems imminent during oncogenic transformation. Therefore, targeting of the Ca^{2+} signalling apparatus in cancer cells could specifically disrupt their Ca^{2+} homeostasis, and so decrease cancer cell proliferation and increase cancer cell apoptosis. Such novel and highly innovative strategies can provide rationale and approaches for the design and development of novel technologies based on Ca^{2+} waves for the diagnosis and treatment of cancer, as well as other disease.

The Ca^{2+}-signalling toolkit

At the beginning of life, Ca^{2+} mediates the process of fertilization and regulates the cell cycle events during the early developmental processes. Once the cells differentiate to perform specific functions, changes in the levels of intracellular Ca^{2+} provide dynamic and highly versatile signals that control a plethora of cellular processes, yet under certain conditions increases in intracellular Ca^{2+} are cytotoxic[4]. For this reason, the intracellular concentration of Ca^{2+}, $[Ca^{2+}]_i$, in resting cells is usually maintained very low, at ~100 nM.

In cells, due to the presence of several charged molecules, the Ca^{2+} diffusion rates are slow. In order to utilize Ca^{2+} as a second messenger, cells have devised an ingenious mechanism of signalling that has overcome the inherent problems associated with lower diffusion rates and potential cytotoxicity of Ca^{2+}, by presenting changes in Ca^{2+} concentration as brief spikes which are often organized as regenerative waves [1]. The universality of Ca^{2+}-based signalling depends on its enormous versatility in terms of amplitude, duration, frequency and localization. The formation of the correct spatio-temporal Ca^{2+} signals is dependent on an extensive cellular machinery named the Ca^{2+} toolkit, which includes the various cellular Ca^{2+}-binding and Ca^{2+}-transporting proteins, present mainly in the cytosol, plasma membrane, ER and mitochondria [5].

To provide for a very fast and effective Ca^{2+}-signalling, the cells use a great amount of energy to maintain an almost 20,000-fold Ca^{2+}-gradient between their intracellular (~100 nM free) and extracellular (~1 mM) Ca^{2+} concentrations. To maintain this Ca^{2+} gradient, the cells chelate, compartmentalize, or remove Ca^{2+} from the cytoplasm through its active extrusion by the plasma membrane Ca^{2+} ATPase (PMCA) and the Na^{+}/Ca^{2+} exchanger (NCX) [6,7].

The increase of intracellular $[Ca^{2+}]$ can be elicited by two fundamental mechanisms (or a combination of both). The first involves Ca^{2+} entry from the extracellular milieu, through the opening of plasma membrane Ca^{2+} channels (traditionally grouped into three classes: voltage operated Ca^{2+} channels (VOCs) [8], receptor operated Ca^{2+} channels (ROCs) [9]and second messenger operated Ca^{2+} channels (SMOCs) [10]. The second universal mechanism for Ca^{2+} signalling is the release of Ca^{2+} from intracellular Ca^{2+} stores, mainly the ER and its specialized form in muscle, the sarcoplasmic reticulum (SR). In these intracellular stores, two main Ca^{2+}-release channels exist that, upon stimulation, release Ca^{2+} into the cytosol, thus triggering Ca^{2+} signalling: the inositol 1,4,5-trisphosphate (IP3) receptors (IP3Rs) and the ryanodine receptors (RyRs) [11,12]. IP3Rs are ligand-gated channels that function in releasing Ca^{2+} from ER Ca^{2+} stores in response to IP3 generation. G protein coupled receptors (GPCRs) can activate phospholipase C-β (PLC-β), and tyrosine-kinase receptors (TKR) can activate

PLC-γ, which then cleave phosphatidylinositol 4,5-bisphosphate (PIP2) into IP3 and diacylglycerol (DAG). IP3 binding to the IP3Rs that are present in the ER, causes efflux of Ca^{2+} from the ER to the cytoplasm resulting in increase in cytosolic Ca^{2+} concentration ($[Ca^{2+}]_c$) from ~100 nM to ~1 μM for several seconds [13,14]. This rise in $[Ca^{2+}]_c$ results in various Ca^{2+}-dependent intracellular events (Figure 1). A variety of cellular proteins with Ca^{2+}-binding affinities ranging between nM to mM are utilized by the cells to buffer the cellular Ca^{2+} increase as well as to regulate cellular processes via Ca^{2+}-signalling. The exact cellular outcome depends on the spatiotemporal characteristics of the generated Ca^{2+} signal [15].

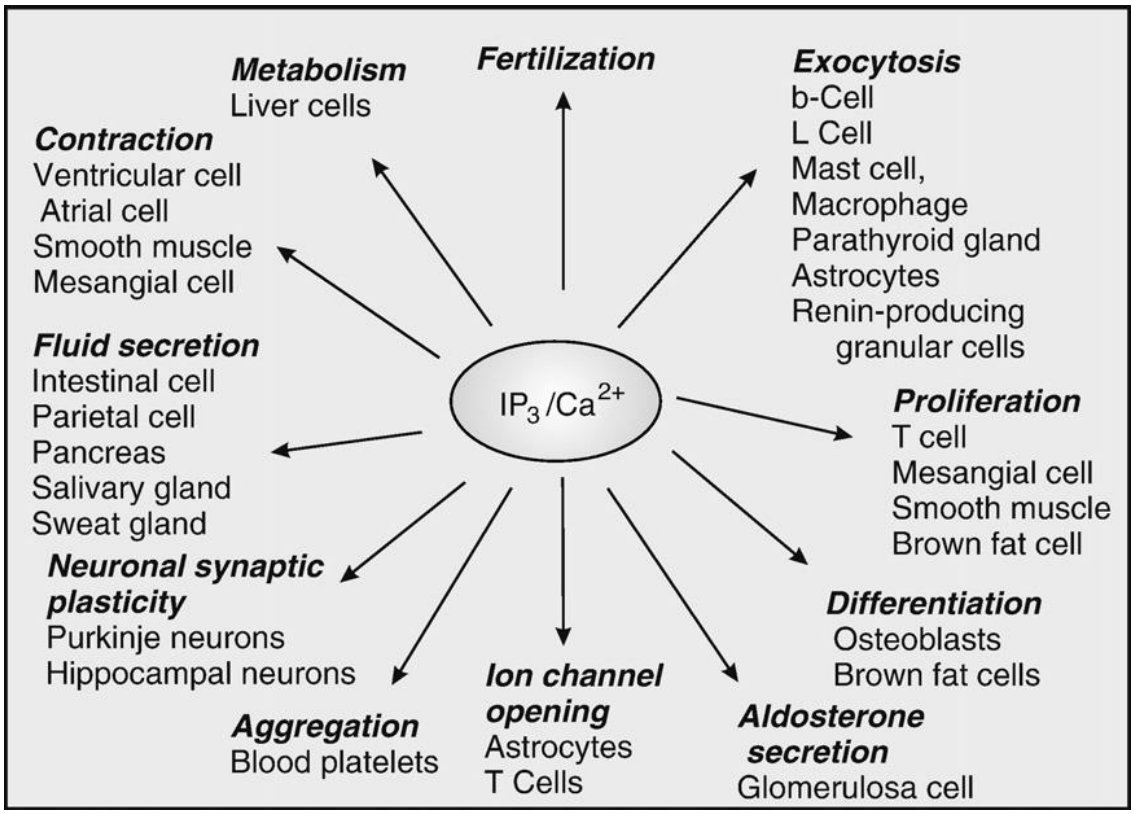

Figure 1. Regulation of multiple cellular processes by the IP3/Ca^{2+} signalling pathway. *(figure from [16])*

Once its downstream targets are activated, basal $[Ca^{2+}]_c$ levels are regained by the combined activity of Ca^{2+} extrusion mechanisms, such as PMCA and NCX, and mechanisms that refill the intracellular stores, like sarco-endoplasmic reticulum Ca^{2+} ATPases (SERCAs) [6]. Due to SERCA activity and intraluminal Ca^{2+}-binding proteins (CABPs), *i.e.* calnexin and calreticulin [17], the ER can accumulate Ca^{2+} more than a thousand-fold excess as compared to the cytosol. Given that PMCAs pump Ca^{2+} out of the cell faster than it can be repleted, IP3R mediated efflux of Ca^{2+} from the ER in response to receptor activation empties the ER, thus a Ca^{2+} entry mechanism is activated. This mechanism is called "Store-operated Ca^{2+} entry"

(SOCE). The molecular determinants of SOCE have been identified in the very last few years and include the ER Ca^{2+} sensors STIM (stromal interaction molecule) 1 and 2, and the specialized plasma-membrane channels Orai1, Orai2 and Orai3 (for a recent review [18]). Although the ER (and its specialized form in muscle, the SR) is generally considered the main intracellular Ca^{2+} store, almost all other organelles play a role in Ca^{2+} signalling: mitochondria (see below) [19], the Golgi apparatus [20], secretory vesicles [21], lysosomes [22], endosomes [23] and peroxisomes [24,25].

Specificity in decoding Ca^{2+} signals can be provided by the affinity of Ca^{2+} sensor as well as its duration, amplitude and intracellular location: in this way a particular Ca^{2+} signal can specifically regulate many different cell functions [26].

ER-mitochondria crosstalk

While the role of the ER as a physiologically important Ca^{2+} store has long been recognized, a similar role for mitochondria have seen a reappraisal only in the past two decades [27]. The uptake of the Ca^{2+} ions into the mitochondrial matrix implies different transport systems responsible for the transfer of Ca^{2+} across the outer and the inner mitochondrial membrane (OMM and IMM respectively). It has long been known that mitochondria can rapidly accumulate Ca^{2+} down the large electrochemical gradient (mitochondrial membrane potential difference, $\Delta\Psi_m$ = -180 mV, negative inside) generated by the respiratory chain [28]. Indeed, based on the chemiosmotic theory, the translocation by protein complexes of H^+ across an ion-impermeable inner membrane generates a very large H^+ electrochemical gradient and mitochondria employ the dissipation of this proton gradient not only to run the endoergonic reaction of ATP synthesis by the H^+-ATPase, but also to accumulate cations into the matrix.

For a long time, however, due to the low affinity of the mitochondrial Ca^{2+} uptake system under physiological conditions (an apparent K_d of 20 to 30 μM under conditions thought to mimic the cytoplasm, estimated in the earlier work with isolated organelles) and the submicromolar global $[Ca^{2+}]_c$ briefly reached after physiological stimulation (which rarely exceed 2-3 μM), this process was considered to take place only in conditions of high-amplitude, prolonged $[Ca^{2+}]_c$ increases, i.e. in the Ca^{2+} overload that is observed in various pathological conditions (such as, for example, excitotoxic glutamate stimulation of neurons) [19]. Mitochondrial Ca^{2+} returned to the limelight in 1992 when Rizzuto, Pozzan and colleagues generated a novel, genetically encoded chemiluminescent indicator, aequorin. This probe, specifically targeted to the mitochondrial matrix, allowed dynamic, accurate and specific monitoring of the $[Ca^{2+}]$ within the matrix of mitochondria in living cells [29]. With this new

tool they could show that mitochondria in living cells undergo very fast and large increases in their matrix Ca^{2+} levels (mitochondrial Ca^{2+} concentration, $[Ca^{2+}]_m$) upon cell stimulation, reaching peaks similar or even larger than those in the cytoplasm, even for normal physiological cytoplasmic Ca^{2+} rises [30]. Similar conclusions could be reached also with fluorescent indicators, such as the positively charged Ca^{2+} indicator rhod-2 (that accumulates within the organelle) [31] and the more recently developed GFP-based fluorescent indicators [32].

While enlivening the interest in mitochondrial Ca^{2+} homeostasis, these data raised an apparent contradiction between the prompt response of the organelle (where $[Ca^{2+}]_m$ rise, in a few seconds, to values above 10 μM, and in some cell types up to 500 μM) and the low affinity of the Ca^{2+} uptake system together with the low concentration of global Ca^{2+} signals observed in cytoplasm. Based on a large body of experimental evidence, it is now generally accepted that the key to the rapid Ca^{2+} accumulation rests in the strategic location of a subset of mitochondria, close to the opening ER or plasma membrane Ca^{2+} channels [30,31,33]. The hypothesis, called "microdomain hypothesis" [26], proposes that microdomains of high $[Ca^{2+}]$ (10-20 μM) can be transiently formed in regions of close apposition between mitochondria and Ca^{2+} channels of the ER/SR or of the plasma membrane [33]. These high Ca^{2+} microdomains rapidly dissipate (due to diffusion) insuring that mitochondria do not overload with Ca^{2+} (Figure 2).

The "microdomain hypothesis" received a number of indirect confirmations in the last 20 years by different groups. More recently, such microdomains in selected regions of contact between ER and mitochondria were finally measured directly, by two complementary studies that demonstrated the existence and amplitude of high Ca^{2+} microdomains on the surface of mitochondria. Giacomello et al. [34] targeted a new generation of FRET-based Ca^{2+} sensors [35] to the OMM and, through a sophisticated statistical analysis of the images, revealed the existence of small OMM regions where $[Ca^{2+}]$ reaches values as high as 15-20 μM. The probe detected Ca^{2+} hotspots on about 10% of the OMM surface that were not observed in other parts of the cell. The Ca^{2+} hotspots were not uniform, and their frequency varied among mitochondria of the same cell. Moreover, classical epifluorescence and total internal reflection fluorescence (TIRF) microscopy experiments were combined in order to monitor the generation of high Ca^{2+} microdomains in mitochondria located near the plasma membrane. With this approach, it could be shown that Ca^{2+} hotspots on the surface of mitochondria occur upon opening of VOCs, but not upon SOCE. Csordás et al. [36] used a complementary approach in which they generated genetically encoded bifunctional linkers consisting of OMM and ER targeting sequences connected through a fluorescent protein, including a low-Ca^{2+}-affinity pericam, and coupled with the two components of the FKBP-

FRB heterodimerization system [37], respectively. Using rapamycin-assembled heterodimerization of the FKBP-FRB-based linker, they detected ER/OMM and plasma membrane/OMM junctions (the latter at a much lower frequency). In addition, the recruited low-Ca^{2+}-affinity pericam reported Ca^{2+} concentrations as high as 25 μM at the ER/OMM junctions in response to IP3-mediated Ca^{2+} release, which is in excellent agreement with the values obtained by Giacomello *et al.*.

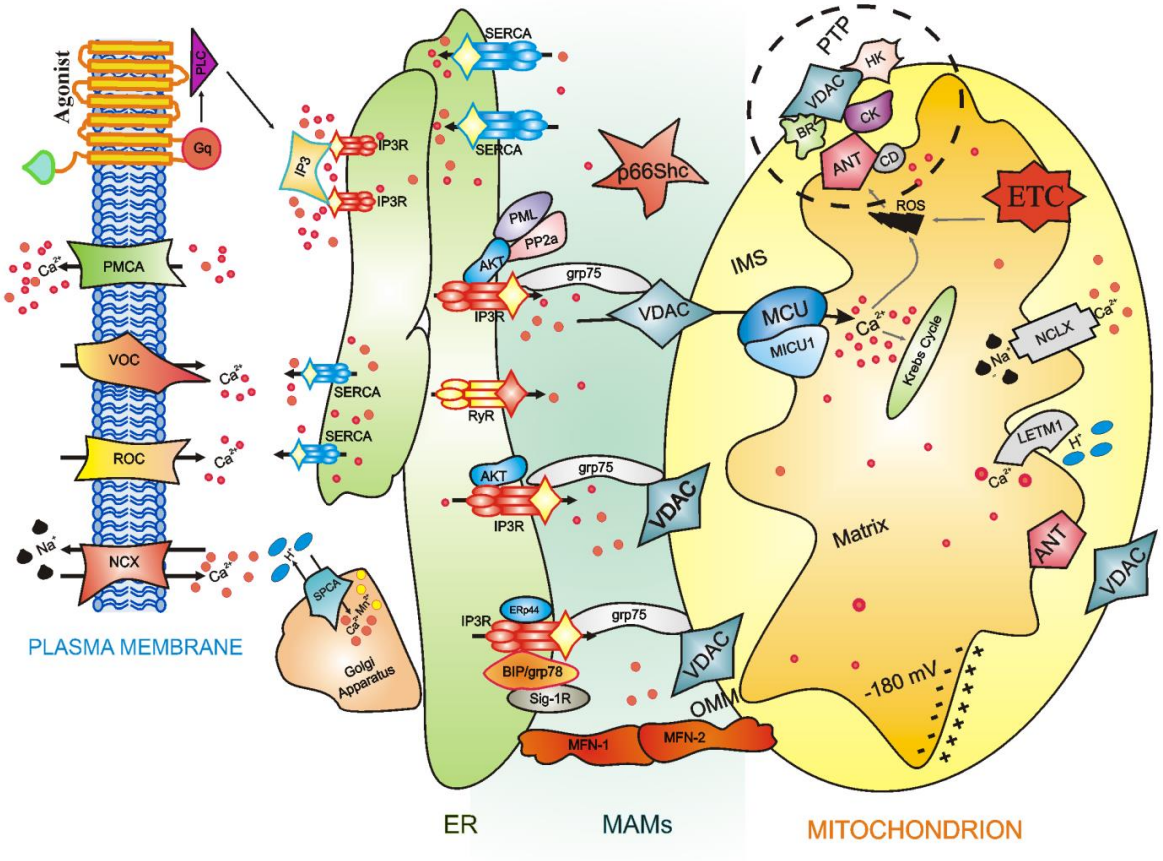

Figure 2. Representation of intracellular Ca^{2+} dynamics. *Cells generate Ca^{2+} signal through two mechanism that use internal and external sources of Ca^{2+}. Calcium enters into the cell through channels and pumps situated on the plasma membrane; these are gated by voltage (VOCs) or external messengers (ROCs). A series of stimuli that act on cell surface receptors triggers the activation of PLC that catalyses the hydrolysis of phosphatidylinositol 4,5-biphosphate to IP3 and DAG. The binding of IP3 to its receptor IP3R stimulates ER Ca^{2+} release and consequently the transfer of Ca^{2+} (red dots) from ER to mitochondria. Mitochondrial surface directly interacts with the ER through contact sites defining hotspot Ca^{2+} signalling units. Mitochondrial Ca^{2+} import occurs through the mitochondrial Ca^{2+} uniporter (MCU) and the H^+/Ca^{2+} exchanger LETM1; conversely, NCLX, mitochondrial Na^+/Ca^{2+} exchanger, together with the PTP, export Ca^{2+} from the matrix. Ca^{2+} levels return to resting conditions through a series of channels and pumps: PMCA and NCX permit the ion extrusion into the extracellular milieu, SERCA (situated on the ER) and SPCA (on the Golgi apparatus) re-establish basal Ca^{2+} levels in intracellular stores. Abbreviations: ANT, adenosine nucleoside transporter; ETC, electron transport chain; HK, hexokinase; CD, cyclophilin D; CK, creatine kinase; BR, benzodiazepine receptor (figure from [38]).*

While based on cell morphology the close proximity between the mitochondria and the ER is expected and indeed often observed, i.e. in neuronal prolongings, a close interaction between ER-resident Ca^{2+} channels and mitochondria in non-excitable cells implies the assembly of a dedicated signalling unit at the organelle interphase.

Calcium release from cellular store

The ER is possibly the largest individual intracellular organelle comprising a three dimensional network of endomembranes arranged in a complex grid of microtubules and cisternae. It is made up of functionally and structurally distinct domains (reviewed extensively by a number of authors [39-42], in relation to the variety of cellular functions played by the organelle, primarily concerning protein synthesis, maturation and delivery to their destination [43,44]. Moreover, the ER is a dynamic reservoir of Ca^{2+} ions, which can be activated by both electrical and chemical cell stimulation [45,46], making this organelle an indispensable component of Ca^{2+} signalling [47-49].

Modern analysis methods enabled the determination of the molecular profile of the ER. This profile reflects the ER's role in signalling, as it comprises a number of components constituting the Ca^{2+} signalling pathway. It contains IP3Rs, RyRs, SERCAs, and in addition to these release channels and pumps, there are buffers (calnexin, calreticulin) and a number of ancillary proteins (FK 506-binding proteins, sorcin, triadin, phosholamban) that contribute to the ER Ca^{2+} signalling system [50].

Many extracellular stimuli, such as hormones, growth factors, neurotransmitters, neutrophins, odorants, and light, function generating IP3 through the phospholipase C isoforms, activated in different manners: G-protein coupled receptors (acting via PLC-β), tyrosine-kinase coupled receptors (PLC-γ), an increase in Ca^{2+} concentration (PLC-δ) or activated by Ras (PLC-ε) [51,52]. The final effector are the IP3Rs, nonselective cationic channels that conduct Ca^{2+}.

Three isoforms of IP3R encoded by different genes have been identified (IP3R1, IP3R2 and IP3R3) with different agonist affinities and tissue distribution [53]. A functional IP3R Ca^{2+} channel is composed of tetramers with six transmembrane domains (of ~3000 amino acids) that can be either homotetramers or, to a lesser extent, heterotetramers of different isoforms. From the structural point of view, several domains are recognized in the protein sequence, with different functions. These include the IP3-binding domain (IP3-BD), i.e. the minimal sequence sufficient for IP3 binding, located near the N-terminus of the protein (aa 226-578). Interestingly, this protein domain contains armadillo-repeat protein structures that are engaged in protein-protein interactions, and mediates intramolecular interactions with other

IP3R domains as well as the association with other regulatory proteins. N-terminally to the IP3-BD, i.e. within aa 1-222, a suppressor region is located that inhibits ligand binding and thus lowers the global receptor IP3 affinity in the physiological range. The six transmembrane-spanning domain is at the very C-terminal end of each subunit, and, between them, an internal coupling domain assures the signal of IP3 binding is transferred to the channel-forming region, hence triggering its opening [54]. Given that the affinity of the IP3-binding core to its ligand is similar for the three isoforms, the tuning of the whole receptor's affinity appears to be due to the isotype-specific properties of the N-terminal suppressor domain [55].

The release of Ca^{2+} from the ER is a nonlinear, cooperative process wherein IP3 binds to four receptor sites on the IP3R, one on each subunit of the tetramer [54]. Small perturbations in conditions such as basal $[Ca^{2+}]_i$, [IP3], and various regulators can cause uncoordinated bursts of local release across a cell. The brief opening of IP3R channels gives rise to localized Ca^{2+} pulses, called "sparks" or "blips" and "puffs" [1]. The smallest Ca^{2+} release events, "blips", probably reflect random openings of single IP3R. Spontaneous clustering of IP3Rs (in particular of IP3R2, due to its higher IP3 affinity) have been proposed to be the underlying mechanism responsible for Ca^{2+} "puffs" observed in the cytoplasm [56]. Recruitment of neighboring IP3Rs and combination of Ca^{2+} "puffs" results in Ca^{2+} waves, ensuring that the Ca^{2+} signal propagates to the entire cell [57], or remains confined to specific subcellular regions[58].

Ca^{2+} oscillations, depend upon both the spatial organization of IP3Rs and their regulation by Ca^{2+}, although the links between IP3R activities and Ca^{2+} oscillations are not fully understood. Ca^{2+} regulates channel activity in a biphasic manner. Early studies demonstrated inhibition of IP3-mediated Ca^{2+} mobilization by micromolar concentrations of Ca^{2+} [59]. Lower concentrations were subsequently found to potentiate the effects of IP3 [60]. In addition, also the ER Ca^{2+} content retains the capability to regulate the channel opening: in permeabilized hepatocytes, an increase in $[Ca^{2+}]_{er}$ enhances the sensitivity of IP3R for its ligand, promoting also spontaneous Ca^{2+} release, but the nature of this direct regulation and the protein involved are still a matter of debate [61]. In this context, the tight spatial relationship between ER and mitochondria, and the capacity of the latter to rapidly clear the high $[Ca^{2+}]$ microdomain generated at the mouth of the IP3R, makes mitochondria an active player in the control of IP3R function. The first clear demonstration of this concept came from the fine work of Lechleiter et al., who demonstrated that energized mitochondria, by regulating the kinetics of ER Ca^{2+} release, finely tune the spatio-temporal patterning of Ca^{2+} waves in Xenopus oocytes. Then, the observation that Ca^{2+} uptake by mitochondria controls the $[Ca^{2+}]$ microdomain at

the ER/mitochondrial contacts and thus the kinetics of IP3R activation/inactivation was extended to a variety of mammalian cell lines, e.g. hepatocytes, astrocytes and BHK-21 cells, thus highlighting its general relevance [62].

Whereas IP3 and Ca^{2+} are essential for IP3R channel activation, other physiological ligands, such as ATP, are not necessary but can finely modulate the Ca^{2+}-sensitivity of the channel [63]. As for Ca^{2+}, the modulation of IP3R by ATP is biphasic: at micromolar concentrations, ATP exerts a stimulatory effect, while inhibiting channel opening in the millimolar range [64,65].

Finally, in their coupling/suppressor domains, the IP3Rs possess consensus sequences for phosphorylation by numerous kinases. Currently, at least 12 different protein kinases are known to directly phosphorylate the IP3R [66], among them: Akt [67], protein kinase A (cAMP-dependent) [68], protein kinase G (cGMPdependent) [69], calmodulin-dependent protein kinase II (CaMKII) [70], protein kinase C (PKC) [71], and various protein tyrosine kinases[72].

Mitochondria: cell physiology and molecular nature of the mitochondrial Ca^{2+} uptake and release machinery

The mitochondrion represents a unique organelle within the complex endomembrane systems that characterize any eukaryotic cell. Complex life on earth has been made possible through the "acquisition" of mitochondria which provide an adequate supply of substrates for energy-expensive tasks. The mitochondrion is a double membrane-bounded organelle thought to be derived from an α-proteobacterium-like ancestor, presumably due to a single ancient invasion occurred more than 1.5 billion years ago. The basic evidence of this endosymbiont theory [73] is the existence of the mitochondrial DNA (mtDNA), a 16.6 Kb circular double-stranded DNA molecule with structural and functional analogies to bacterial genomes (gene structure, ribosome). This mitochondrial genome encodes only 13 proteins (in addition to 22 tRNAs and 2 rRNAs necessary for their translation), all of which are components of the electron transport chain (mETC) complexes (I, III and IV), while the whole mitochondrial proteome consists of more than 1000 gene products. Thus, one critical step in the transition from autonomous endosymbiont to organelle has been the transfer of genes from the mtDNA to the nuclear genome. At the same time, eukaryotes had to evolve an efficient transport system to deliver nuclear-encoded peptides inside mitochondria: TIM (Transporters of the Inner Membrane), TOM (Transporters of the Outer Membrane) and mitochondrial chaperones (such as hsp60 and mthsp70) build up the molecular machinery that allows the newly-synthesized unfolded proteins to enter mitochondrial matrix [74].

Mitochondria are defined by two structurally and functionally different membranes: the plain outer membrane, mostly soluble to ions and metabolites up to 5000 Da, and the highly selective inner membrane, characterized by invaginations called *cristae* which enclose the mitochondria matrix. The space between these two structures is traditionally called intermembrane space (IMS), but recent advances in electron microscopy techniques shed new light on the complex topology of the inner membrane. *Cristae* indeed are not simply random folds but rather internal compartments formed by profound invaginations originating from very tiny "point-like structures" in the inner membrane [75]. These narrow tubular structures, called *cristae junctions*, can limit the diffusion of molecule from the intra-*cristae* space towards the IMS, thus creating a micro-environment where mETC complexes (as well as other proteins) are hosted and protected from random diffusion.

Mitochondria were identified as the powerhouse for energy production in eukaryotic cells thanks to decades of extensive biochemical work on carbohydrate metabolism and organelle morpho-functional characterization, carried out in the first half of the 20th century by leading scientific figures such as Krebs, Corey, Claude, Palade and many others. Mitochondria are the main site of ATP production. When glucose is converted to pyruvate by glycolysis, only a small fraction of the available chemical energy has been stored in ATP molecules; the main enzymatic systems involved in this process are the tricarboxylic acid (TCA) cycle and the mETC. Products from glycolysis and fatty acid metabolism are converted to acetyl-CoA which enters the TCA cycle where it is fully degraded to CO_2. More importantly, these enzymatic reactions generate NADH and $FADH_2$ which provide reducing equivalents and trigger the electron transport chain. mETC consists of five different protein complexes: complex I (NADH dehydrogenase), complex II (succinate dehydrogenase), complex III (ubiquinol cytochrome c reductase), complex IV (cytochrome c oxidase) and complex V that constitutes the F_1F_0-ATP synthase. Electrons are transferred from NADH and $FADH_2$ through these complexes in a stepwise fashion: as electrons move along the respiratory chain, energy is stored as an electrochemical H^+ gradient across the inner membrane, thus creating a negative mitochondrial membrane potential (estimated around -180 mV against the cytosol). H^+ are forced to re-enter the matrix mainly through complex V which couples this proton driving force to the phosphorylation of ADP into ATP, according to the chemiosmotic principle. ATP is then released to IMS through the electrogenic Adenine Nucleotide Translocase (ANT) which exchange ATP with ADP to provide new substrate for ATP synthesis. Finally, ATP can easily escape the IMS thanks to the mitochondrial porin of the outer membrane, VDAC (voltage-dependent anion channel).

With the general acceptance of the chemiosmotic hypothesis, it has become clear that the ΔΨ across the mitochondrial inner membrane is the driving force for mitochondrial Ca^{2+} accumulation [76]. Thus, Ca^{2+} enters the mitochondrial matrix down its electrochemical gradient, that can be generated either by the electron flow in the mETC or by reversal of the ATP synthase. Mitochondrial Ca^{2+} accumulation plays a key role in the regulation of many cell functions, ranging from ATP production to cell death. Mitochondrial Ca^{2+} uptake and release is central not only for the regulation of cellular Ca^{2+} homeostasis, but is vital also for the regulation of intramitochondrial enzymes concerned with the utilization of oxidizable substrates. However, excess Ca^{2+} accumulation by mitochondria is a common event in the process of cell death, by both necrosis and apoptosis [77].

Despite the basic mechanisms of mitochondrial Ca^{2+} homeostasis have been firmly established for decades, the molecular identities of the channels and transporters responsible for Ca^{2+} uptake and release (schematized in Figure 3) have remained mysterious until very recently.

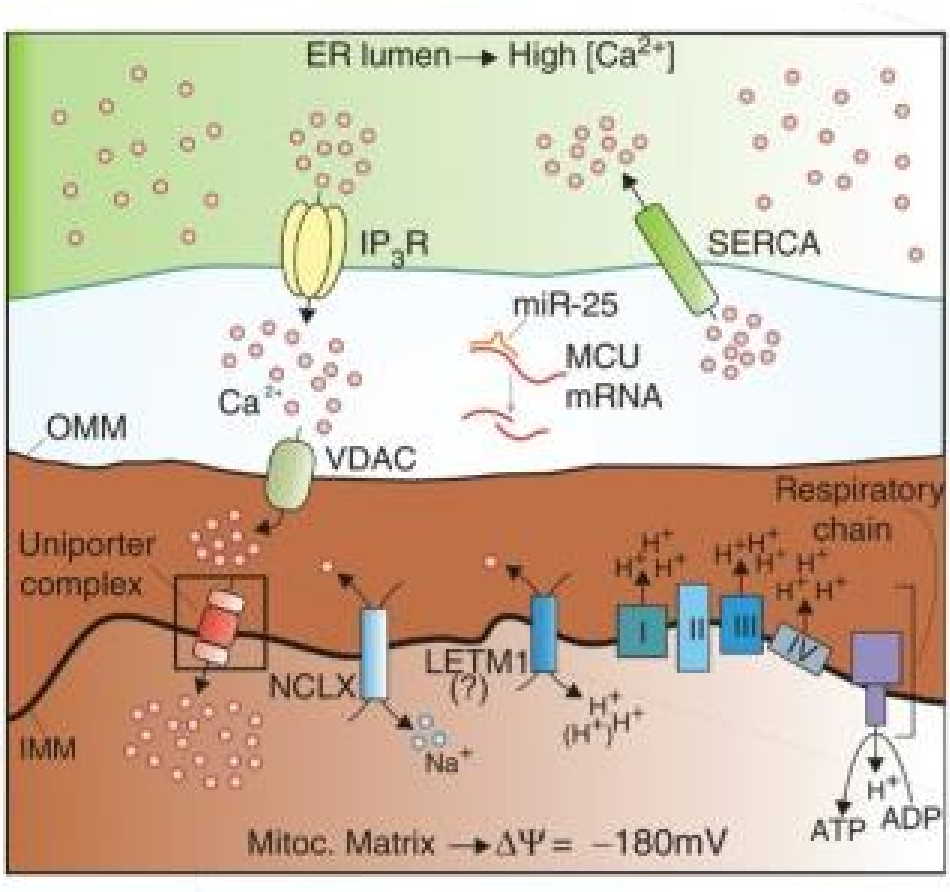

Figure 3. Schematic representation of the mitochondrial Ca^{2+} homeostasis machinery. *Figure modified from* [78]

Several studies have identified three essential proteins mediating the processes of calcium influx and efflux:

Mitochondrial Calcium Uniporter (MCU)

The main transporters involved in the uptake of Ca^{2+} into mitochondria is the MCU, characterized by a low affinity for Ca^{2+}; in fact, MCU takes up Ca^{2+} in the micromolar range and experiments in permeabilized cells report a K_d of the uniporter of 10 μM [79]. In addition, a biphasic effect of calcium on the MCU has been reported: beyond a certain level, cytosolic Ca^{2+} inactivates the uniporter, preventing further Ca^{2+} uptake and this process might avoid an excessive accumulation of the cation in mitochondria[80].

In spite of repeated efforts by different researchers, the molecular identity of the MCU has remained elusive. Among the early candidates proposed for the MCU were the uncoupling proteins UCP2/3 [81], but experiments in different tissues of mice lacking UCP2 and UCP3 showed a normal Ca^{2+} uptake[82]. Recently, Perocchi and colleagues demonstrated that MICU1 (mitochondrial calcium uptake 1), also known as FLJ12684 or CBARA1, has a key role in regulating the classically defined uniporter [83]. MICU1 is associated with the IMM and has two canonical EF hands that are essential for its activity and it caused a significant suppression of the $[Ca^{2+}]_m$ signal evoked by an IP3-linked agonist. Silencing MICU1 does not impair mitochondrial respiration or membrane potential but abolishes Ca^{2+} entry in intact and permeabilized cells, and attenuates the metabolic coupling between cytosolic Ca^{2+} transients and activation of matrix dehydrogenases.

More recently, in 2011, two distinct laboratories have been identified a transmembrane protein (CCDC109A) that fulfilling the criteria for being the MCU [84,85]. Indeed, in planar lipid bilayers CCDC109A showed channel activity with electrophysiological properties as those previously reported for the MCU [86]. The over-expression of CCDC109A (that now is called "MCU"), increases mitochondrial Ca^{2+} uptake and sensitizes cells to apoptotic stimuli, and the employment of short interfering RNA (siRNA) silencing of MCU strongly reduced mitochondrial Ca^{2+} uptake. This reduction is specific for mitochondria (Ca^{2+} cytosolic levels remain almost unaffected), does not induce impairment of the electrochemical gradient or change in mitochondrial morphology and the induction of specific mutations at the level of the putative pore-forming region reduce the mitochondrial calcium uptake and blocks the channel activity of the protein [84,85] .

Finally, in 2012, it has been identified CCDC90A, referred to as MCUR1 (mitochondrial calcium uniporter regulator 1), as an integral membrane protein required for MCU-dependent mitochondrial Ca^{2+} uptake [87]. MCUR1 binds to MCU and regulates ruthenium-red-sensitive MCU-dependent Ca^{2+} uptake. MCUR1 knockdown does not alter MCU localization, but abrogates Ca^{2+} uptake by energized mitochondria in intact and permeabilized cells. Ablation of MCUR1 disrupts oxidative phosphorylation, lowers cellular ATP and activates AMP

kinase-dependent pro-survival autophagy. Thus, MCUR1 is a critical component of a mitochondrial uniporter channel complex required for mitochondrial Ca^{2+} uptake and maintenance of normal cellular bioenergetics.

LETM1

As described above, MCU only takes up Ca^{2+} in the micromolar range, but evidence has shown that mitochondria are able to take up Ca^{2+} also at much lower concentrations, as recently reported by Jang and colleagues who identified a high-affinity mitochondrial Ca^{2+}/H^{+} exchanger capable of importing calcium in the nanomolar range[88]. This group conducted a genome-wide RNAi screen in *Drosophila* cells stably expressing a mitochondria-targeted ratiometric Pericam and identified the gene CG4589 (*Drosophila* homolog of the human gene LETM1, leucine zipper-EF-hand containing transmembrane protein 1) as a regulator of mitochondrial Ca^{2+} and H^{+} concentrations, supporting electrogenic import of Ca^{2+} (one Ca^{2+} in for one H^{+} out).

However, the effective role of LETM1 as Ca^{2+}/H^{+} exchanger still remains a subject of discussion, since its activity is blocked by treatment with CGP37157 (channel inhibitor that mediates mitochondrial calcium efflux) and red/Ru360 (inhibitor of MCU). Furthermore, LETM1 is associated with K^{+} homeostasis, and the loss of LETM1 lowers mitochondrial membrane potential, and the mitochondrial H^{+}/Ca^{2+} exchanger turned out to be non-electrogenic (one Ca^{2+} in for two H^{+} out) [88,89].

NCLX/NCKX6

A Na^{+}-dependent mechanism that mediates mitochondrial Ca^{2+} efflux has been demonstrated, but the molecular identity of this transporter has also remained elusive. In a recent study, Palty and co-workers showed that the Na^{+}/Ca^{2+} exchanger NCLX is enriched in mitochondria, where it is localized to the cristae [90]. This protein was identified as a member of the Na^{+}/Ca^{2+} exchanger situated in the ER or plasma membrane, but Palty et al., shown that in several tissues endogenous NCLX is enriched primarily in mitochondria, but not in ER and plasma membrane. The same observation is achieved overexpressing the protein in different cell lines, and the results show that expression of NCLX enhances mitochondrial Ca^{2+} efflux; this is blocked by CGP37157 and by mutations in the catalytic site of NCLX. Besides, the role of NCLX as a mitochondrial Na^{+}/Ca^{2+} exchanger is supported by evidence that NCLX mediates Li^{+}/Ca^{2+} exchange, a functional property that, among NCX proteins, is shared exclusively with the mitochondrial exchanger [90]

Remodelling ER-mitochondria Ca^{2+} transfer in cell survival and death

ER and mitochondria functions are intimately connected. A major area of functional interaction between the ER and mitochondria is the control of Ca^{2+} signalling, that is a topic of major interest in physiology and pathology. These two organelles form a highly dynamic interconnected network within which they cooperate to generate Ca^{2+} signals. The mitochondria play an important role in shaping the Ca^{2+} signal released from the ER. During normal signalling, there is a continuous flow of Ca^{2+} between these two organelles. The normal situation is for most of the Ca^{2+} to reside within the lumen of the ER except during Ca^{2+} signalling when a small bolus is periodically released to the cytoplasm and is then re-sequestered with a proportion passing through the mitochondria. At equilibrium, therefore, the bulk of internal Ca^{2+} is in the ER where it not only functions as a reservoir of signal Ca^{2+} but it also plays an essential role in maintaining the activity of the chaperones responsible for protein processing [26]. However, despite controlling many processes essential for life, Ca^{2+} arising from the ER can be a potent death-inducing signal [91,92].

The release of Ca^{2+} from ER stores by IP3Rs has been implicated in multiple models of apoptosis as being directly responsible for massive and/or a prolonged mitochondrial Ca^{2+} overload. The requirement of IP3Rs for Ca^{2+}-dependent cell death is exemplified by the resistance to apoptosis of cells in which InsP3R expression has been ablated or reduced [93,94]. Mitochondria seem to be the downstream effectors of this pathway, as KO of IP3R3 significantly decreased agonist-induced mitochondrial Ca^{2+} uptake [95]. In this picture, the three isoforms of the IP3R appear to play distinct roles. IP3R3 seems to play a selective role in the induction of apoptosis by preferentially transmitting apoptotic Ca^{2+} signals into mitochondria, whereas IP3R1 predominantly mediates cytosolic Ca^{2+} mobilization [96,97]. However, other studies have shown that the type 1 isoform can also mediate apoptosis [98].

Several observations underline the significance of the role of the ER-mitochondrial Ca^{2+} flux in stimulating apoptosis. Indeed, a wide number of apoptotic stimuli, such as ceramide, arachinodic acid, and oxidative stress induced by H_2O_2 or menadione, trigger both a progressive release of Ca^{2+} from the ER and an activation of the capacitative Ca^{2+} influx [99,100]. This sustained ER Ca^{2+} release, in turn, induced a mitochondrial Ca^{2+} overload with a consequent release of mitochondrial proteins involved in the apoptotic process (Figure 4).

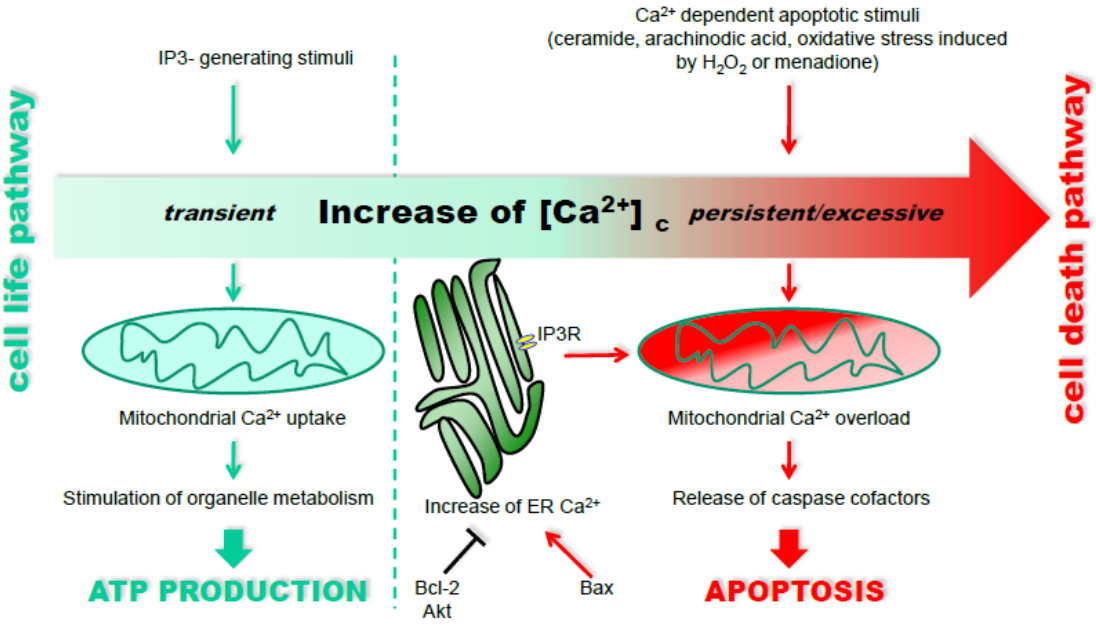

Figure 4. Differential decoding of Ca^{2+}-linked stimuli evoking the activation of cell metabolism or apoptosis. *(figure modified from [92])*

Since ER and mitochondria play significant roles in the regulation of cell proliferation and apoptosis, the remodelling of Ca^{2+} signalling machinery in ER and mitochondria of cancer cells seems imminent during oncogenic transformation, to limit death-inducing Ca^{2+} signals during cancer.

The first indication came from the observation that in cancer cells the increased expression of anti-apoptotic members of the Bcl-2 family of proteins (Bcl-2 and Bcl-X_L), or decreased expression of the pro-apoptotic BH3-only proteins (Bax or Bak) can protect these cells from apoptosis by modulating intracellular Ca^{2+} signals. These proteins reside in the ER, cytosol and mitochondria as homo o heterodimers. Of interest, the proapoptotic protein Bcl-2 affects ER-mitochondrial Ca^{2+} crosstalk, as the over-expression of Bcl-2 reduces the Ca^{2+} content of the ER [101] making the cells resistant to apoptosis. Similarly, genetic ablation of the proapoptotic proteins Bax and Bak that drastically increases the resistance to death signals also results in a dramatic reduction in ER Ca^{2+} content, and consequently in a reduction of the Ca^{2+} that can be transferred to mitochondria [100]. The use of a Bax/Bak double-knockout model system demonstrated that Bcl-2 forms a macromolecular complex with the IP3Rs. The decreased level of Bax and Bak hereby correlated inversely with the amount of Bcl-2 bound to the IP3R, the phosphorylation status of the IP3R and the Ca^{2+} leak from the ER, leading to the conclusion that Bcl-2 regulated ER Ca^{2+}-store content by regulating the phosphorylation status and the activity of the IP3R. The phosphorylation of IP3R1 was proposed to be due to protein kinase A, but the role of other kinases could not be dismissed [102].

IP3R phosphorylation appears to be a key common feature for modulation of channel function and, as consequence, apoptotic signalling. IP3Rs possess consensus sequences for phosphorylation by numerous kinases, including the pro-survival protein kinase Akt. The consensus site for phosphorylation by Akt has been identified at the carboxyl terminus (serine 2618) of all three mammalian IP3R isoforms and is conserved from mammals to flies [67]. This phosphorylation event decreases IP3-stimulated Ca^{2+} release from the ER and so diminishes flux of Ca^{2+} to the mitochondria following stimulation with pro-apoptotic agonists, thereby reducing apoptosis [103,104]. This is an interesting observation, because in some cancer cells in which Akt is constitutively active (e.g. prostatic carcinoma cells), IP3Rs are hyper-phosphorylated [67]. These data suggest that this functional interaction between Akt and IP3Rs is retained in tumour cells, endowing them with a significant survival advantage by limiting Ca^{2+}-dependent death signalling.

ER-mitochondria Ca^{2+} transfer appears to be a key sensitizing in various apoptotic routes. Hence, therapeutic modulation of targets that regulate $[Ca^{2+}]_{er}$ and/or ER-mitochondrial Ca^{2+} transfer may be able to augment apoptosis in cancer cells without disrupting global Ca^{2+} homeostasis. However, the precise molecular definition of this process still awaits a fine clarification of the macromolecular complex assembled at the interphase between the two organelles.

Mitochondria-associated membranes: role of structural and regulatory proteins in the control of Ca^{2+} transfer between ER and mitochondria

The association between ER and mitochondria was first described by Copeland and Dalton over 50 years ago in pseudobranch gland cells [105]. By the beginning of the 70s, the contacts between mitochondria and ER had been visualized by several groups [106,107]. Electron micrograph images of quickly frozen samples [108] and experiments in living cells with the two organelles labelled by means of targeted spectral variants of GFP (mtGFP(Y66H,Y145F) and erGFP(S65T)) [33], demonstrated conclusively that such physical interactions between the two organelles indeed exist. These latter experiments revealed the presence of overlapping regions of the two organelles and allowed to estimate the area of the contact sites as 5-20% of the total mitochondrial surface (Figure 5). The distance between the ER and the OMM was originally estimated to be approximately 100 nm [109,110]. More detailed morphological studies, carried out by Achleitner *et al.* in 1999, indicated that the distance between the ER and mitochondria in the areas of interaction varied between 10 and 60 nm [111]. Importantly, a direct fusion between membranes of the ER and mitochondria was not observed in any case, and the

membranes invariably maintained their separate structures. The authors of this pioneering paper proposed that a distance of less than 30 nm between the two organelles could be considered as an association. More recently, electron tomography techniques allowed to estimate that the minimum distance is even shorter (e.g. 10-25 nm) [112]. This distance thus enables ER proteins to associate directly with proteins and lipids of the OMM. Further development of microscopic techniques allowed detailed analysis of such contacts with high resolution in three dimensions [113].

The interactions between ER and mitochondria at the contact sites are so tight and strong, that upon subcellular fractionation (at the step of mitochondria purification), a unique fraction, originally named 'mitochondria-associated membranes" (MAMs), can be isolated [114,115]. More recently, the isolation procedures was improved and adapted to isolate the MAMs fraction from yeast, different organs, tissues, and various cell lines [111,116,117]. The molecular analysis of both "crude" mitochondria and MAMs fractions demonstrated that, apart from specific ER and mitochondrial proteins, they also contain proteins which are abundant in the plasma membrane. However, research on the morphological organization of mitochondria and ER with respect to the plasma membrane is much less extensive. Modifications in the subcellular fractionation procedure enabled the isolation of the "plasma membrane associated membranes" (PAMs) fraction. In general, PAMs fractions have been described as the center of interactions between plasma membrane and the ER [118,119], but the presence of mitochondrial proteins in these fractions indicates that mitochondria interact actively also with the plasma membrane [120,121]. The MAMs have a pivotal role in several cellular functions related to bioenergetics and cell survival. MAMs have been originally shown to be enriched in enzymes involved in lipid synthesis and trafficking between ER and mitochondrial membranes, including long-chain fatty acid-CoA ligase type 4 (FACL4) and phosphatidylserine synthase-1 (PSS-1) [115,122,123]. The MAMs have since been shown to be enriched in functionally diverse enzymes involved not only in lipid metabolism but also in glucose metabolism [124,125].

More recently, the same subcellular fraction has been shown to contain Ca^{2+}-sensing ER chaperones and oxidoreductases, as well as key Ca^{2+} handling proteins of both organelles [126,127]. Together, these data have led to the conclusion that the MAMs are not only a site of lipid synthesis and transfer, but also function as a fundamental hub of cellular signalling that controls a growing number of processes associated with both organelles, ranging from ER chaperone-assisted folding of newly synthesized proteins to the fine-tuning of physiological and pathological Ca^{2+} signals from ER to mitochondria.

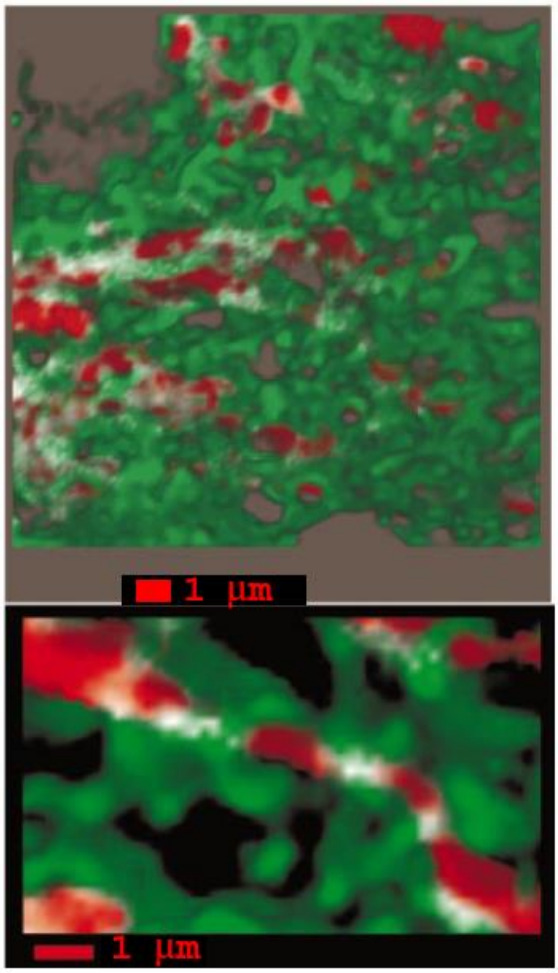

Figure 5. High-resolution 3D imaging of ER-mitochondria contact sites. *Combined 3D imaging of mitochondria and ER in a HeLa cell transiently expressing mtGFP(Y66H,Y145F) and erGFP(S65T). The mitochondrial and ER images are represented in red and green, respectively; the overlaps of the two images are white. On the bottom, a detail of the main image (80-nm pixel) (figure from [33]).*

The importance of MAMs began to emerge when it was found that, after cell stimulation, mitochondria were able to uptake Ca^{2+} directly from IP3Rs[30]. It was thus possible to identify specialized signaling microdomains, selectively enriched in critical Ca^{2+} signaling elements, labelled as "hotspots zones", where Ca^{2+} is transferred from the ER into mitochondria. The interactions between the two organelles are modulated by mitochondria-shaping proteins and chaperone proteins. MFN-1 and -2 (mitofusin-1 and -2) belong to the first group and stabilize the interaction between adjacent mitochondria, regulate ER morphology and calcium homeostasis, and directly tether ER to mitochondria, thus facilitating efficient Ca^{2+} uptake by mitochondria [113]. The hsp70 homologous cytosolic chaperone grp75 (glucose-regulated protein 75) tethers the N-terminal domain of the type-1 IP3Rs to the isoform 1 of VDAC, generating a molecular bridge that enhances the Ca^{2+} accumulation in mitochondria [128]. Recently identified, the Sigma-1 ER receptor (Sig-1R) selectively resides at the MAMs, forms a Ca^{2+}-sensitive chaperone complex with BiP/GRP78 (78-kDa glucose-regulated protein GRP78, also referred to as the immunoglobulin binding protein BiP) and associates with isoform 3 of IP3R. Upon activation of IP3Rs, which causes the decrease of Ca^{2+} concentration at the MAM, redistribution of Sig-1Rs occurs, from MAMs to the periphery of the

ER: here Sig-1Rs dissociates from BiP/GRP78 and the chaperone activity of free Sig-1Rs attenuates the aggregation of IP3R3[95].

Mitochondria-associated membranes and autophagy

Autophagy (derived from the ancient Greek meaning 'to eat oneself') is a process by which cells undergo partial autodigestion to briefly prolong their survival under starvation conditions. Autophagy provides the nutrients necessary to maintain cell viability. Although autophagy could be aspecific, it is now clear that autophagy specifically targets invading bacteria [129,130], protein aggregates [131], and organelles such as mitochondria [132]and ER [133].

Autophagy is up-regulated in response to extra- or intra-cellular stress, and defects in autophagy play significant roles in several human pathologies, including cancer and neurodegeneration [134].

The molecular basis of autophagy has been studied extensively, mainly in yeast. These studies have revealed over 30 autophagy related genes (ATG), 18 of which are essential for autophagosome generation. Importantly, Atg proteins involved in the formation of autophagosomes are evolutionarily conserved from yeast to humans, and the corresponding yeast and human proteins have similar functions [135]. When autophagy is induced, a membrane cisterna called the isolation membrane or phagophore encloses a portion of the cytoplasm, resulting in the formation of the autophagosome. This initial sequestration step is generally thought to be non-selective. The outer membrane of the autophagosome then fuses with the lysosomal membrane. The formation of the autophagosome is clearly central to the autophagic process, but the details of how the phagophore membrane forms and the compartment from which it originates remain unknown. In yeast, the phagophore membrane forms around a cytosolic structure known as the pre-autophagosomal structure (PAS), but there is no evidence of PAS formation in mammalian cells, and the source of the mammalian phagophore remains uncertain [136]

MAMs are important for the initiation and execution of the autophagic machinery as a primary component. To date, mitochondria and the ER are known to be involved in autophagosome biogenesis. Initially, several ER proteins were found to be localized to the autophagosome membrane. Subsequently, electron and fluorescence microscopy have demonstrated that the ER and the initial isolation membrane of autophagosomes (phagophore) are juxtaposed and that upon starvation-induced autophagy, the cell forms the so-called omegasome, which is a phosphatidylinositol 3–phosphate compartment connected to the ER that is fundamental for autophagosome formation. Alternatively, autophagosomes may be derived from mitochondria. It has been demonstrated that during starvation, the OMM "gifts" some mitochondrial-derived

membranes for use in autophagosome biogenesis. Furthermore, studies have also identified a crucial role for the ER-mitochondria connection in autophagy induction. Indeed, MFN2 KO-derived cells are unable to undergo autophagy, supporting the possibility of a lipid contribution from the ER to the mitochondria [137]. Additionally, these studies provided an additional indication of the intimate relationship between MAMs and autophagosomes. Immunofluorescence and electron microscopy and subcellular fractionation illustrated in detail how specific pre-autophagosome/autophagosome markers (ATG14 and ATG5) localize to MAMs under starvation conditions. Consistent with this finding, DCFP1 (double FYVE domain-containing protein 1) also translocates to the omegasome upon starvation. In contrast, in PACS-2 KO and MFN2 KO cells, both the accumulation of autophagic markers and the translocation of ER-related proteins were significantly reduced, indicating a stable role of MAMs during the completion of autophagosomes [138]. Although these findings have provided evidence regarding the origin of autophagosomes, several questions remain unanswered. In particular, the role of MAMs in the molecular mechanism of autophagy remains unclear. It is well known that the serine/threonine kinase mTOR (mammalian target of rapamycin) is the primary regulator of autophagy. The activity of TOR is inhibited under nutrient starvation, which has been known as a crucial step for autophagy induction in eukaryotes [139,140]. This kinase exists in two protein complexes: mTOR complex1 (mTORC1) and mTOR complex2 (mTORC2)[141]. Interestingly, mTORC2 has been found to localize to MAMs, where it activates AKT. Once activated, AKT appears to control MAMs integrity and mitochondrial physiology through PACS and hexokinase (HK2) phosphorylation. Furthermore, mTORC2-AKT regulates IP3R3 phosphorylation and Ca^{2+} release at MAMs [142]. Despite this finding, the involvement of mTORC2 in autophagy remains debatable. Nevertheless, it has been found that Rab32, a MAMs protein that is essential for autophagosome formation [143], is a critical regulator of mTORC2 activity [144]. Overall, these findings suggest an active role for this complex in autophagosome formation and the regulation of autophagic activity. Additional MAMs proteins appear to regulate autophagy [145] Different forms of specialized autophagy have recently been discovered and comprehensively reviewed [146]. One of the most important of these forms is mitophagy [132], which is responsible for the selective removal of damaged mitochondria. Several studies have demonstrated that two genes, PINK1 (PTEN-induced kinase 1) and parkin, are involved in the maintenance of a healthy population of mitochondria. Indeed, the PINK1-parkin axis recognizes defective mitochondria, rapidly isolates them from the mitochondrial network and, finally, degrades them through the ubiquitin-proteosome and autophagic pathways [147]. Recently, it has been demonstrated that mitochondria supply membrane material not only during serum starvation but also during drug-induced autophagy, introducing a novel mechanism of parkin-associated mitophagy [148]. This study

may offers new avenues for the discovery of novel roles for the ER-mitochondria contact sites in the regulation of the molecular pathways of general and selective autophagy.

Mitochondria-associated membranes and inflammation

MAMs have recently been shown to play a central role in the modulation of various key processes, including inflammasome signaling. A link between inflammation and the ER-mitochondria interface was established for the first time in 2011 in a study by Zhou and colleagues, who demonstrated a new role for mitochondria in NLRP3 inflammasome activation [149].

The NLRs are composed of 22 human genes that are characterized by the presence of a central nucleotide-binding oligomerization (NACHT) domain, C-terminal leucine-rich repeats (LRRs) and an N-terminal effector domain. Upon activation, select NLR family members form multiprotein complexes (termed inflammasomes) that serve as platforms for caspase-1 activation and the subsequent proteolytic maturation of the potent proinflammatory cytokine IL-1β[150]. Due to its association with numerous inflammatory diseases, the NLRP3 inflammasome is currently the most fully characterized, well-studied inflammasome. The key components of a functional NLRP3 inflammasome include NLRP3, the adaptor protein ASC (apoptosis-associated speck-like protein containing a caspase recruitment domain) and caspase-1[151]. Upon sensing a wide variety of danger signals, NLRP3 oligomerization and recruitment of ASC and procaspase-1 trigger the autoactivation of caspase-1 and the maturation and secretion of proinflammatory cytokines, such as IL-1β. Resting NLRP3 localizes to the cytosol and ER structures, whereas upon inflammasome activation using nigericin (an antibiotic) or monosodium urate, both NLRP3 and its adaptor ASC colocalize to the MAMs fraction. Thus, by virtue of its ER-mitochondria localization upon activation, the NLRP3 inflammasome is strategically located to receive signals emanating from mitochondria.

Previous studies have indicated that ROS represent the common integrator across several stimuli that activate the NLRP3 inflammasome, and in addition to the ER and peroxisomes [152], mitochondria are the primary source of ROS; however, the source of NLRP3-activating ROS and its underlying mechanisms remain unclear.

Zhou and colleagues observed a correlation between mitochondrial ROS activity and the presence of IL-1β in the supernatant of the human THP1 macrophage cell line. To avoid cellular damage, ROS-generating mitochondria are constantly removed by mitophagy; these authors found that inhibition of the autophagic machinery affectsIL-1β production, resulting in the accumulation of

defective and ROS-producing mitochondria, which potentiates NLRP3-dependent inflammasome activation.

Although these results indicated that the prolonged presence of damaged, ROS-producing mitochondria is implicated in inflammasome activation, this evidence remained indirect. However, this finding suggests that MAMs may become locally enriched in ROS or ROS-derived signaling molecules and recruit ROS-sensing proteins.

Another NLRP3 binding partner, TXNIP, redistributes to MAMs/mitochondria in response to oxidative stress [153] or NLRP3 inflammasome activation [154]. In resting cells, TXNIP interacts with TRX and is therefore unavailable for NLRP3 interaction.

Inflammasome activators, such as uric acid crystals, induce the dissociation of TXNIP from thioredoxin in a ROS-sensitive manner and allow it to bind NLRP3 and translocate to MAMs/mitochondria[154], raising the possibility that TXNIP is involved in IL-1β production through NLRP3 under ER stress conditions. TXNIP is a critical signaling node that links ER stress and inflammation. TXNIP is induced by ER stress through the PERK and IRE1 pathways, induces IL-1β mRNA transcription, activates IL-1β production by the NLRP3 inflammasome, and mediates ER stress-mediated β-cell death [155].

The observation that perhaps best exemplifies the crucial role of NLRP3 at ER–mitochondria contacts is the identification of the adaptor MAVS (mitochondrial anti-viral signaling) as the mitochondrial anchor for NLRP3 inflammasome formation[156]. MAVS decodes antiviral signals that are primarily received and conveyed to the mitochondria by RIG-1 and MDA5 [157].

In addition to RIG-1, several other proteins that function in the area surrounding the mitochondria fine-tune the activities and functions of MAVS. Among these factors, STING (stimulator of IFN genes) resides ER-facing side of the MAM. STING interacts with RIG-1, likely stabilizing it at the ER–mitochondria interface, and is able to activate both the NF-kB and IRF3 transcription pathways to induce the expression of type I interferon [158].

Recently, it has been demonstrated that MAVS is required for optimal NLRP3 activity, mediating recruitment of NLRP3 to mitochondria, promoting the production of IL-1β and the pathophysiological activity of the NLRP3 inflammasome [156].The recruitment, which depends on a short N-terminal sequence in NLRP3, promotes ASC “speckle” formation and the downstream biochemical events associated with the activity of the inflammasome .Contrary to these results, which support a role for MAVS in the activation of the NLRP3 inflammasome via nonviral stimuli such as LPS plus nigericin or LPS plus ATP, Park and colleagues demonstrated that MAVS regulates NLRP3 activation primarily in response to stimuli that directly engage MAVS, such as infection with Sendai virus [159]. MAVS facilitates the recruitment of NLRP3 to the mitochondria and

may enhance its oligomerization and activation by bringing it in close proximity to mitochondrial ROS. Collectively, these findings highlight the central role of MAMs in the coordination of inflammasome formation.

p53 at the endoplasmic reticulum regulates apoptosis in a Ca^{2+}-dependent manner

p53 is a master regulator of cell fate

In 1979 six different research groups, independently, reported the discovery of a 53KDa protein, present in both human and murine cells, five of this shows how the protein was able to bound the T-large antigen from SV40, while the sixth that the protein was present in several murine tumor cell types[160-164]. Initially believed as an oncogene, because of its correlation to the SV40 antigen, in 1989, the TP53 gene was found mutant in tumor cells compared to the one of neighbouring sane tissues. Definitely TP53 was labelled as an oncosuppressor gene, and the p53 used to that date to show its oncogenic activity was effectively a mutant [165].

Later TP53 has been found as one of the most mutant genes in human tumors and, to date, more than 25000 mutations have been reported, most of that as missense mutations. These natural occurring mutations has been reported also to be often dominant negative or gain of function for oncogenic activities. Mutations in p53 alleles are found in more than 50% of human tumors, most of it are concentrated within the DBD, in just a few position known as Hot Spot. These mutations are able to impair proper p53 transcription regulation, but recently several other roles has been proposed (see later).

The p53 protein is composed of at least 4 domains:

- N-terminal trans-activational domain,
- A proline-rich domain, for protein interactions (such as for Mdm2),
- A DNA binding domain (DBD),
- An oligomerization domain (OD), principal target for post-transactional modifications such as phosphorylation, acetylation, methylation, ubiquitinilation, sumoilation, neddylation, which can influence protein stability or its interactions.

The presence of a DBD and a trans-activational domain make p53 a transcription factor involved in processes like cell cycle block, control of proliferation, apoptosis induction and others all equally important in tumor suppression.

In normal conditions p53 is present at very low levels, due to its interaction with the E3-ubiquitin ligase Mdm2. This interaction allows constant ubiquitinilation of p53 and its consequent degradation via proteasome. During several stress conditions different proteins can phosphorylate

the binding site for Mdm2 on p53 proline-rich domain inhibiting p53 degradation, allowing a rapid accumulation of the protein and engage of its activities [166].

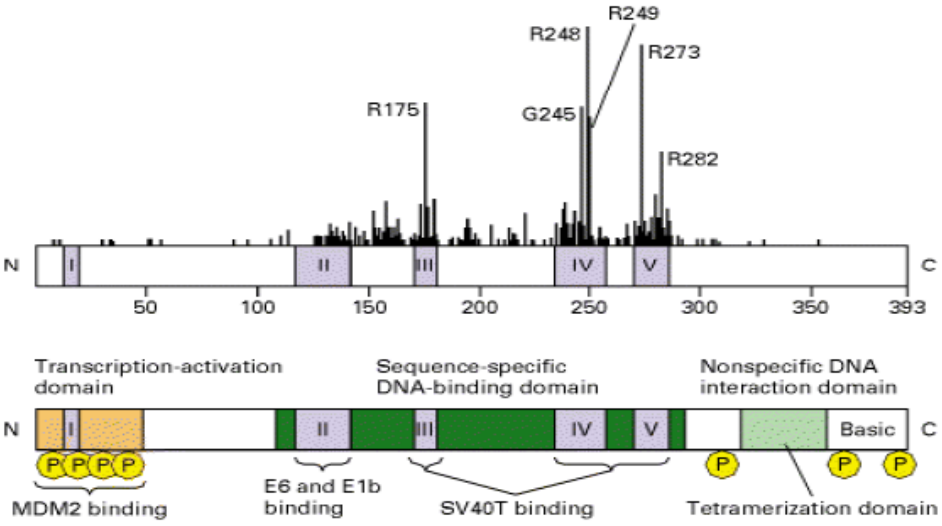

Figure 6. Representation of domains of p53. *Domains are represented in different colours; yellow labels indicate phosphorylation sites while black bars on upper panel indicate Hot Spot mutation found in human tumours.*

This peculiarity of p53 response to stress, bid researchers to usually not describe p53 activation event (in order of lacking an enzymatically activity), but of p53 stabilization.

P53 stabilization is induced by a plethora of stimuli, not only of genotoxic nature, but also:

- telomeres erosion,
- serum starvation,
- hypoxic damage,
- ribosomal stress,
- oncogene activation.

With the ultimate fate to induce cell cycle arrest or apoptosis, but also favoring DNA repair and genomic stability, senescence, survival, regulation of metabolism (specially inhibition of glycolysis and promotion of respiration), regulation of autophagy, oxidative stress regulation, cell motility and cell differentiation. All these aspects evidence p53 as an overall regulator of cell fate and tissutal homeostasis, requiring, within the cell, the presence of a huge amount of regulators of p53 that could act directly (i.e. Mdm2), but specially by post-translational regulation and subcellular localization. Ability of p53 to regulate gene expression is in turn fundamental to orchestrate all the response describe above and to date hundreds of genes has been found directly regulated p53 because of the presence of one or more of its consensus sequence i.e. p53AIP1, Apaf-1, BAX, Caspase-1 and Caspase 6, cathepsin D, DINP1, DR4, DR5, Fas, IGF-BP3, NOXA, p85, PERP, PIDD, PIG3, PTEN, PUMA, Scotin, p21, E124/PIG8.

Signals stabilizing p53 are not acting all through the same participants or mechanism, i.e. ARF protein that bounds and inhibits Mdm2 is activated by oncogenes, but is not involved during DNA damage stress [167]. Similarly the ribosomal protein L11 allows p53 stabilization after ribosomal stress [168]. Interestingly the genotoxic activation pathway (induced by radiotherapy and many chemotherapeutic agents) recently has been suggested as the most primitive, but not as the most relevant in order of tumor suppression [169], while the most efficient from this point of view appears to be exactly the once activated by oncogene activated and mediated by ARF [170].

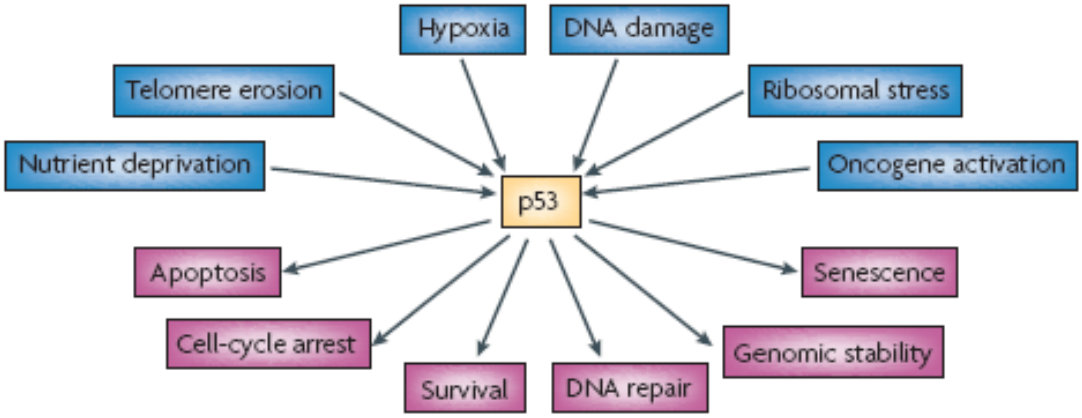

Figure 7. The many routes of p53. *Blue boxes indicates the activating signals induced in different stress conditions, while pink boxes display several induced answers by p53 accumulation. Figure source (109)*

P53 stabilization has been recently linked to metabolism, even during non-genotoxic conditions. During glucose deprivation p53 activate the AMP kinase (AMPK) that in turn allow cell survival [171] moreover Matoba and co-workers in 2006 shown how p53 [172] in basal condition favors the expression and assembly of Respiratory Complex IV favoring cell respiration. Loss of p53 in turn would favor cell growth and tumor formation even in presence of low nutrient conditions and appearance of Warburg effect.

Moreover p53 has been implicated also in metabolism of reactive oxygen species as both antioxidant and pro-oxidant. Link between p53 and ROS starts with observation that p53 could induce genes able to promote ROS production [173] as PIG3 and Proline Oxidase [174] as well as it is able to inhibit expression of antioxidant genes [175]. This would increase sensitivity to p53 dependent apoptosis and, through DNA damage, to induce a feedback loop for p53 activation.

Nonetheless p53 is also able to induce genes like sestrines [176], glutathione peroxidase [177], aldehyde dehydrogenase [178], allowing reduction of levels of ROS.

The mitochondrial route of p53

The first hint of a transcription-independent apoptotic activity of p53 dates back to 1994–1995, when it was shown that p53-dependent apoptosis occurred in the presence of transcriptional or translational inhibitors, and that p53 truncation mutants lacking transcriptional activity can still trigger apoptotic function [179,180]. Later studies suggested that direct p53 signaling is participating in regulating caspase activity [181,182]. However, these studies did not provide any mechanistic explanation and until the beginning of the new century the novel, transcription-independent proapoptotic function of p53 remained enigmatic. Today, the subject is intensely studied. It is clearly established that in response to a stress signal, cytoplasmic p53 rapidly translocates to mitochondria, where it interacts with multi-domain members of the anti- and proapoptotic Bcl-2 family members to either inhibit or activate them. This direct action of p53 results in robust mitochondrial outer membrane permeabilization (MOMP), unleashing the enzymatic apoptotic machinery of caspases and of chromatin degradation.

The breakthrough study that first showed a direct role of p53 in mitochondrial apoptosis came from Marchenko et al, demonstrating that during p53-dependent apoptosis, a fraction of stress-stabilized wild-type p53 rapidly translocates to the mitochondrial outer membrane. p53 translocation precedes changes of mitochondrial membrane potential, cytochrome c release and caspase activation[183]. As definitive proof, a mitochondrially targeted p53 fusion protein that bypasses the nucleus and has no residual transactivation function was able to induce apoptosis and long-term growth suppression as efficiently as conventional p53 when expressed in several p53-null cancer cell lines [183,184]. Subsequent studies from Moll's lab established that mitochondrial translocation of endogenous wtp53 occurs during the full spectrum of p53-activating cellular stress categories (various types of DNA damage, hypoxia, oncogene deregulation, oxidative damage) in different cell types (human and mouse; primary, immortal and malignant; epithelial, mesenchymal and lymphoid/myeloid) [185-187]. This translocation occurs during p53-dependent apoptosis but not during p53-induced cell cycle arrest or p53-independent apoptosis [183-185,187],Mechanistic insights into the mitochondrial function of wtp53 came when it was realized that mitochondrially translocated p53 interacts directly with members of the Bcl-2 family, which are central in governing the induction of mitochondrial outer membrane permeabilization. In response to stress, wtp53 interacts with and neutralizes the anti-apoptotic members Bcl-xL and Bcl-2. This interaction stimulates MOMP and subsequent apoptosis and is associated with disruption of inhibitory complexes between Bcl-xL or Bcl-2 with MOMP inducing members (i.e. BH3-only and Bax/Bak) that pre-exist in unstressed cells[184,185,187,188]. Only the p53 core domain but not its amino- and carboxyterminal regions interacts [189].

The core domain of mitochondrial p53 also directly interacts with pro-apoptotic Bak, which constitutively resides in the outer mitochondrial membrane [184,190]. This interaction liberates Bak from pre-existing inhibitory complexes with the anti-apoptotic Mcl-1 protein [190].

Similarly to Bcl-xL/2 interactions, conserved residues of the p53 core domain participate in Bak interaction [191]. Nonetheless affinity for Bcl-2/Xl is apparently 10 times higher compared to binding with Bak/Bax that displays a lower acidic surface neither a BH4 domain, suggesting that p53 preferentially binds to Bcl-2/Xl.

A different explanation for non-nuclear p53 has been proposed involving PUMA. In physiological condition cytolasmic p53 would be sequestered in an inhibitory complex with Bcl-Xl. In response to stress p53 would translocate to the nucleus where promote transcription of its target PUMA. PUMA, in turn, disrupt this complex by binding Bcl-Xl and allowing p53 to activate Bak monomer within cytosol [192,193]. Mitochondrial translocation to p53 has been shown to be PUMA and Bax indipendent and would allow not only Bak/Bax oligomerization on the OMM, but involved also VDAC, inducing a complex formation with cyclophillin D.

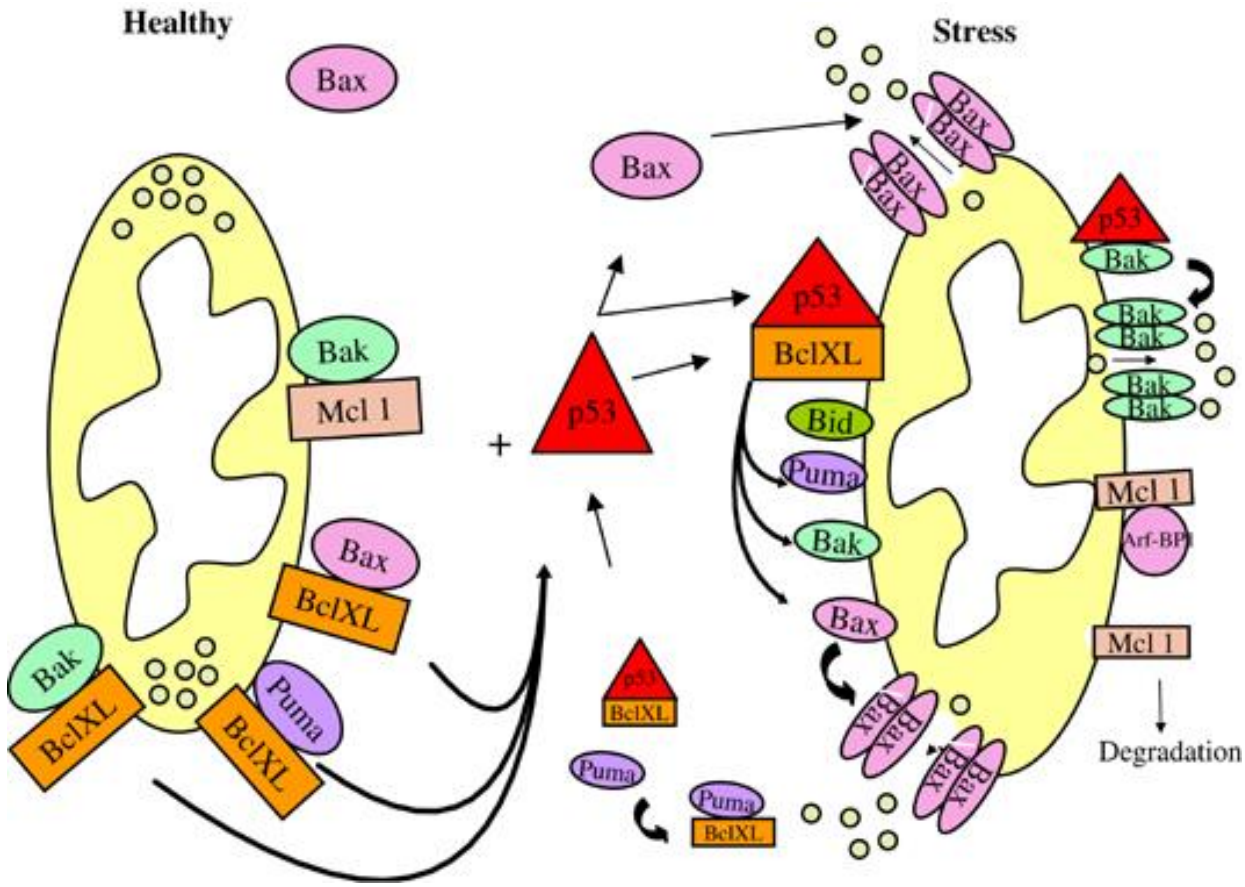

Figure 8. The Bcl-2 model for mitochondrial p53. *In normal condition on OMM Bcl-2/XL and Mcl-1 maintain Bax andBak inhibited, p53 by removal of Bcl-2/Xl/Mcl-1 allow the generation of a permeability transition state. Figure source* [186].

Studies on negative dominant heterozygosity for p53 with naturally occurring mutants show how the gene transcription is impaired in this condition, while the mitochondrial route appear completely normal [194]. Should be noticed that, while nuclear p53 act as a tetramer (or dimer of dimers), the mitochondrial path appear exerted by monomeric p53, explaining why this route appear not affected by tumor derived missense mutants. This phenomenon has been explained as a security mechanism versus dominant negative mutation.

Recently also has been show how p53 interacts with Mdm4, allowing translocation to mitochondria and binding to Bcl-2 [195]. Moreover, while interaction between p53 and Bcl-2 occurs even in physiological conditions, interaction between Mdm4 and Bcl-2 is dependent by apoptotic stimulation. This evidences counteract the idea that Mdm4 would be a negative regulator of p53, while propose a more fine regulation of p53 levels during transition between physiological state and stressed conditions[196,197].

Despite these interesting evidences collected about physiology of p53 still is not clear neither which are all the cytoplasmic functions of p53 nor which are the pathways allowing p53 to choose its path and specially P53 does not show any translocation sequence (at least within the plethora of the known once).

The most relevant post-translational modification linked to this route for p53 is a monoubiquitinilation actually [198]. Monoubiquitinilation are known as regulatory events linked to protein compartmentalization [199,200], despite the role for ubiquitin in proteasomal degradation, where at least 4 copy of the protein has to be linked to the target to induce is removal [201].

P53 monoubiquitinilation is apparently driven by Mdm2 (as the poliubiquitinilation that mediate its degradation), but still is not clear what determine the “stop” after the first labelling step. Once to mitochondria p53 is rapidly deubiquitinilated by HAUSP, impeding a further ubiquitinilation and allowing engagement of apoptosis initiation.

The mitochondrial p53 induction of apoptosis has been addressed to radiotoxicity in organs like thymus and spleen where appear to translocate faster compared to the nuclear translocation.

Nonetheless this pathway has been also linked to cerebral ischemia and reperfusion damage in kidney [202], to such a big extent that inhibiting this mitochondrial route, with a drug called pifithrin can allow tissue survival reducing the toxicity due to chemotherapy [203].

Introduction

The master tumor suppressor p53 is the hub of numerous signaling stress pathways that control cell fate. The inactivation of p53 function is a pivotal aspect of tumor formation in different human cancers. Its activity is crucial for regulating efficient cell death in cancer cells upon cellular stress [204] evoked by chemotherapeutic drugs or radiation. Many cancer cells, however, contain a mutant TP53 gene or a nonfunctional p53 protein and are thus unable to respond efficiently to these treatments. Indeed, more than 50% of human cancers harbor somatic p53 gene mutations [205]. In addition to sporadic tumors, inherited heterozygous loss-of-function mutations in TP53 cause Li–Fraumeni syndrome, which confers a high familial risk of various types of cancer [206]. However, the mechanisms by which wild-type p53 suppresses tumor growth and influences the response to drug treatment by mediating apoptosis are not yet fully understood. Two pools of p53, cytoplasmic and nuclear, have been well established to independently respond to stress [198] through transcription-dependent and -independent mechanisms [207,208], both of which are regulated by posttranslational modifications that allow its accumulation and the full activation of its proapoptotic functions [209]. The cytoplasm is the main source of p53 involved in the non-transcriptional pathway through mitochondrial translocation, whereas the nuclear p53 pool is responsible for transcription dependent mechanisms [198,208,209]. Giorgi and colleagues recently demonstrated the unexpected localization of the promyelocytic leukemia protein (PML) at the endoplasmic reticulum (ER) and at mitochondria-associated membranes (MAMs) [210], a specialized domain of close contact between the ER and mitochondria that is involved in maintaining a dynamic cross-talk between the two organelles [126]. PML is a tumor suppressor that physically interacts and synergizes with p53 during apoptosis induction [211]. ER–mitochondrial cross-talk is fundamental for the upregulation of mitochondrial metabolism in stimulated cells [212] and plays a key role in decoding Ca^{2+}-mediated apoptotic signals [92,95,112,213]. The down-regulation of ER–mitochondrial Ca^{2+} transfer caused by B-cell lymphoma 2 (Bcl-2) overexpression or PML impairment is important for the antiapoptotic effects of these proteins [214].

Recent studies have suggested that p53 participates in apoptosis induction by acting directly at mitochondria. Because p53 can mediate apoptosis without its DNA-binding domain (the domain proposed to be fundamental for the targeting of p53 to mitochondria), the mitochondrial localization of p53 is likely not the only transcription-independent mechanism by which p53 promotes apoptosis[180]. In this project we investigated and discuss whether an extra nuclear localization of p53 could mediate its tumor-suppressive function through a nontranscriptional, Ca^{2+}-dependent pathway.

Results

p53 Accumulation at the ER/MAM compartments after anticancer treatments enhances cell death.

To establish whether another nonmitochondrial p53 aspect could be involved in a nontranscriptional proapoptotic pathway, we verified the intracellular localization of p53 using biochemical and immunofluorescence techniques. Using a previously described subcellular fractionation protocol [117], we purified ER and MAM fractions from the human colon cancer HCT- 116 $p53^{+/+}$ cell line. Similar to PML, p53 was localized to the ER and MAMs as well as the cytosolic fraction (Fig. 9A) under untreated conditions.

Therefore, we investigated whether adriamycin (ADRIA), a chemotherapeutic agent, or H_2O_2, an oxidative stress mediator, would change the subcellular localization of p53. An enrichment at the ER/MAMs was detected after p53 induction by either treatment (Fig. 9 B and C). We confirmed p53 accumulation at the ER/MAMs by immunofluorescence using digital imaging 3D deconvolution (Fig. 9 D–F). The colocalization of p53 and the ER was analyzed in $p53^{+/+}$ primary (MEFs) as an overlap between the p53 and ER-marker (Sec61b-GFP) signals. The suitability of a colocalization analysis was verified by sampling the cytoplasmic portion of each cell and performing the randomized Costes et al. method [215]. In all of the analyzed samples, the colocalization probability was higher than 99%. As expected, the overlap of p53 signal and ER-marker signal was increased in response to stress (Fig. 9G). MEFs have previously been shown to be resistant to apoptosis induced by thapsigargin (TG) in the absence of p53 [216]. In addition, p53 localizes to the ER/MAM compartments.

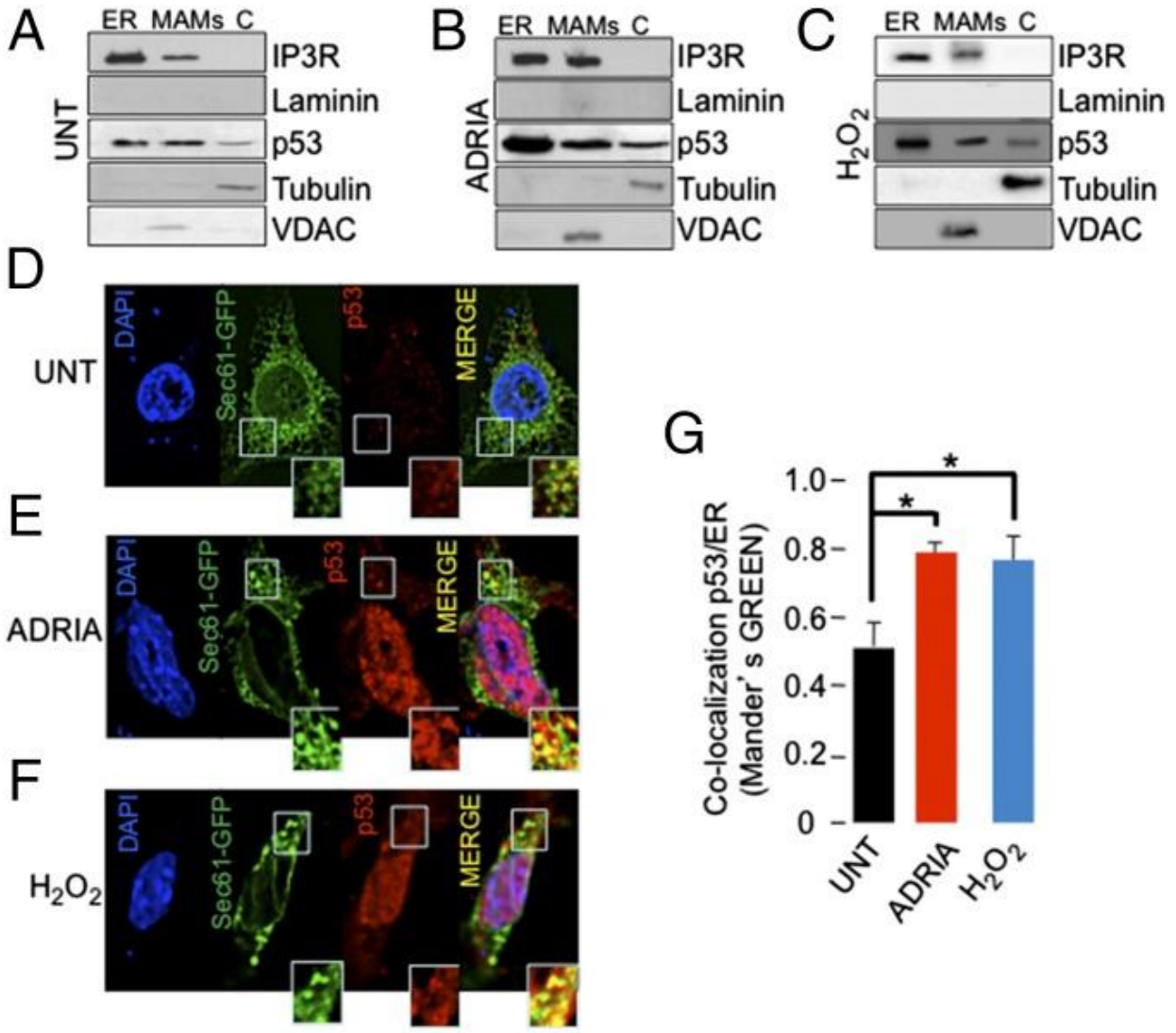

Figure 9. p53 localizes at the ER and MAMs. (A–C) *Detection of p53 by immunoblotting in HCT-116 $p53^{+/+}$ fractions. (A) p53 localization in untreated condition (UNT). Accumulation of p53 at the ER and MAMs in HCT-116 $p53^{+/+}$ cells after adriamycin (ADRIA) induction (1 μM, 6 h) (B) or afterH_2O_2 treatment (500μM, 6 h) (C). (D–F) Colocalization of p53 (red) and Sec61-GFP (used as ERmarker; green) in $p53^{+/+}$ MEFs under untreated conditions (UNT) (D) and after ADRIA (E) or H_2O_2 (F). (Insets) A higher magnification of the images is presented. (G) p53 activation increased its ER colocalization. Colocalization of p53 and ER in $p53^{+/+}$ MEFs quantified as the proportion of total ER marker overlapping the p53 signal (by Mander's coefficient colocalization method). To allow for a better appreciation of colocalization of p53 with the ER, a cytoplasmic portion was selected and the contrast was increased.*
*Bars, SEM; *P < 0.05.*

Therefore, we investigated whether p53 could be a fundamental component of the ER stress-induced apoptotic pathway. Using different ERstress inducers, we showed a marked reduction in the number of apoptotic cells in $p53^{-/-}$ MEFs compared with wild-type (WT) cells using flow cytometry analysis (Fig. 10 A and B), cytochrome c release (Fig. 10 C and D), and automated cell analysis based on morphological parameters and propidium iodide staining (Fig. 10 E). Apoptotic cell death, evoked by H_2O_2, was blocked in cells pretreated with a caspase inhibitor (Fig. 10 F) but enhanced after ADRIA-induced p53 accumulation at the ER/MAMs (Fig. 10 G–I)

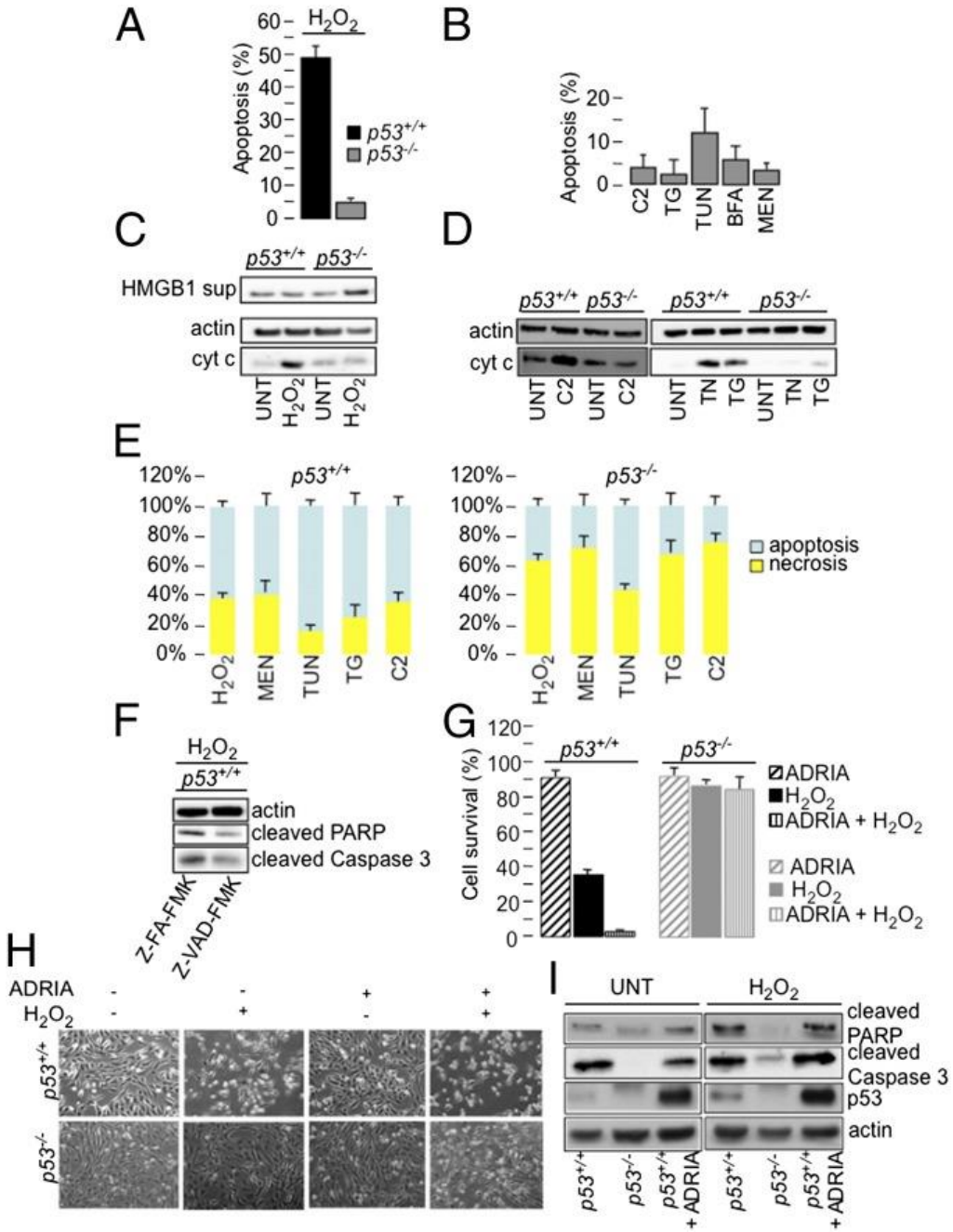

Figure. 10. Activation and accumulation of p53 at the ER/MAMs render cells more prone to death. *(A and B) Percentage of apoptosis induced by (A) H_2O_2 (500 μM, 12 h) in $p53^{+/+}$ or $p53^{-/-}$ MEFs or (B) ceramide (C2; 60 μM, 12 h), thapsigargin (TG; 2 μM, 12 h), tunicamycin (TUN; 6 μM, 12 h), brefeldin A (BFA; 5mg/mL, 12 h), or menadione (MEN; 15 μM, 12 h) in $p53^{-/-}$ MEFs. The data show the percentage of cell death in the whole cell population negative for annexin- V-FITC and propidium iodide (PI) staining, as analyzed by flow cytometry. (C) Detection of cytosolic cytochrome c release and supernatant HMGB1 release (a necrotic marker) by immunoblotting in $p53^{+/+}$ or $p53^{-/-}$ MEFs treated with H_2O_2 (500 μM, 12 h) compared with the untreated condition. Actin was used as a loading control for the cytosolic fraction. (D) Cytosolic cytochrome c release in $p53^{+/+}$ and $p53^{-/-}$ MEFs treated with C_2 (60 μM, 12 h), TUN (6 μM, 12 h), or TG (2 μM, 12 h). (E) Percentage of apoptosis versus necrosis analyzed by automated imaging and cell scoring based on morphological parameters and PI staining in $p53^{+/+}$ and $p53^{-/-}$ MEFs treated with H_2O_2 (500 μM, 12 h), MEN (15 μM, 12 h), TUN (6 μM, 12 h), TG (2 μM, 12 h), or C_2 (60 μM, 12 h). (F) Z-VADFMK treatment inhibits cell death in $p53^{+/+}$ MEFs (H_2O_2, 500 μM, 6 h). (G) Quantification of cell survival induced by H_2O_2 (500 μM, 12 h) through automated nucleus count analysis. Bars, SEM. (H) Representative microscopic fields of $p53^{+/+}$ and $p53^{-/-}$ MEFs under untreated conditions, pretreated with ADRIA (1 μM, 6 h) and then H_2O_2 (1 mM, 12 h). (I) Detection of apoptosis by immunoblotting in $p53^{+/+}$ and $p53^{-/-}$ MEFs and $p53^{+/+}$ pretreated with ADRIA (1 μM, 6 h) under untreated conditions and with H_2O_2 (500 μM, 6 h).*

p53 induction at the ER/MAMs regulates Ca^{2+} homeostasis, allowing for mitochondrial fragmentation and apoptosis.

The key process connecting apoptosis to the ER–mitochondrial interaction is an alteration in Ca^{2+} homeostatic mechanisms [217-219] that results in massive and/or prolonged mitochondrial Ca^{2+} overload [217,220,221]. We thus examined the effect of p53 down-regulation and induction on Ca^{2+} homeostasis. Using recombinant aequorin probes [222], $[Ca^{2+}]$ was measured selectively in the cytosol and in organelles acting as a source (ER) or target (mitochondria) of cellular Ca^{2+} signals. A striking difference was evident in $[Ca^{2+}]_{ER}$ steady-state levels (Fig. 11 A). After p53 induction by ADRIA the $[Ca^{2+}]_{ER}$ was higher, whereas the loss of p53 caused a reduction in the $[Ca^{2+}]_{ER}$ compared with WT. In agreement with the $[Ca^{2+}]_{ER}$ data, the $[Ca^{2+}]$ increases evoked by agonist stimulation (ATP) in the cytosol and in the mitochondria were significantly higher after ADRIA treatment and lower in $p53^{-/-}$ MEFs than in WT MEFs (Fig. 11 B and C). In contrast, ADRIA treatment in $p53^{-/-}$MEFs had no effect on Ca^{2+} homeostasis (Fig. 11 A–C, blue traces). The effect of p53 at the ER was also confirmed by analyzing mitochondrial Ca^{2+} uptake in permeabilized cells exposed to the same $[Ca^{2+}]$. These data indicate that the p53-dependent Ca^{2+} responses previously described were due to alterations of the source of the Ca^{2+} signals, the ER.

As mentioned above, there is a strong agreement in the literature linking Ca^{2+} transfer from the ER to the mitochondria and the effects of apoptotic stimuli [217-219,221] Using the ER-targeted, FRET-based Ca^{2+}-sensitive D1ER-YC4.3 probe, we measured the effect of p53 on the progressive release of Ca^{2+} from the ER caused by H_2O_2. The normalized FRET ratio (proportional to $[Ca^{2+}]$ER) was observed to correlate with p53 levels (Fig. 11 D). Administration of H_2O_2 caused a progressive depletion of Ca^{2+} from the ER (as revealed by a reduction in the normalized FRET ratio) with consequent increases in $[Ca^{2+}]$ in the cytosol (Fig. 11 E) and mitochondria (Fig. 11 F).

Furthermore, this event appeared to be proportional to p53 levels. To assess whether the observed ER Ca^{2+} overload is a proapoptotic condition, we analyzed the mitochondrial morphology after apoptotic stress induction. The mitochondria of WT p53 and $p53^{-/-}$ MEFs were labeled with targeted GFP, and the mitochondrial structure was evaluated by confocal microscopy.

Treatment with H_2O_2 for 3 h caused a strong reduction in the average mitochondrial volume in WT cells, as expected, upon network breakage (Fig. 11 G, i and ii, and H, i and ii). The induction of p53 by ADRIA alone did not significantly affect mitochondrial morphology (Fig. 11 G, iii, and H, iii), whereas ADRIA treatment followed by H_2O_2 exposure induced a stronger increase in the fragmentation index value (Fig. 11 G, iv, and H, iv) compared with H_2O_2 alone. $p53^{-/-}$ cells treated with H_2O_2 did not show significant changes in the mitochondrial network (Fig. 11 I and J).

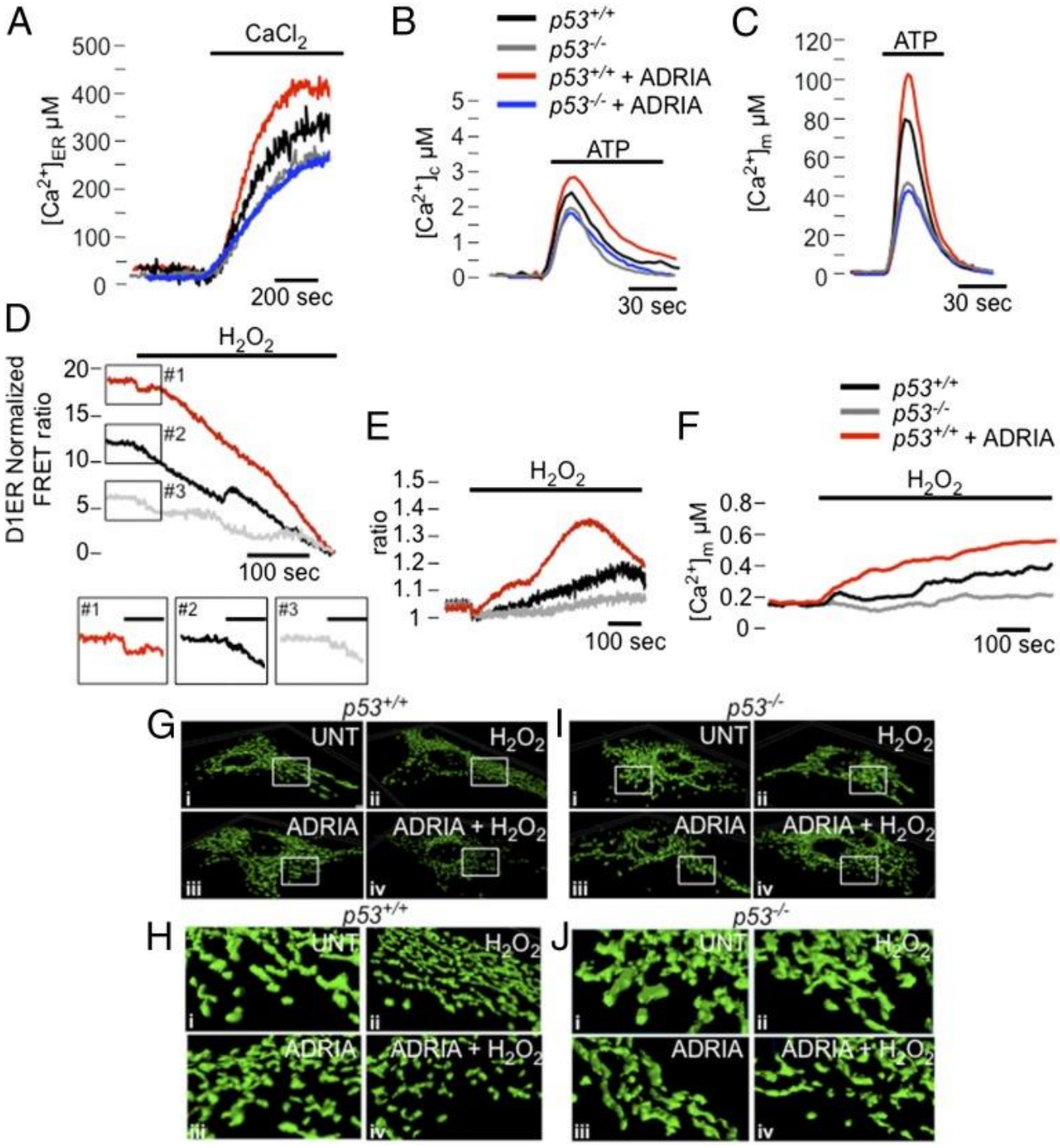

Figure 11. Deregulation of Ca^{2+} homeostasis after p53 induction is a stress signal for mitochondrial structure and a trigger for apoptosis. *(*A–C*) Measurements of $[Ca^{2+}]$ using recombinant aequorin upon agonist stimulation (100 µM ATP) in the ER (*A*), cytosol (*B*), and mitochondria (*C*). (*D*) ER Ca^{2+} release induced by H_2O_2 measured using a FRET-based Ca^{2+}-sensitive D1ER-YC4.3 probe; the normalized FRET ratio of D1ER-YC4.3 was assumed as the intraluminal $[Ca^{2+}]$. (*Insets*) A magnified portion of the first 2 min of the recording as basal. (*E*) Cytosolic Ca^{2+} response induced by H_2O_2 (2 mM) in MEFs loaded with the Ca^{2+}-sensitive fluorescent dye Fura-2. The kinetic behavior of the $[Ca^{2+}]_c$ (Ca^{2+} concentration within cytoplasm) response is presented as the ratio of fluorescence at 340 nm/380 nm. (*F*) Analysis of $[Ca^{2+}]_m$ (Ca^{2+} concentration within mitochondrial matrix) during oxidative stress upon H_2O_2 stimulation (2 mM). Isosurface rendering of representative* $p53^{+/+}$ *(*G *and* H*) and* $p53^{-/-}$ *(*I *and* J*) MEFs expressing mitochondrial GFP in basal conditions (UNT), after adriamycin (1 µM, 6 h), and/or H_2O_2 exposure (500 µM, 3 h). (*H *and* J*) High-resolution imaging of mitochondrial fragmentation during p53 activation and oxidative stress induction in* $p53^{+/+}$ *and* $p53^{-/-}$ *MEFs.*

Naturally Occurring p53 Mutants Lose Their Ability to Modulate Ca^{2+} Responses.

To exclude the possibility that a transcription-dependent pathway of p53 accounts for its effect on Ca^{2+} homeostasis (and, in turn, on the sensitivity of ER-stress apoptotic stimuli), we used different strategies: specific drugs blocking the transcriptional arm of p53 (Fig. 12 A) and p53-targeted chimeras, p53-ΔNLS (a nuclear import-deficient p53 mutant; Fig. 12 B and C) and ER-p53 (a chimera containing the human p53-ΔNLS protein targeted to the outer surface of the ER; Fig. 12 B and C) [223].As pharmacological treatments, we used α-amanitin, a highly specific and potent inhibitor of RNA polymerase II transcription, or a combination of pifithrin α, which selectively blocks p53-mediated transcription, and ADRIA to activate the remaining p53 pathways [224]. As expected, we observed increased mitochondrial Ca^{2+} responses under both conditions (Fig. 12 A), reflecting increased ER Ca^{2+} release and indicating a nontranscriptional role for p53 in Ca^{2+} modulation. Moreover, the expression of p53-ΔNLS or ER-p53 chimeras in $p53^{-/-}$ MEF (Fig. 12 D),enhanced mitochondrial Ca^{2+} signaling, similar to the effect of p53 induction by ADRIA (Fig. 12 C). This effect was further associated with a reestablished sensitivity to apoptosis induced by ER stress (Fig. 12 E), as determined by cell count analysis (Fig. 12 F) and PARP and caspase 3 cleavage (Fig. 12 G).

In contrast, MDA-MB 468 cells, harboring the p53 273H mutant, were not sensitive to p53-ADRIA induction (Fig. 13 A). Accordingly, naturally occurring p53 mutants expressed in HCT-116 $p53^{-/-}$ cells lost their ability to increase the Ca^{2+} response (Fig. 13 B).

Moreover, those mutants were unable to modulate Ca^{2+} homeostasis also failed to rescue the sensitivity to apoptosis after oxidative stress treatment (Fig. 13 C–E). These data show that Ca^{2+}-mediated apoptosis is a transcription-independent pathway regulated by p53 at ER/MAMs.

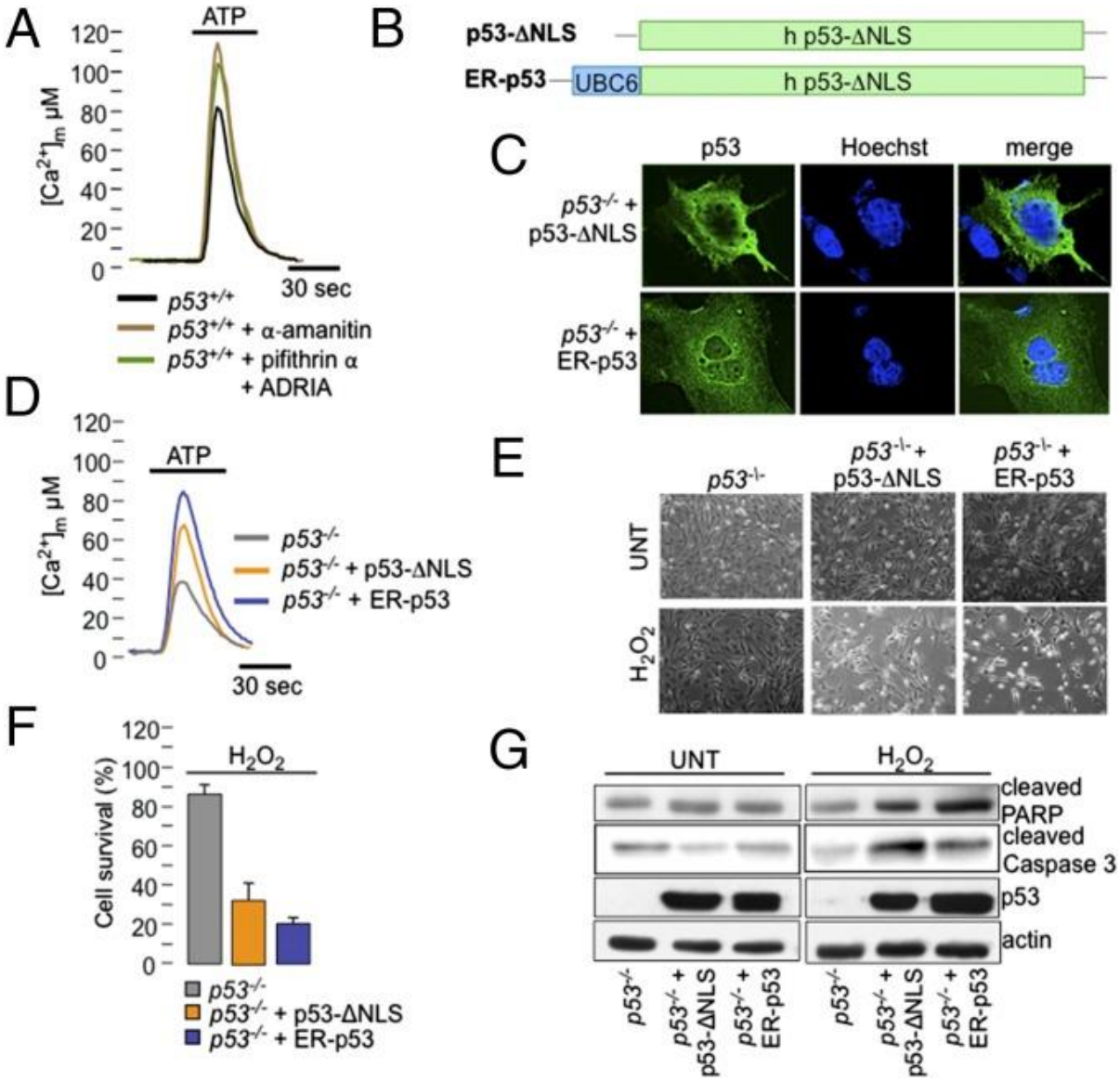

Figure 12. p53 controls mitochondrial Ca^{2+} homeostasis and, in turn, apoptotic sensitivity from ER/MAM compartments. *(*A*) Agonist-dependent $[Ca^{2+}]_m$ response in* $p53^{+/+}$ *MEFs after pharmacological block of the transcriptional arm of p53. (*B*) Schematic representation of p53-ΔNLS and ER-p53 chimeras. (*C*) Immunofluorescence images of* $p53^{-/-}$ *MEF cells expressing the p53-ΔNLS or ER-p53 constructs stained with anti-p53 antibody (green) and Hoechst (nuclear marker). (*D*) Mitochondrial Ca^{2+} response in* $p53^{-/-}$ *MEFs after the reintroduction of an ER-targeted chimera, ER-p53 or p53-ΔNLS. (*E*) Representative microscopic fields, from three independent experiments, of* $p53^{-/-}$ *MEFs expressing p53-ΔNLS and ER-p53 before and after H_2O_2 treatment (1 mM, 12 h). (*F*) Evaluation of cell-death induction by H_2O_2 (500 µM, 12 h) through automated nucleus count analysis in* $p53^{-/-}$ *MEFs,* $p53^{-/-}$ *MEFs expressing ER-p53, and* $p53^{-/-}$ *MEFs expressing p53-ΔNLS. Bars, SEM. (*G*) Analysis of apoptotic markers by immunoblot in* $p53^{-/-}$ *MEFs and* $p53^{-/-}$ *MEFs expressing p53-ΔNLS and ER-p53 under untreated conditions and after H_2O_2 treatment (500 µM, 6 h).*

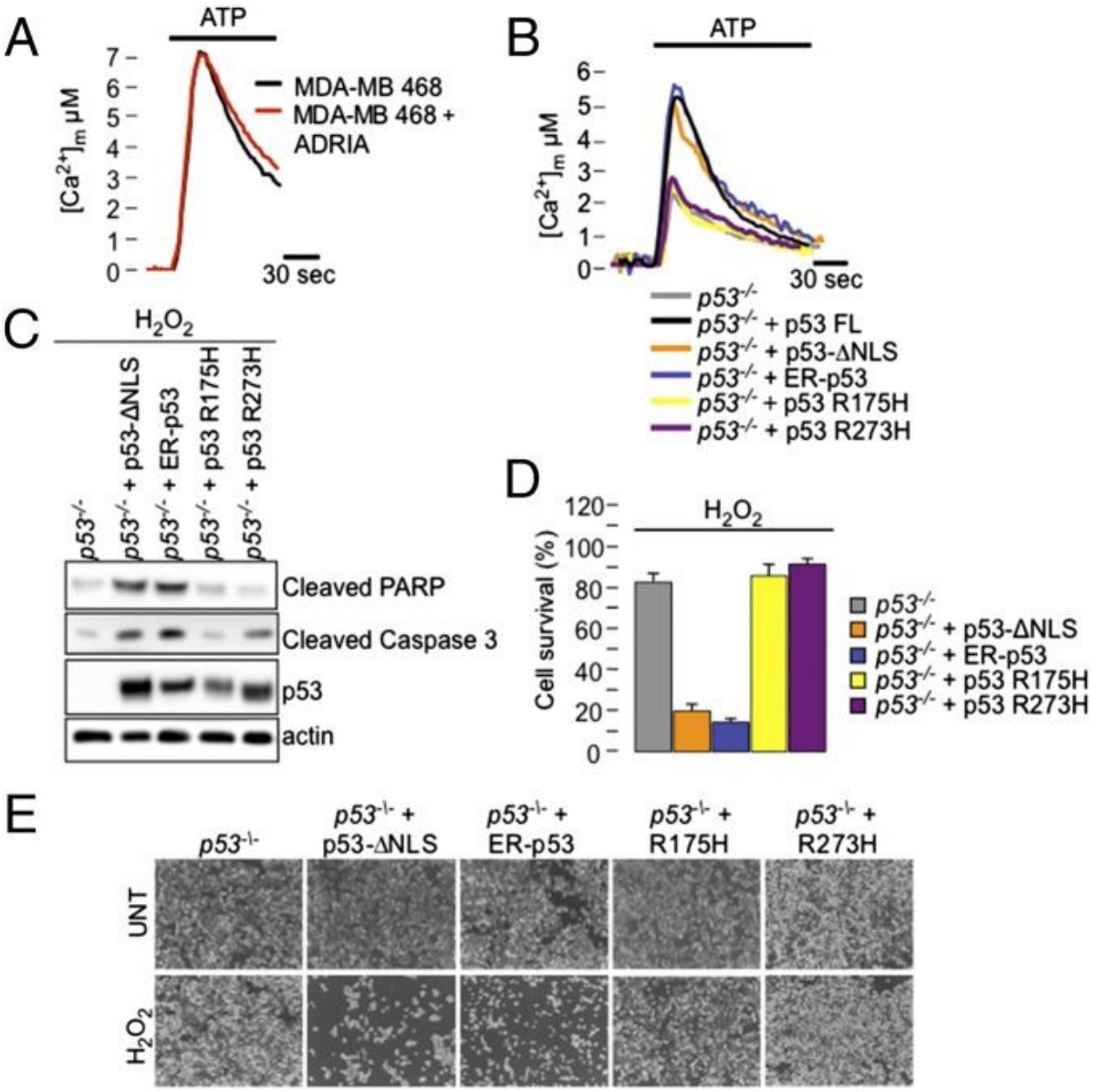

Figure 13. p53 mutants cannot modulate the mitochondrial Ca^{2+} response and thus apoptosis. *(*A*) Mitochondrial [Ca^{2+}] after ATP stimulation measured in MDA-MB 468 cells, harboring p53 273H mutation, under control conditions and after adriamycin treatment (1 µM, 6 h). (*B*) Mitochondrial Ca^{2+} response after agonist stimulation in HCT-116* p53$^{-/-}$ *cells and HCT-116* p53$^{-/-}$ *cells after reintroduction of the p53-ΔNLS and ER-p53 chimeras or naturally occurring p53 mutants R175H and R273H. (*C *and* D*) Evaluation of apoptosis induction in HCT-116* p53$^{-/-}$ *cells expressing p53-ΔNLS and ER-p53 chimeras or naturally occurring p53 mutants R175H and R273H after treatment with H_2O_2 using (*C*) immunoblot detection of cleaved PARP and cleaved caspase 3 (500 µM, 6 h) and (*D*) automated cell count analysis (500 µM, 12 h). Bars, SEM. (*E*) Representative images of HCT-116* p53$^{-/-}$ *cells expressing different p53 constructs under untreated conditions and after H_2O_2 treatment (1 mM, 12 h).*

p53 modulates Ca^{2+} homeostasis and apoptosis by interacting with the Sarco/ER Ca^{2+}-ATPase pump at the ER, changing its redox state.

To dissect the mechanism by which WT p53 exerts its impact on Ca^{2+} homeostasis upon activation and accumulation at ER/MAM compartments, we examined whether p53 modulates the activity of sarco/ER Ca^{2+}-ATPase (SERCA) pumps, which mediate ER Ca^{2+} re-accumulation. Thus, we tested whether p53 functionally and physically interacts with SERCA. The in vitro interaction between p53 and endogenous SERCA was first detected using an MBP pull-down assay (Fig. 14 A) in H1299 cells lacking p53. Next, we mapped the region of p53 involved in the interaction with SERCA. To this end, we used HA-tagged p53 deletion constructs: HAp53 1–175, HAp53 175–393, HAp53 294–393, and the full-length HA-p53. In coimmunoprecipitation experiments performed in H1299 cells transfected with the HA-p53 constructs, SERCA selectively bound to the C-terminal regulatory domain of p53, a region where posttranslational modifications can modify the interaction of p53 with partner proteins (Fig. 14 B). However, the interacting fragment alone was not sufficient to modulate Ca^{2+} homeostasis and apoptosis (data no shown), suggesting that the entire p53 protein (or the majority of it) is required for its biological activity. Interestingly, the naturally occurring p53 mutants R175H and R273H were unable to be coimmunoprecipitated with the SERCA protein. In contrast, the p53-ΔNLS protein retained this ability (Fig. 14 C). Finally, to establish whether p53 has a direct effect on SERCA activity, we analyzed the kinetics of ER Ca^{2+} accumulation both in vivo and in vitro. The Ca^{2+} accumulation rate was higher in the ER vesicles isolated from the liver of $p53^{+/+}$ mice treated intraperitoneally with ADRIA compared with those obtained from $p53^{+/+}$ and $p53^{-/-}$ mice (Fig. 14 D). Similarly, the rate of ER Ca^{2+} accumulation, measured in MEFs, increased proportionally in a time-dependent manner with the induction of p53 by ADRIA, indicating a stimulatory role of p53 in SERCA activity (Fig. 14 E).

Next, we investigated the possible mechanism by which p53 stimulates SERCA activity upon binding. To this end, we analyzed whether p53 activation affects the oxidative state of the SERCA protein, which is known to modulate its activity [225]. We thus compared the level of hyperoxidized sulfenylated proteins in HCT-116 $p53^{+/+}$ and MDA-MB 468 cells after the induction of WT p53 and mutant p53, respectively. Cells and lysates were exposed to dimedone, a chemical that selectively modifies sulfenylated cysteines, and the dimedone-modified proteins were detected by immunoblotting with an antibody to dimedone [226]. To understand whether the levels of sulfenylated SERCA were different in HCT-116 $p53^{+/+}$ and MDA-MB 468 cells, both cell types were exposed to dimedone to quench the sulfenylated cysteines, and the proteins were immunopurified using a monoclonal SERCA antibody. Immunoblotting of the SERCA immunocomplex with an antibody to dimedone revealed the presence of sulfenylated SERCA, which was lower in HCT-116 $p53^{+/+}$ cells

treated with doxorubicin (Fig. 14 F). In contrast, in MDA-MB 468 cells, SERCA oxidation was unchanged after ADRIA treatment. These results were then confirmed by measuring SERCA activity. Fig. 14 G shows that ADRIA required WT p53 to be effective. Indeed, in MDA-MB 468 cells, SERCA activity was not sensitive to ADRIA induction of p53.

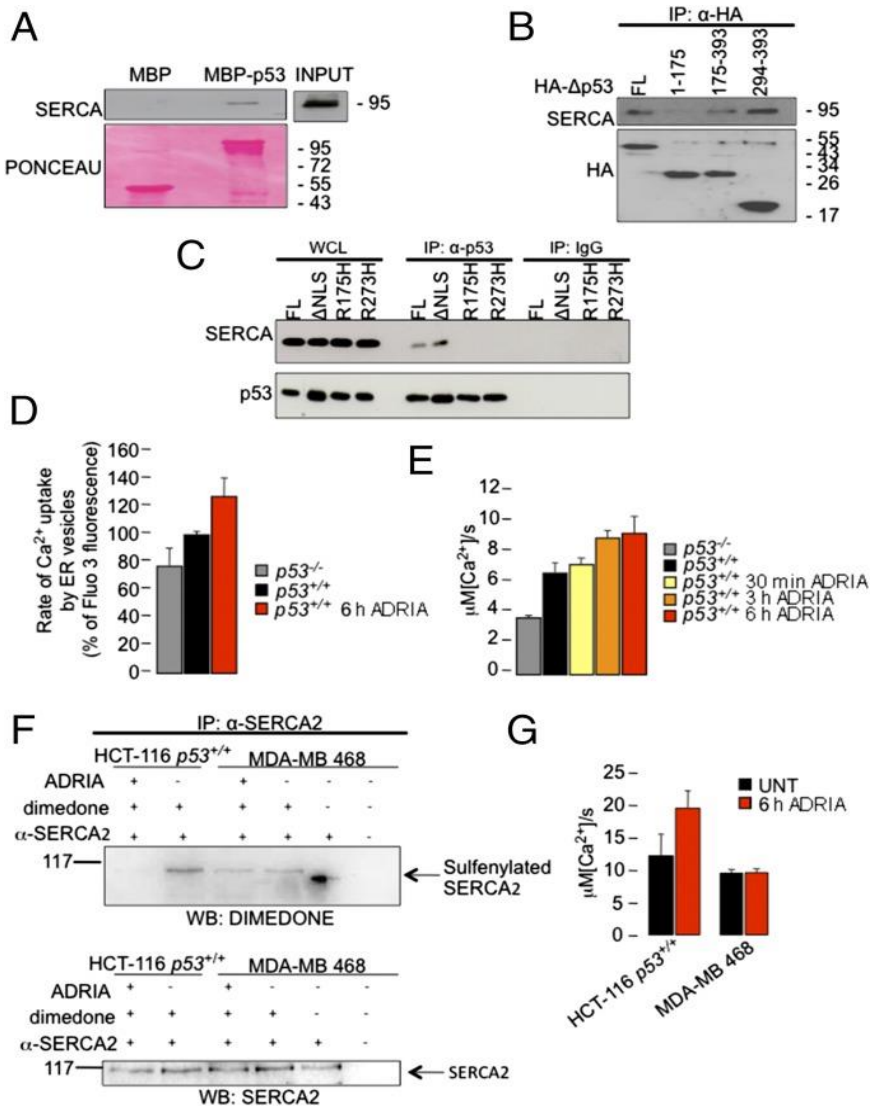

Figure 14. p53 interacts with SERCA and stimulates Ca^{2+} accumulation in the ER, changing the SERCA oxidative state. *(A) In vitro binding of endogenous SERCA to MBP-p53. H1299 cell lysates were incubated with bacterially expressed MBP-p53 protein or MBP as a control. Ponceau staining shows the amount of MBP proteins used in the experiments. (B) Full-length (FL) and HA-tagged p53 deletion mutants transiently expressed in H1299 cells were immunoprecipitated by anti-HA antibody and analyzed by Western blot (WB). IP, immunoprecipitation. (C) H1299 cells were transiently transfected with different p53 constructs (FL, full-length p53 WT; ΔNLS, p53-ΔNLS; R175H, p53 R175H; R273H, p53 R273H) and then harvested for immunoprecipitation and immunoblotting as indicated. WCL, whole cell lysate. (D and E) Rate analysis of Ca^{2+} uptake measured in the ER vesicles isolated from the (D) liver of $p53^{-/-}$ and $p53^{+/+}$ mice and $p53^{+/+}$ mice treated with adriamycin (1 µM, 6 h) or (E) ER compartments of $p53^{-/-}$ and $p53^{+/+}$ MEFs at different times after ADRIA (1 µM, 30 min, 3 h, 6 h) treatments. (F) Immunoblot with an antibody reactive to dimedone-conjugated cysteine residues of the protein sample extracts from HCT-116 $p53^{+/+}$ and MDA-MB 468 cells after ADRIA induction that were immunopurified using a monoclonal SERCA2 antibody. Cells with an active p53 reveal lower cysteinyl sulfenic acid-modified SERCA. (G) Analysis of ER Ca^{2+} uptake in HCT-116 $p53^{+/+}$ and MDA-MB 468 cells after ADRIA induction. Bars, SEM.*

Discussion

In recent years, it has become evident that the ER, mitochondria, and region of close contact between these two organelles (MAMs) play a central role in different human diseases, including cancer [92,227]. One important process occurring in these intracellular domains is apoptosis. A key signal transduction pathway connecting apoptosis to ER–mitochondrial interactions is an alteration in Ca^{2+} homeostatic mechanisms [38]. The switch from a life to a death signal has been argued to occur when Ca^{2+} signaling between the ER and mitochondria is distorted, leading to a breakdown of mitochondrial function [126]. Interestingly, in recent years, many tumor suppressor proteins, such as PML [210]and PTEN [228], have been demonstrated to be localized to the ER and at MAMs, where they modulate cell death. In the present study, we investigated whether p53 also shares this intracellular localization and whether, as for PML, PTEN, Bax, and Bak, p53 regulates apoptosis in a Ca^{2+}-dependent manner. p53 is a well-known tumor suppressor that coordinates different cell-death programs, mainly associated with its function as a transcription factor. Several studies have, however, described a transcription-independent function for p53, although the importance of the cytoplasmic pool of p53 for p53-mediated apoptotic cell death remains highly controversial. We showed that a fraction of p53 is associated with the ER and MAMs. We demonstrated that this nonnuclear fraction of p53 is able to modulate Ca^{2+} homeostasis in response to both physiological and pathological stimulation. The activation and accumulation of p53 at ER/MAM compartments induced by anticancer drugs or stress allow apoptotic stimuli to rapidly and efficiently overload mitochondria with Ca^{2+}, a priming step for the release of caspase cofactors and induction of apoptosis via the intrinsic pathway. As a consequence, cells are more prone to die through mitochondrial permeability transition pore opening [229], mitochondrial fragmentation, and cytochrome c release. p53 present in the ER/MAM fraction physically interacts with SERCA, thus potentiating in vitro and in vivo Ca^{2+} accumulation in the ER lumen under stress conditions. In cancer cells, this proapoptotic mechanism is impaired due to the functional inactivation of p53, contributing to disease progression. In agreement with these results, SERCA overexpression, and thus its increased activity, and the subsequent ER Ca^{2+} overload have been previously demonstrated to increase spontaneous apoptosis [230]. Our data suggest that the activation of WT p53 reduces the oxidation of SERCA (Fig. 14), thus modulating SERCA activity. Indeed, prooxidative modification of SERCA decreased its activity [225], and a critical cysteine in the SERCA sequence [231]that regulates this posttranslational modification is accessible from the cytosolic compartment [232], where p53 is localized. Altogether, these results reveal a previously unidentified Ca^{2+}-dependent mechanism through which p53 exerts its potent proapoptotic role in response to anticancer treatments.

Intravital imaging reveals p53-dependent cancer cell death induced by phototherapy via calcium signaling

Introduction

The development of malignant tumors results from the deregulated proliferation of cells or from the inability of cells to undergo apoptotic death [233]. Consequently, apoptosis induction in tumor cells is one of the aims of anti-cancer therapy. Studies during the past decade have highlighted the importance of calcium (Ca^{2+}) signaling in the regulation of key aspects of cell death. In particular, the modulation of Ca^{2+} signaling can change cell sensitivity to apoptotic signals, such as chemotherapeutic agents [219]. Several studies have indicated that the Ca^{2+} content of the ER determines cell sensitivity to apoptotic stress and that perturbation of ER Ca^{2+} homeostasis appears to be a key component in the development of several pathologies. Therefore, changes in the Ca^{2+} flux are regulated by Ca^{2+} release from the ER store toward the cytosol, and mitochondria can promote the survival of cancer cells, reducing sensitivity to apoptotic signals [217]. Although the majority of the mechanisms related to intracellular Ca^{2+} transport have been successfully elucidated either in vitro or in cultured cells, we still know little regarding the actual physiological role of these processes in the context of the tumor environment primarily due to technical limitations. However, recent advancements in imaging have allowed researchers to visualize transient changes in Ca^{2+} levels in live mice [234].

We recently demonstrated that tumor suppressors could modulate cell sensitivity to apoptosis by regulating Ca^{2+} transfer from the ER to mitochondria [99,210,228]; however, this intriguing signaling pathway has never been investigated in the tumor environment.

This study is the first to demonstrate the direct measurements of intracellular Ca^{2+} dynamics in vivo within tumor masses. Importantly, the methodology used in the present study is readily applicable to all the currently available fluorescent probes for following any intracellular parameter of interest. Finally, in the present study, we demonstrate Ca^{2+}-dependent p53-mediated apoptosis induced by phototherapy in cancer cells. This approach will generate new opportunities for elucidating chemoresistance signaling in tumors and for developing new anti-cancer therapy.

Results

We adopted the well-known tumor suppressor p53 to generate a tumor model related to the loss of an onco-suppressor [235,236]. The mechanism of action of p53 is dependent on its transcription factor activity. Recently, a cytoplasmic fraction of p53 was suggested to directly modulate apoptosis via its cytoplasmic localization [209], which is a common requirement for tumor suppressors that can regulate ER-to-mitochondria Ca^{2+} transfer.

We generated the following two stable clones to verify the relevance of the modulation of Ca^{2+} homeostasis by p53 in the tumor environment: the mouse embryo fibroblast (MEF) $p53^{-/-}$ clone that was transduced with H-RASV12 ($p53^{-/-}$ clone) and the MEF $p53^{-/-}$ clone that was transduced with H-RASV12 with re-introduced wild type (wt) p53 ($p53^{+/+}$ clone) (Fig.15 A). We tested the anchorage-independent growth, Ca^{2+} response and apoptotic sensitivity of these clones in vitro. As expected, the $p53^{-/-}$ clone formed approximately twice as many colonies in soft agar (Fig.15 B). Moreover, the $p53^{-/-}$ clone displayed lower mitochondrial Ca^{2+} uptake after agonist stimulation, as analyzed by aequorin technology, compared to that of the $p53^{+/+}$ clone (Fig. 15 C and D). This result indicates that p53 modulates intracellular Ca^{2+} homeostasis, presumably by blocking the Ca^{2+} responses generated from the ER, which is a condition that is known to be sufficient to reduce apoptotic sensitivity. Thus, we tested the sensitivity of these two clones to a Ca^{2+}-dependent apoptotic stimulus, H_2O_2. As consequence of less Ca^{2+} mobilization, the $p53^{-/-}$ clone exhibited protection from apoptosis when compared to the MEFs clone expressing wt p53 (Fig.15 E). These results suggested that the efficacy of the apoptotic Ca^{2+} signals is p53-dependent.

The next step was to identify a stimulus that could induce an apoptotic Ca^{2+} signal within tumor masses using a drug currently applied in clinical cancer therapy. We selected the anti-cancer photosensitizer aluminum phthalocyanine chloride (phthalocyanine) for this purpose. Phthalocyanine is a light-activatable agent used in cancer photodynamic therapy (PDT) [237]. PDT combines a drug called a photosensitizer or photosensitizing agent with a specific type of light to kill cancer cells preferentially because these cells are more prone to accumulate this drug. Indeed, when the photosensitizer drug in tumors absorbs the light, an active form of oxygen is produced that destroys nearby cancer cells [238]. Several photosensitizers have been shown to localize to intracellular organelles, including the ER, where these photosensitizers promote reactive oxygen species (ROS)-mediated cell death upon illumination with suitable wavelengths of visible (red) light [239]. Because different pro-oxidant agents (i.e., H_2O_2 and menadione) can produce Ca^{2+}-dependent cell death, we hypothesized that phthalocyanine should also produce a Ca^{2+} signal that results in a toxic effect. Thus, we analyzed the sensitivity of these clones to phthalocyanine in vitro.

Phthalocyanine photo-activation with a LED light resulted in a rapid increase in the $[Ca^{2+}]c$ that slowly returned to basal levels, as measured using the ratiometric Ca^{2+} indicator Fura-2. Interestingly, the $p53^{-/-}$ clone had an impaired Ca^{2+} response (Fig. 15 F and G), and were more resistant in terms of cell death upon phthalocyanine treatment compared to the $p53^{+/+}$ clone, as indicated by the number of pyknotic nuclei appearing after LED irradiation (Fig.15 H).

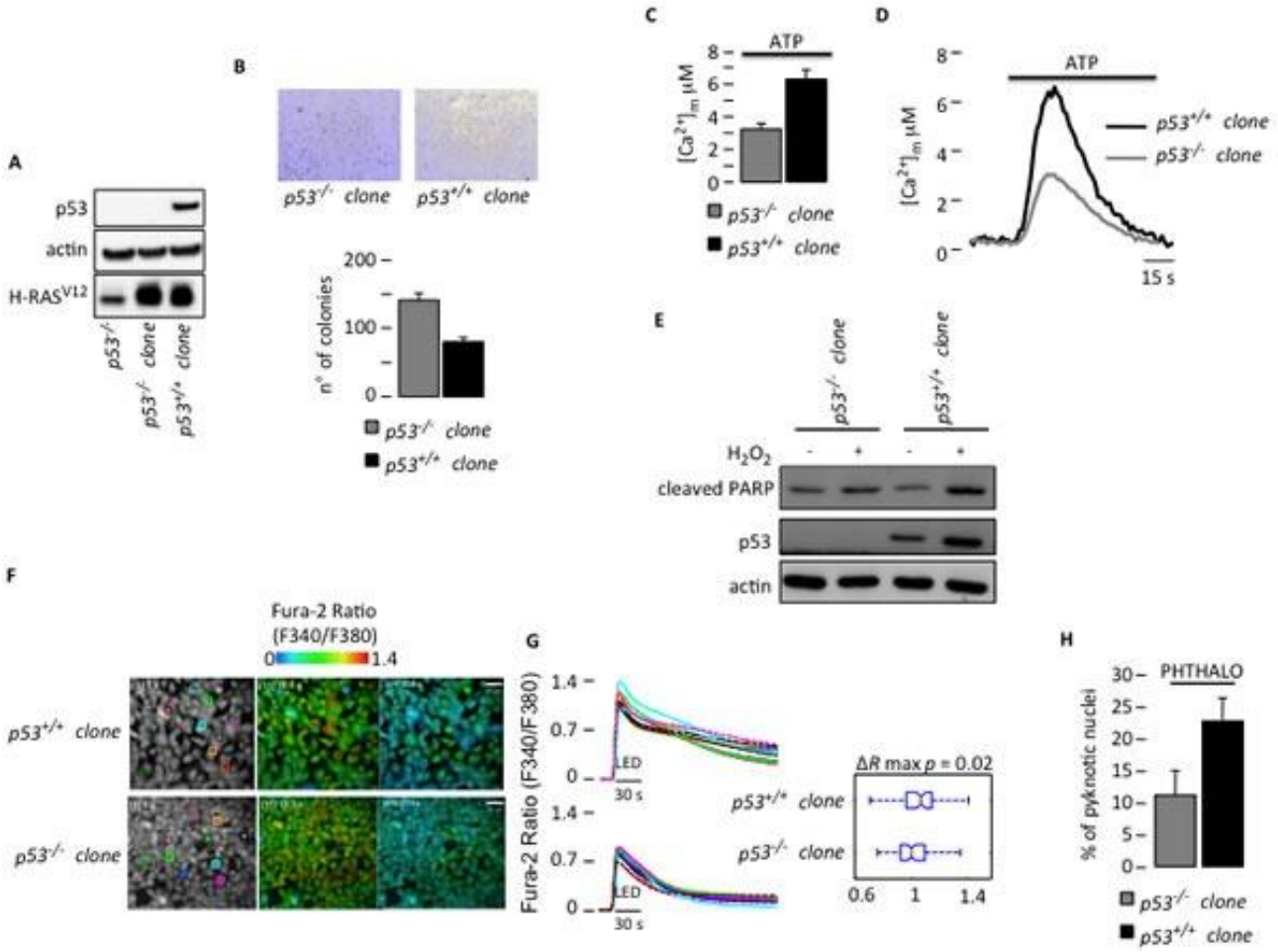

Figure 15. Defective Ca^{2+} homeostasis and apoptosis due to a lack of p53 *(A) Generation of H-RAS^{v12}-transduced MEF clones. (B) Anchorage-independent growth of H-RAS^{v12}-transduced MEFs ($p53^{+/+}$ clone and $p53^{-/-}$ clone). Pictures in the upper part are representative of colonies formed. For each well all colonies larger than 0.1 mm in diameter were counted using ImageJ software. (C) Mitochondrial Ca^{2+} response obtained with a mitochondria-targeted aequorin chimera after agonist stimulation with ATP (100 µM) ($p53^{+/+}$ clone: $[Ca^{2+}]_m$ peak 6.23 ± 0.44; $p53^{-/-}$ clone: $[Ca^{2+}]_m$ peak 2.99 ± 0.21) ($p < 0.01$). (D) Representative traces of mitochondrial Ca^{2+} transient. (E) Apoptotic sensitivity of H-RAS^{v12}-transduced MEF clones (500 µM H_2O_2 for 6 hours). (F) Cytosolic Ca^{2+} response of H-RAS^{v12}-transduced MEF clones loaded with Fura-2 dye upon phthalocyanine (15 µM) photo-activation with visible (red) light from a 650 nm light emitting diode (LED). Microscopic fields of analyzed cells. (G) The ratio of Fura-2 fluorescence 340 nm/380 nm averaged with the color-matched regions of interest (ROIs) shown in (F), accompanied by statistical analysis. (H) Cell death analysis using the percentage of pyknotic nuclei in H-RAS^{v12}-transduced MEF clones upon phthalocyanine (15 µM) photo-activation.*

Next, we tested the involvement of p53 in the generation of pro-apoptotic Ca^{2+} signals evoked by cancer PDT in vivo. We developed a new intravital fluorescent microscopy technique to investigate Ca^{2+} signaling in single cells in tumor masses in live mice during PDT. The MEFs of the two clones were injected either subcutaneously or into a skinfold chamber [240] placed on the dorsal skin of athymic mice [241] (Fig.16 A). Subcutaneous tumors were excised after 2 weeks, and as expected, the $p53^{-/-}$ clone developed tumors that were double in size compared with the tumors that developed from $p53^{+/+}$ clone (Fig.16 B). Tumors in the dorsal skinfold chamber were loaded with phthalocyanine and the ratiometric Ca^{2+} indicator Fura-2. Ca^{2+} signaling was monitored in live mice using a spinning disk confocal microscope (Fig.16 C). Live ratiometric Ca^{2+} images within the tumor mass and representative traces of the cytosolic Ca^{2+} response after phthalocyanine photo-activation are shown in Fig. 16 C and D. Higher Ca^{2+} responses were evoked in the tumor mass that developed from the $p53^{+/+}$ clone compared to those from the tumor mass that developed from the $p53^{-/-}$ clone (Fig. 16 C and D).

These results strongly suggest that the absence of a functional p53 precludes the generation of an efficient Ca^{2+} response during chemotherapeutic PDT that subsequently prevents the induction of apoptosis to limit tumor growth.

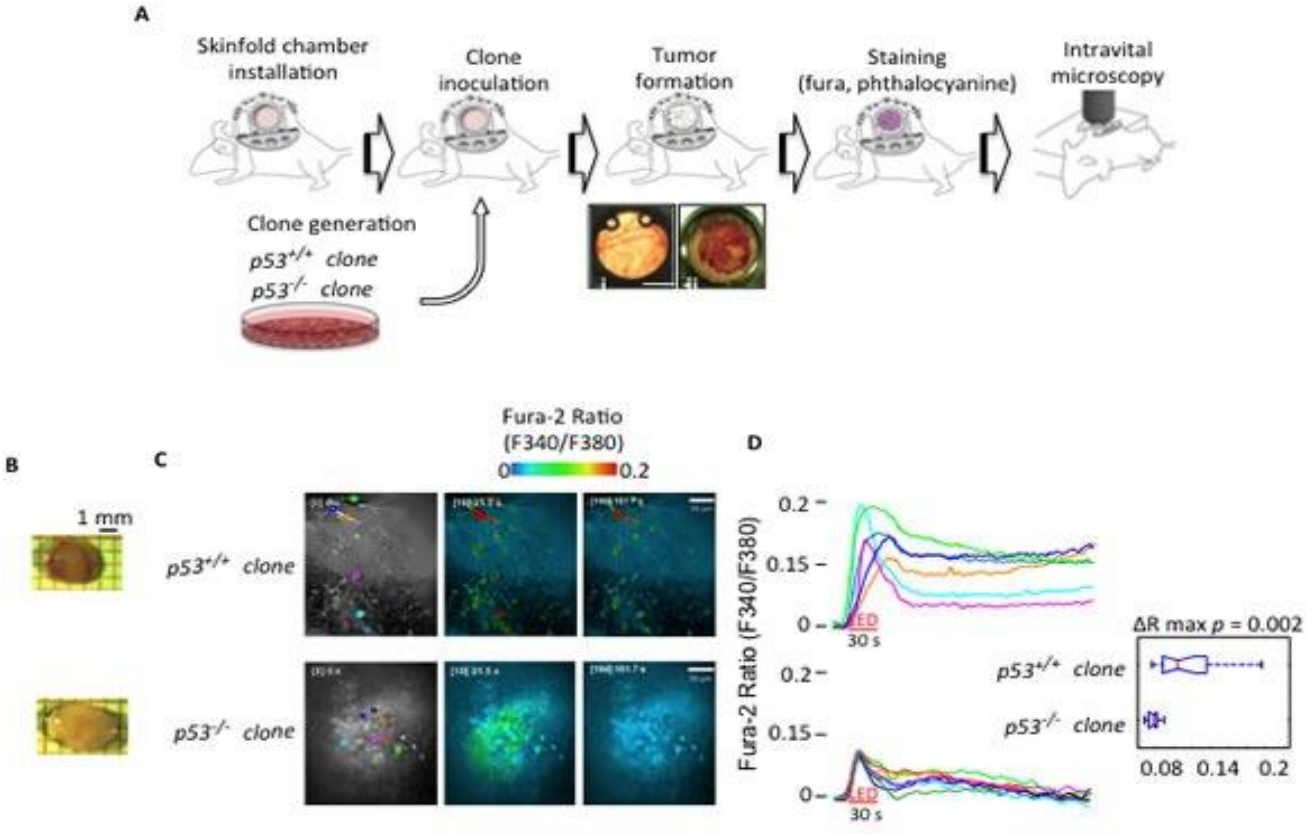

Figure 16. Intravital Ca^{2+} imaging in tumor masses *(A) Schematic representation of the skinfold chamber technique used to allow tumor formation and subsequent analysis by ratiometric confocal spinning disk intravital microscopy. (B) Representative images of tumor masses originated by the indicated H-RAS^{v12}-transduced MEF clones ($p53^{+/+}$ and $p53^{-/-}$ clones) injected in athymic mice. (C) Cytosolic Ca^{2+} response measured within the tumors obtained by H-RAS^{v12}-transduced MEF clones injected into skinfold chambers mounted on athymic mice. Microscopic fields of analyzed cells. (D) The ratio of Fura-2 fluorescence 340 nm/380 nm accompanied by statistical analysis.*

To demonstrate this hypothesis, we modulated the Ca^{2+} response in vitro and in vivo to confirm the relation between p53-dependent differences in Ca^{2+} handling and apoptotic behavior. Because we determined that the $p53^{-/-}$ MEF clones have a reduced response to PDT due to reduced Ca^{2+} signaling, we used two different genetic strategies to restore the Ca^{2+} response and apoptosis: i) overexpression of the mitochondrial Ca^{2+} uniporter (MCU) [78] and ii) overexpression of sarco-ER Ca^{2+}-ATPase pumps (SERCA)[241]. The overexpression of the MCU construct in the $p53^{-/-}$ clone increased the ability of mitochondria to accumulate Ca^{2+}. Indeed, the $[Ca^{2+}]$m rise evoked by agonist stimulation and measured using aequorin technology was increased in the $p53^{-/-}$ clone overexpressing MCU compared to the $p53^{-/-}$ clone (Fig. 17 A and B). These increased values were comparable to those observed in the $p53^{+/+}$ clone (Fig.15 C), which is consistent with previous publications [84,85]. We then analyzed the effect of MCU overexpression after PDT. Interestingly, PDT induced a Ca^{2+} response also in the mitochondrial matrix. In fact, cells transfected with the Ca^{2+}-sensitive FRET-based probe 2mtD3cpv [35] and treated with phthalocyanine displayed a progressive increase in the FRET ratio (proportional to the $[Ca^{2+}]$m) after photo-activation-induced Ca^{2+} waves. Furthermore, the stimulated Ca^{2+} uptake by mitochondria was significantly increased after MCU introduction (Fig. 17 C and D). This increased mitochondrial Ca^{2+} responsiveness was associated with a re-established apoptotic sensitivity induced by PDT in vitro (Fig.17 E).

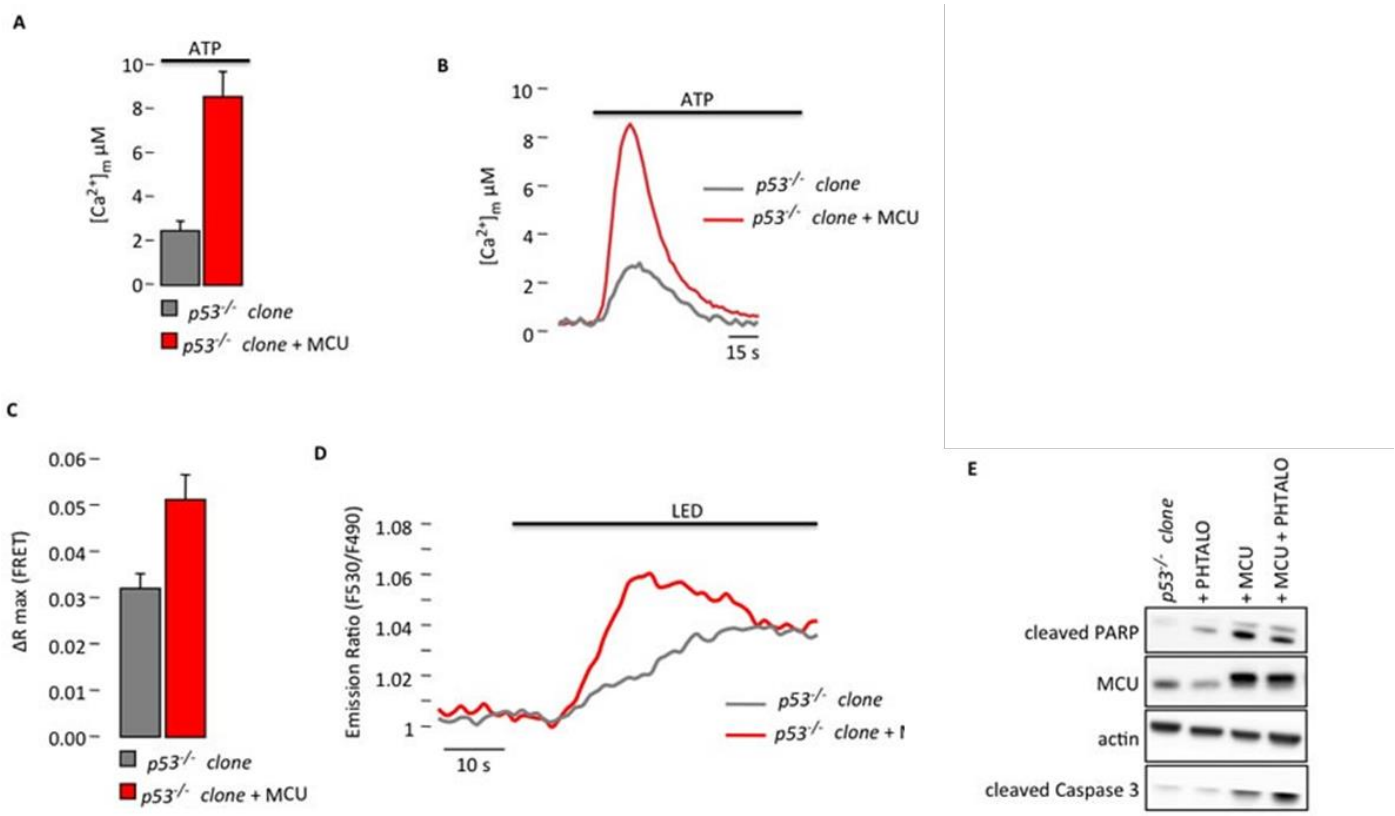

Figure 17. Increased Ca^{2+} response in $p53^{-/-}$ MEF clones after MCU overexpression restores sensitivity to PD*(A) Mitochondrial Ca^{2+} response after agonist (100 µM ATP) stimulation of $p53^{-/-}$ MEF clone in resting condition or after MCU overexpression ($p53^{-/-}$ clone: $[Ca^{2+}]_m$ peak 2.20 ± 0.45; $p53^{-/-}$ clone + MCU: $[Ca^{2+}]_m$ peak 8.28 ± 1.45) ($p < 0.01$). (B) Representative traces of mitochondrial Ca^{2+} transient. (C) and (D) Single-cell FRET measurements of PDT-induced mitochondrial Ca^{2+} uptake that are expressed as the maximal variation in the emission ratio ($p53^{-/-}$ clone: ΔR max 0.0311 ± 0.0043; $p53^{-/-}$ clone + MCU: ΔR max 0.0512 ± 0.0054) ($p < 0.05$). (E) Immunoblotting for typical apoptotic markers in $p53^{-/-}$ clone upon phthalocyanine (15 µM) photo-activation (PHTALO)*

As additional approach we used the overexpression of SERCA. Indeed its increased activity, and the subsequent ER Ca^{2+} overload have been previously demonstrated to promote apoptosis [230]. In our studies, the overexpression of SERCA pumps in the $p53^{-/-}$ clone restored the mitochondrial Ca^{2+} response after agonist stimulation (Fig. 18 A and B) as in the $p53^{+/+}$ clone (Fig.15 C). Similar to the results obtained after MCU overexpression, also PDT-evoked Ca^{2+} release from the ER into the cytosol was increased (Fig. 18 C and D), as measured using the ratiometric Ca^{2+} indicator Fura-2. Consequently, apoptotic sensitivity was rescued in the cells overexpressing SERCA pumps (Fig. 16 E). These results support the evidence that the alteration of Ca^{2+} homeostasis observed in the absence of p53, is determinant for sensitivity to apoptosis and that modulating mitochondrial Ca^{2+} handling is possible to re-sensitize cells to death.

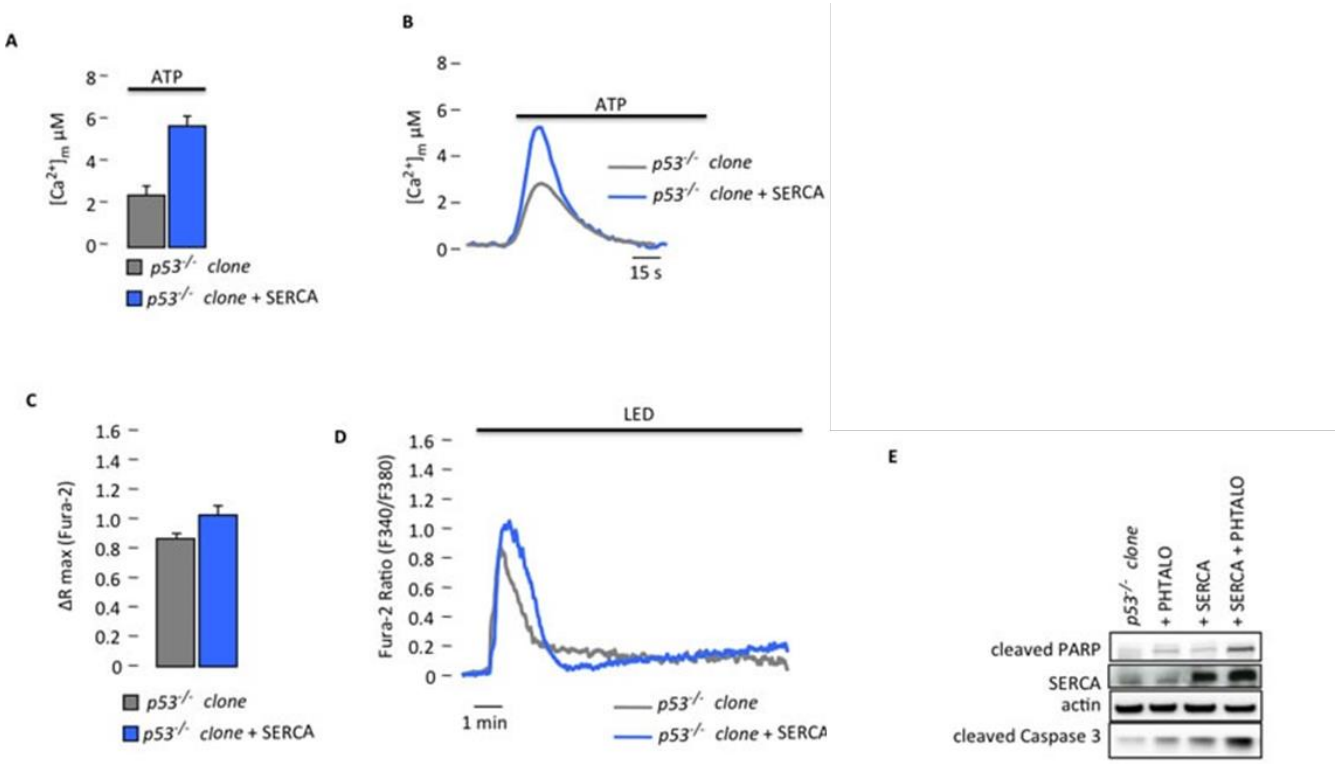

Figure 18. Increased Ca^{2+} response in $p53^{-/-}$ MEF clones after SERCA overexpression restores sensitivity to PDT *(A) Mitochondrial Ca^{2+} response after agonist (100 µM ATP) stimulation of $p53^{-/-}$ clone in resting condition or after SERCA overexpression ($p53^{-/-}$ clone: $[Ca^{2+}]_m$ peak 2.51 ± 0.31; $p53^{-/-}$ clone + SERCA: $[Ca^{2+}]_m$ peak 5.40 ± 0.56) ($p < 0.01$). (B) Representative traces of mitochondrial Ca^{2+} transient. (C) and (D) Ratiometric single-cell measurements of PDT-induced Ca^{2+} waves by Fura-2 that are expressed as the maximal variation in the excitation ratio ($p53^{-/-}$ clone: ΔR max 0.85 ± 0.02; $p53^{-/-}$ clone + SERCA: ΔR max 1.05 ± 0.06) ($p < 0.01$). (E) Immunoblotting for typical apoptotic markers in $p53^{-/-}$ clone upon phthalocyanine (15 µM) photo-activation (PHTALO).*

Moreover, we used an approach for preventing Ca^{2+} signaling [242] in the *p53*$^{+/+}$ clone to mimic the Ca^{2+} signaling conditions observed both *in vitro* and *in vivo* in the *p53*$^{-/-}$ clone to test the dependency of PDT-induced apoptosis on mitochondrial Ca^{2+} uptake. Using BAPTA-AM, which is a well-known membrane permeable Ca^{2+} chelator, we were able to reduce the $[Ca^{2+}]_m$ response evoked by agonist stimulation (Fig. 19 A and B) to values similar to those observed in the *p53*$^{-/-}$ clone (Fig. 15 C). We further assessed the effect of the chelator after PDT treatment on either the cytosolic (Fig. 19 C and D) or mitochondrial Ca^{2+} response (Fig.19 E and F). The reduced ability of mitochondria to accumulate Ca^{2+} was associated with reduced sensitivity to PDT-induced apoptosis (Fig.19 G) as observed previously in the *p53*$^{-/-}$ clone (Fig.15 H), probably due to a defective opening of the mitochondrial permeability transition pore [229].

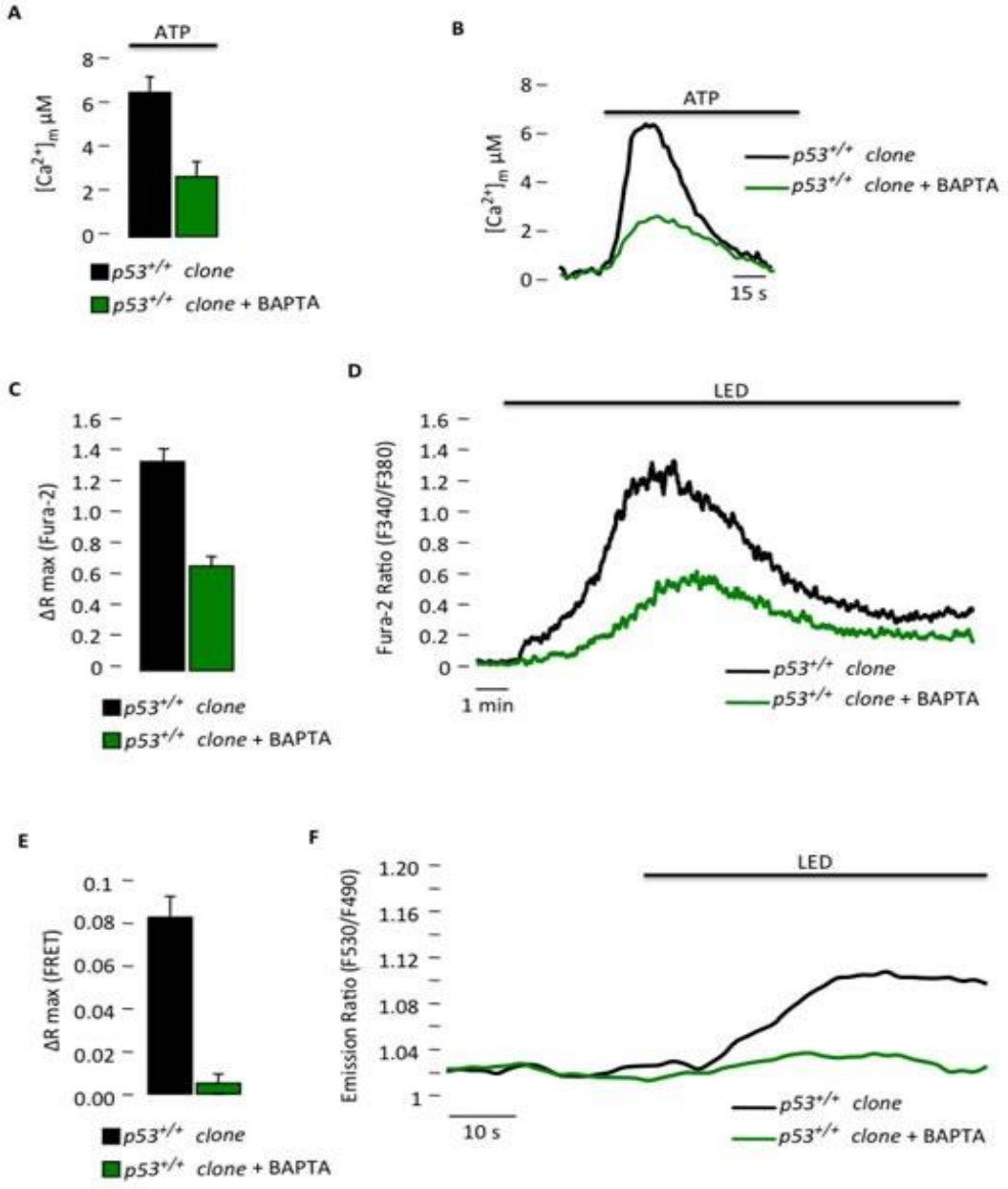

Figure 19. Reduced Ca^{2+} response in $p53^{+/+}$ MEF clones with a Ca^{2+} chelator blocks the sensitivity to PDT *(A) Mitochondrial Ca^{2+} response after agonist (100 µM ATP) stimulation of $p53^{+/+}$ clone in resting condition or after BAPTA-AM loading ($p53^{+/+}$ clone: $[Ca^{2+}]_m$ peak 6.33 ± 0.97; $p53^{+/+}$ clone + BAPTA: $[Ca^{2+}]_m$ peak 2.59 ± 0.83) ($p < 0.05$). (B) Representative traces of mitochondrial Ca^{2+} transient. (C) and (D) Ratiometric single-cell measurements of PDT-induced Ca^{2+} waves by Fura-2 that are expressed as the maximal variation in the excitation ratio ($p53^{+/+}$ clone: ΔR max 1.35 ± 0.07; $p53^{+/+}$ clone + BAPTA: ΔR max 0.63 ± 0.04) ($p < 0.01$). (E) and (F) Single-cell FRET measurements of PDT-induced mitochondrial Ca^{2+} uptake that are expressed as the maximal variation in the emission ratio ($p53^{+/+}$ clone: ΔR max 0.0824 ± 0.0102; $p53^{+/+}$ clone + BAPTA: ΔR max 0.0048 ± 0.0045) ($p < 0.01$). (G) Immunoblotting for typical apoptotic markers in $p53^{+/+}$ clone upon phthalocyanine (15 µM) photo-activation (PHTALO)*

Then, we also validated our findings *in vivo*. First, we directly verified in the tumor masses (derived from the $p53^{+/+}$ clone) grown in skinfold chambers and found that the activation of phthalocyanine was unable to induce a significant increase in Ca^{2+} concentration in the presence of BAPTA (Fig. 20 A). Then, we directly linked Ca^{2+} response with apoptotic behavior using SR-FLIVO,

which is a fluorescent probe used to detect apoptosis *in vivo*. Indeed, as shown in the lower panel of Figure 20 B, tumors treated with PDT exhibited reduced levels of caspase activity in the presence of BAPTA compared to levels of apoptosis in tumors not exposed to this Ca^{2+} chelator (Fig.20 B, upper panel). To further investigate the correlation between Ca^{2+} and apoptosis *in vivo,* two groups of mice were injected subcutaneously with the $p53^{+/+}$ clones to induce tumor formation. After 14 days, the animals were pre-treated with a control (vehicle) or with BAPTA-AM for 1 hour at the level of the tumor nodules, irradiated with PDT and then injected with SR-FLIVO to image caspase-positive tumor cells. Figure 20 C clearly shows that the inhibition of Ca^{2+} signals reduced apoptotic activation *in vivo* (as previously observed *in vitro*). Finally, tumor nodules were excised and imaged by confocal microscopy (Fig. 20 D) or homogenized for Western blot analysis (Fig. 20 E). Tumor cells treated with BAPTA displayed significantly decreased fluorescence (and thus, reduced apoptosis due to the inhibition of caspase activation) compared to that of the tumors not treated with BAPTA ($p53^{+/+}$ clone). These results were confirmed by immunoblotting the extracted tumors with anti-caspase 3 antibody (Fig. 20 E).

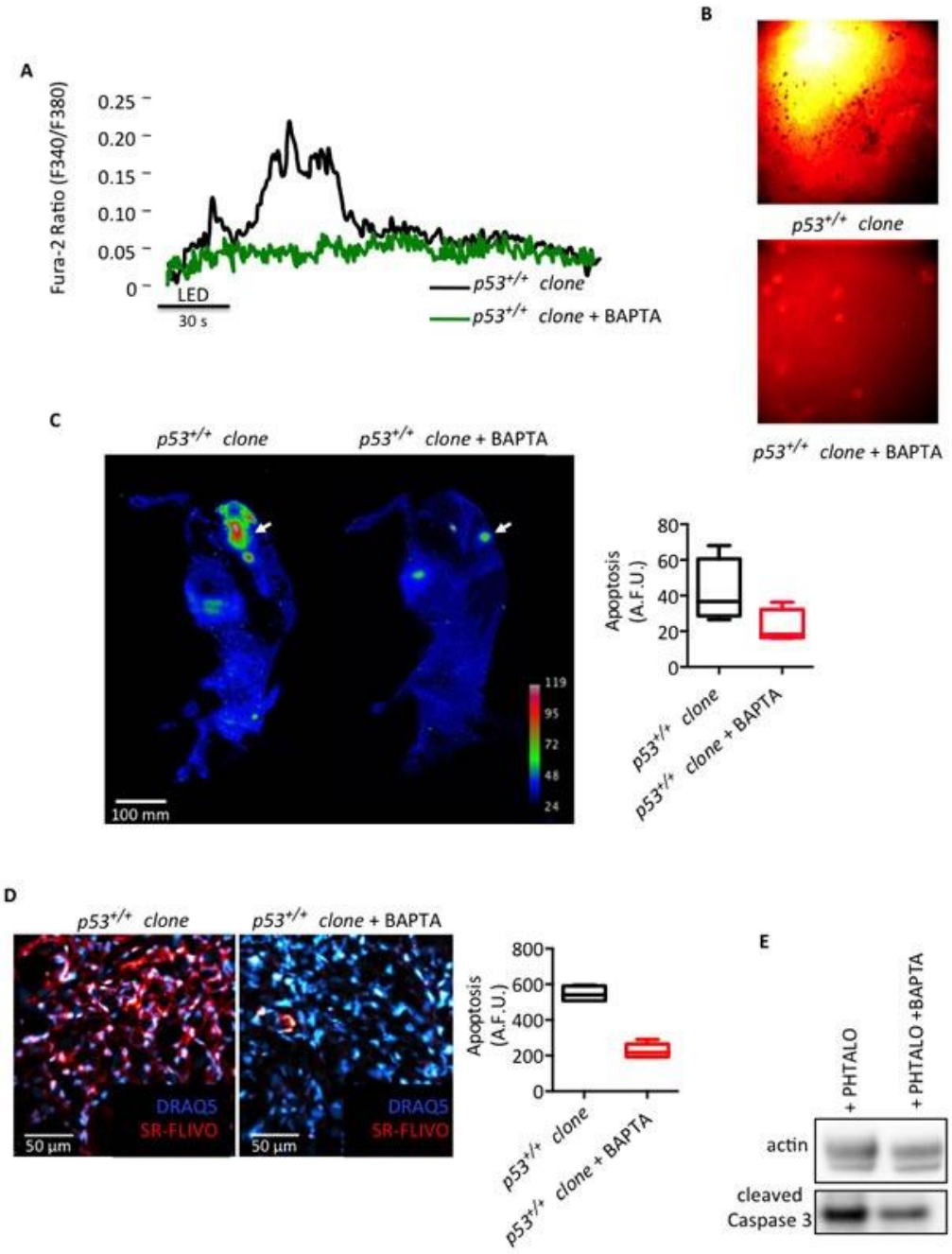

Figure 20. Ca^{2+} signal in tumor masses is required for the anticancer effect of PDT *(A) Cytosolic Ca^{2+} response measured within the tumors in the skinfold chambers as the ratio of Fura-2 fluorescence 340 nm/380 nm induced upon phthalocyanine (15 µM) photo-activation. (B) Levels of apoptosis measured as caspase activity (SR-FLIVO) within the tumor masses in the skinfold chambers. (C) In vivo imaging of apoptosis as the intensity of fluorescence (SR-FLIVO) emitted by a subcutaneous tumor mass upon phthalocyanine (15 µM) photo-activation. (D) Analysis of apoptosis in tumor tissue sections prepared upon in vivo phthalocyanine (15 µM) photo-activation and tumor excision. (E) Immunoblotting of homogenized tumors excised upon in vivo phthalocyanine (15 µM) photo-activation.*

Discussion

Our ability to elucidate the details of intracellular signaling has improved remarkably in recent years. Technological innovations resulting from the development of new specialized optical

microscopes and from the introduction of fluorescent indicators and proteins allow us to visualize events within a cell in real time and space [222]. These tools provide high sensitivity and great versatility while minimally perturbing the cell under investigation.

Much of the recent progress in understanding the biology of cancer cells has been achieved *via* the study of key components of signaling and regulatory pathways. A widely studied signal transduction pathway in cancer cells is intracellular Ca^{2+} homeostasis [92]. Ca^{2+} plays roles in both tumor progression and the efficacy of chemotherapeutic agents, and the participation of this cation in the apoptotic process has been extensively demonstrated [237]. The link of Ca^{2+} to cancer and apoptosis was initially accepted with the discovery that the classical antiapoptotic protein Bcl-2 affected Ca^{2+} signaling. In particular, the antiapoptotic members of the Bcl-2 family cause a reduction in the ER Ca^{2+} concentration, while the opposite is true for proapoptotic proteins. Indeed, apoptotic sensitivity correlates with the total ER Ca^{2+} load and depends on the ability of cells to transfer Ca^{2+} from the ER to the cytosol [238]. Strikingly, proteins other than the proapoptotic members of the Bcl-2 family act by modulating Ca^{2+} homeostasis. Indeed, in recent years, many other onco-suppressor proteins have been shown to reduce the Ca^{2+} release in the ER (albeit through completely different molecular mechanisms) and, consequently, to block the apoptotic responses[99,210,239,240,243]. However, all of these mechanisms have been successfully elucidated *in vitro*. In contrast, no data regarding the role of intracellular Ca^{2+} homeostasis are available in the context of the tumor environment *in vivo* in mice.

In the present study, we combined the dorsal skinfold chamber technique with intravital microscopy to elucidate the involvement of p53 in the control of intracellular Ca^{2+} signals and apoptosis in three-dimensional tumor masses in living mice. The obtained data strongly indicate that p53-dependent dysregulated Ca^{2+} homeostasis causes reduced ER Ca^{2+} release that is associated with reduced responsivity to apoptotic stimulation. More interestingly, we showed that Ca^{2+} signals with amplitudes that are directly dependent on the presence of p53 and that are tightly linked with the generation of apoptosis in cancer cells are generated when the anti-cancer photosensitizer phthalocyanine, which is used in the photodynamic therapy of cancer, is activated. To our knowledge, this study is the first to report the direct measurements of intracellular Ca^{2+} dynamics *in vivo* within tumor masses under physiological conditions. Moreover, this imaging approach can be applied successfully to all the various GFP moieties and chimeras, as well as to all of the fluorescent probes that are available, to follow intracellular parameters of interest.

Overall, these results provide new insights into p53 pathways underlying cancer and a method to monitor the kinetics of intracellular signals in tumor masses *in vivo* to verify the efficacy of anticancer treatments.

PML at mitochondria-associated membranes is critical for the repression of autophagy and cancer development

PML and cell death

The promyelocytic leukemia (PML) protein is a tumor suppressor frequently lost or aberrant in hematopoietic malignancies and human solid tumors [244,245]. Its gene was originally identified at the break point of the t(15;17) chromosomal translocation of acute promyelocytic leukemia (APL), a distinct subtype of acute myeloid leukemia. As a consequence of this translocation, PML fuses to the retinoic acid (RA) receptor alpha (RARα) gene. Two fusion genes are generated encoding PML-RARα and RARα-PML fusion proteins, which coexist in the leukemic cells, blocking hematopoietic differentiation [246]. PML has therefore, become the object of intense research on the basis of this premise. Since then, PML has been shown to regulate diverse cellular functions, such as transcriptional regulation, DNA-damage response, sumoylation process, cellular senescence, neoangiogenesis and apoptosis [247].

PML, also known as TRIM19, belongs to a large family of proteins harboring a distinctive zinc-finger domain termed the RING domain, followed by two additional zinc fingers called B-boxes and an a-helical coiled-coil motif, which are collectively referred to as the RBCC domain. The RBCC domain mediates protein–protein interactions and is responsible for PML homomultimerization and nucleation of the PML-NBs [248,249]. Also, PML RBCC domain mediates heterodimerization with PML–RARα [248]. The C-terminal region of PML is less structured and varies between PML isoforms. Alternative splicing of C-terminal exons determines the existence of at least seven PML isoforms characterized by different C-terminal regions. The variability of the C-terminal part of PML isoforms is important for the recruitment of different interacting partners and therefore for the specific functions of each isoform [250].

PML is typically concentrated in subnuclear macromolecular structures termed PML-nuclear bodies (PML-NBs), of which PML is the essential component. PML-NBs have a diameter of 0.2-1 μm and the shape of a doughnut. PML-NBs are multiprotein dynamic structures that undergo significant changes in number, size and position, particularly in response to cellular stress [251]. They critically depend on PML to be correctly assembled [252]. PML functionally interacts with a large number of proteins within PML-NBs; some are in direct physical contact with PML, while others are not [249]

PML SUMOylation and noncovalent binding of PML to SUMOylated PML through the SUMO-binding motif constitutes the nucleation event for subsequent recruitment of SUMOylated proteins

and/or proteins containing SUMO-binding motifs to the PML-NBs [252]. *Pml* null mice and cells are protected from multiple and diverse apoptotic stimuli [253]. A possible explanation for why *Pml* null cells are resistant to many apoptotic stimuli can be ascribed to the fact that PML can act as a pleiotropic factor in the functional regulation of several pro-and antiapoptotic pathways. Indeed, PML is functioning as a part of a complex tumor-suppressive network.

For instance, it is well established that PML is an important factor in the regulation of both p53-dependent and –independent apoptotic pathways [211].

PML has been shown to interact with the phosphatase PP2A and to modulate its activity on specific targets. *Via* PP2A PML can modify the sensitivity to pro-survival and pro-apoptotic cues in at least two ways: (i) recruiting PP2A phosphatase to nuclear PML-NBs, thereby de-phosphorylating and inactivating AKT and its pro-survival functions [254]; (ii) recruiting PP2A to the inositol1,4,5-trisphosphate receptor, IP3R-3, to modulate Ca^{2+} release and storage at the endoplasmic reticulum (ER). The physical structures where both this regulation is achieved and cytoplasmic PML is localized are MAMs. Indeed, sensitivity to apoptosis is dependent on the ability of cells to transfer Ca^{2+} from the ER to the mitochondria. Ca^{2+} release, in turn, induces mitochondrial Ca^{2+} loading, with a consequent release of mitochondrial proteins involved in the apoptotic process, such as cytochrome c, the apoptosis initiating factor AIF, and the complex of second mitochondria-derived activator of caspases (SMAC) with the direct IAP binding protein with low pI (DIABLO) [92,99]. Conditions that reduce ER Ca^{2+} storage, and thus Ca^{2+} release from the ER to the mitochondria, lower the probability of Ca^{2+} dependent apoptosis[99]. In $Pml^{-/-}$ MEFs, both ER steady-state (Ca^{2+}) values and the increase of cytosolic Ca^{2+} concentration after treatment with apoptotic stimuli like H_2O_2 are significantly smaller than in $Pml^{+/+}$ MEFs [210]. PML appears to be essential for PP2A tethering to the ER localized receptor IP3R-3, favoring IP3R-3 dephosphorylation and Ca^{2+} storage. Conversely, IP3R-3 is hyper-phosphorylated in the absence of PML and this modification decreases the Ca^{2+} release from the ER and the overload of mitochondria increasing the apoptotic threshold [214].

PML and autophagy

As already mentioned, autophagy is a catabolic process that allows lysosomal-mediated degradation of unnecessary or dysfunctional cellular components. Autophagy functions as an adaptive mechanism, which grants cell survival under several stress conditions (e.g., starvation, hypoxia) and maintains cellular integrity by clearing of subcellular debris and regeneration of metabolic precursors [255,256]. In cells growing in a nutrient-rich environment [134,257] autophagy is negatively regulated by mTOR and AKT signaling. PML inhibits the AKT-mTOR signaling pathway, thus suggesting an involvement in the regulation of autophagy. A study from Laane and colleagues [258] shows that impairment of autophagy by siRNA-mediated repression of the autophagy regulator BECN1 interferes with glucocorticoid dexamethasone-mediated lymphoblastic leukemia cell death. Dexamethasone treatment leads to PML up-regulation, its interaction with AKT, and PML-dependent AKT dephosphorylation, which was required for dexamethasone-dependent cytotoxicity effects on thymocytes. Conversely, autophagy was shown to contribute to ATRA mediated differentiation and PML-RARα degradation in NB4 cells, where PML-RARα is targeted to lysosomes by the ubiquitin binding adaptor protein p62/SQSTM1 [259,260]. These studies coherently associate PML activity with autophagy induction and tumor suppression in acute promyelocytic leukemia. However, the role of autophagy in tumorigenesis and tumor maintenance is still controversial.

PML Expression in Human Tumors

About 95% of human acute promyelocytic leukemia (APL) cases harbor the oncogenic fusion gene PML-RARα as a result of the translocation t(15;17), whose breakpoints are located within the PML and the retinoic acid receptor α, RARα loci on chromosome 15 and 17, respectively. In principle, PML function in these cells is impaired by two concomitant events: PML haplo-insufficiency, for the presence of a single WT PML autosome and the expression of PML-RARα, which might interfere with the function of the WT PML protein. PML is involved in the regulation of many cellular functions and some of them, such as the activation of P53 by the DNA damage checkpoint response, rely on its localization and organization in subnuclear structures called PML-nuclear bodies (PML-NBs). PML-RARα functions as a dominant negative factor in the process of PML-NB assembly, causing a microspeckled distribution of PML. In this context, treatment with retinoic acid and arsenic, two agents that induce disease-remission in APL patients, leads to PML-RARα degradation, cell differentiation, re-assembly of PML-NBs, and tumor regression. These

"therapeutic" effects establish a correlation between PML-NB assembly and tumor suppression, yet formal evidence that PML-NBs per se are responsible for tumor suppression is still missing. Indeed, it cannot be excluded that APL regression is due, exclusively, to other missing PML-RARα-associated functions after its degradation. Notably, expression of X-RARα chimera, which does not interfere with PML-NB assembly (P50-RARA, GCN4-RARα), and where X represents a coiled-coil domain mediating RARα homodimerization, maintains transforming potential, and recapitulates the main biological properties of PML–RARα [261,262]. However, the expression of X-RARα fusion proteins in mice, like P50-RARα or GCN4-RARA, is not sufficient to drive tumorigenesis as PML-RARα or the CCPML-RARα protein, where the RARα is fused to the coiled-coil region of PML, do [261]. $Pml^{-/-}$ mice expressing P50-Rarα do not show increased incidence or acceleration of leukemia onset. This suggests that loss of Pml cannot complement P50-Rarα in restoring the leukemogenic potential to a level comparable to that of PML-RARα, and that the PML-RARα oncogene does not simply interfere with Pml and Rarα functions but has additional activities that cannot be recapitulated by separating the two components in this way [262]. In contrast with this observation, $Pml^{-/-}$ Pml-Rarα transgenic-mice show increased incidence and acceleration of leukemia onset [263]. Therefore is not clear if PML-NBs really exert tumor suppressive functions or not.

Immunohistochemical analysis of PML expression in human tumors of different histologic origins shows that PML expression-levels are reduced in a considerable number of cases, as compared to the corresponding normal tissues. PML expression is absent in 49% of central nervous system (CNS) tumors (in 100% of medulloblastomas and over 90% of oligodendroglial tumors), 17% of colon adenocarcinomas, 21% of lung tumors, 27% of prostate adenocarcinomas, 31% of breast adenocarcinomas, 49% of germ cell tumors, and 68% of non-Hodgkin's lymphomas (in 83% of diffuse large-cell lymphomas and 77% of follicular lymphomas)[245]. In addition, PML low-expression correlates with bad prognosis and high-grade tumors for breast adenocarcinomas and prostate carcinomas [245]. PML is phosphorylated by the extracellular signal-regulated kinase ERK2 which facilitates the recruitment of the peptidyl-prolyl cis/trans isomerase PIN1 and the following degradation of PML by the proteasome [264,265]. Given the frequent activation of ERK2 in several types of tumors, due to the sustained action of paracrine growth factors or mutations, the ERK2/PML axis may partly explain why PML expression is low in a considerable fraction of human tumors. However, mutational analysis of the PML gene in 132 samples from different primary tumors and human cell lines showed that PML is rarely mutated or subjected to LOH mutations. Moreover, the few PML mutations detected did not correlate with PML protein-loss, suggesting that mutation is not the main mechanism of PML inactivation in the tumor types analyzed [245].

Triple negative breast cancer (TNBC) is a noticeable exception to the common theme of PML loss in tumors. PML expression is strongly associated with TNBC and basal high tumor-grade breast cancers, which are among the most undifferentiated and untreatable breast cancers [266]. Here, high levels of PML expression correlate with early tumor recurrence, a signature of poor prognosis, and mutations of the tumor-suppressor P53 [267]. In vitro experiments performed on MCF10A cells overexpressing PML show increased survival to anoikis via the regulation of PPAR- δ and fatty acid oxidation, suggesting a crucial role for PML in the regulation of cell metabolism [267].

Chronic myeloid leukemia (CML) is also an exception. Indeed, high levels of PML expression correlate with bad prognosis in CML, and its function is critical to maintain leukemic initiating cells [268]. PML degradation induced by As_2O_3 (arsenic trioxide) treatment allows exit from quiescence and exhaustion of cancer stem cells (CSCs) in a murine model of the disease. This parallels the role of PML in hematopoietic stem cells (HSCs) where it is highly expressed and controls HSC self-renewal and symmetric division through its regulation of mTOR and PPAR-δ signaling (fatty acid oxidation) [268]. Additional proof of the general role that PML plays in stem cell homeostasis comes from studies on the nervous system. In mice PML expression is restricted to neural progenitor cells (NPCs) in the developing neocortex where PML regulates NPC proliferation and differentiation [269].

In summary, analysis of PML expression in human tumors reveals two distinct situations: (i) reduced/loss-of expression in different tumor types, most frequently in CNS tumors, which suggests that PML may be a tumor suppressor; (ii) high expression in CML and TNBC tumors, which, on the contrary, rely on PML expression to, respectively, maintain unlimited self-renewal and survive under metabolic stressing conditions. A controversial picture emerges from all these observations, indicating that the role of PML in human malignancies is context dependent.

Introduction

To become cancerous, cells must overcome the foolproof mechanism of cell death and hence reduce their propensity to activate self-destructive catabolic pathways in response to hostile environmental clues [270]. The induction of apoptosis is the major route of cell death that is targeted by many chemotherapeutic drugs, yet is antagonized by multiple cellular processes including one particularly important one, namely autophagy.

Autophagy plays dual roles in cancer; it can function as either a tumor suppressor by preventing the accumulation of damaged proteins and organelles or as a survival pathway by suppressing apoptosis and promoting the growth of established tumors [271-275].

Recent studies have indicated that autophagy represents an important mechanism underlying chemotherapy resistance in leukemia [276,277] and in solid cancers [272,277,278], although the exact molecular mechanism underlying the effects of autophagy on tumorigenesis must be further elucidated.

Here, we propose a new role of promyelocytic leukemia protein (PML) in the negative regulation of autophagy. PML is a tumor suppressor that was initially identified because of its dysregulation during the pathogenesis of acute promyelocytic leukemia (APL) [279]. The fusion oncoprotein PML/RARα can upregulate the activation of constitutive autophagy in APL cells, thereby contributing to the anti-apoptotic function of PML/RARα [276]. However, the precise mechanisms by which PML regulates autophagy remain unknown.

Because PML dysregulation is associated with an extensive range of malignancies including solid tumors [245], we reasoned that completely understanding all of the molecular pathways that require PML for the control of cell death and, consequently, of cancer progression is fundamental.

Results

PML represses the autophagic process

To determine the possible involvement of Pml in the autophagic process, we monitored autophagosome levels in wild type ($Pml^{+/+}$) primary MEFs matched with $Pml^{-/-}$ MEFs, either under normal conditions (fed) or after serum deprivation (starved). Autophagosomes were detected as fluorescent cytoplasmic dots that concentrated the fusion protein microtubule-associated proteins 1 light chain 3A (MAP1LC3A, best known as LC3) fused to green fluorescent protein (GFP) in live imaging experiments. Such GFP-LC3-positive dots were more frequent in $Pml^{-/-}$ than in WT MEFs under basal conditions (Figures 21A and 21B). Following nutrient deprivation, autophagosome formation was induced in WT MEFs at levels similar to those found in $Pml^{-/-}$ cells under fed conditions; conversely, autophagosome formation did not change significantly after starvation in $Pml^{-/-}$ MEFs (Figures 21 A, 21B). The redistribution of LC3 to autophagosomes is usually accompanied by its lipidation, causing an increase in its electrophoretic mobility (and hence a shift from LC3-I to LC3-II) [280]**.** Accordingly, detection of the conversion of LC3-I to LC3-II *via* immunoblotting confirmed that $Pml^{-/-}$ MEFs contained higher levels of LC-3-II than WT MEFs in baseline conditions (Figure 21C). Transmission electron microscopy (TEM) confirmed the increase in baseline autophagosomes in $Pml^{-/-}$ MEFs (Figure 21D).

Increased abundance of LC3-II was also detectable in the livers and skeletal muscles of adult $Pml^{-/-}$ mice (Figure 21E) compared with WT animals. Interestingly, as observed above *in vitro*, LC3-II could be induced *via* starvation (food deprivation for 24 h) only in WT mice (but not in $Pml^{-/-}$ mice), in which LC3-II reached the same level as the one observed in $Pml^{-/-}$ mice under fed conditions. Thus, we analyzed whether *Pml* might affect the formation of autophagosomes. We found that two autophagosome markers, ATG14 and STX17 [138], were markedly shifted to the MAM compartments in $Pml^{-/-}$ MEF, suggesting increased autophagosome biogenesis in the absence of *Pml* (Figures 21F).

Pharmacological blockade of autophagy using 3-methyladenine (3-MA), an inhibitor of the Beclin 1-dependent class III phosphoinositide 3-kinase (PI3K), blocked the excessive formation of autophagosomes in $Pml^{-/-}$ MEFs, meaning that WT and $Pml^{-/-}$ MEFs contained similar amounts of LC3-GFP puncta (data no shown). Conversely, blockade of the last step of autophagy (which depends on lysosomal proteases) by means of leupeptin *in vivo* [281] failed to reduce the difference in LC3-II formation observed between WT and $Pml^{-/-}$ mouse livers (data no shown). Similarly, bafilomycin A1 of NH_4Cl, which both abolish the acidification of lysosomes, caused an increase in the abundance of LC3-II in both WT and $Pml^{-/-}$ MEFs, yet did not abolish the difference in LC3-II

formation between MEFs with the two genotypes, suggesting that the absence of *Pml* truly induces an increase in autophagic flux. .

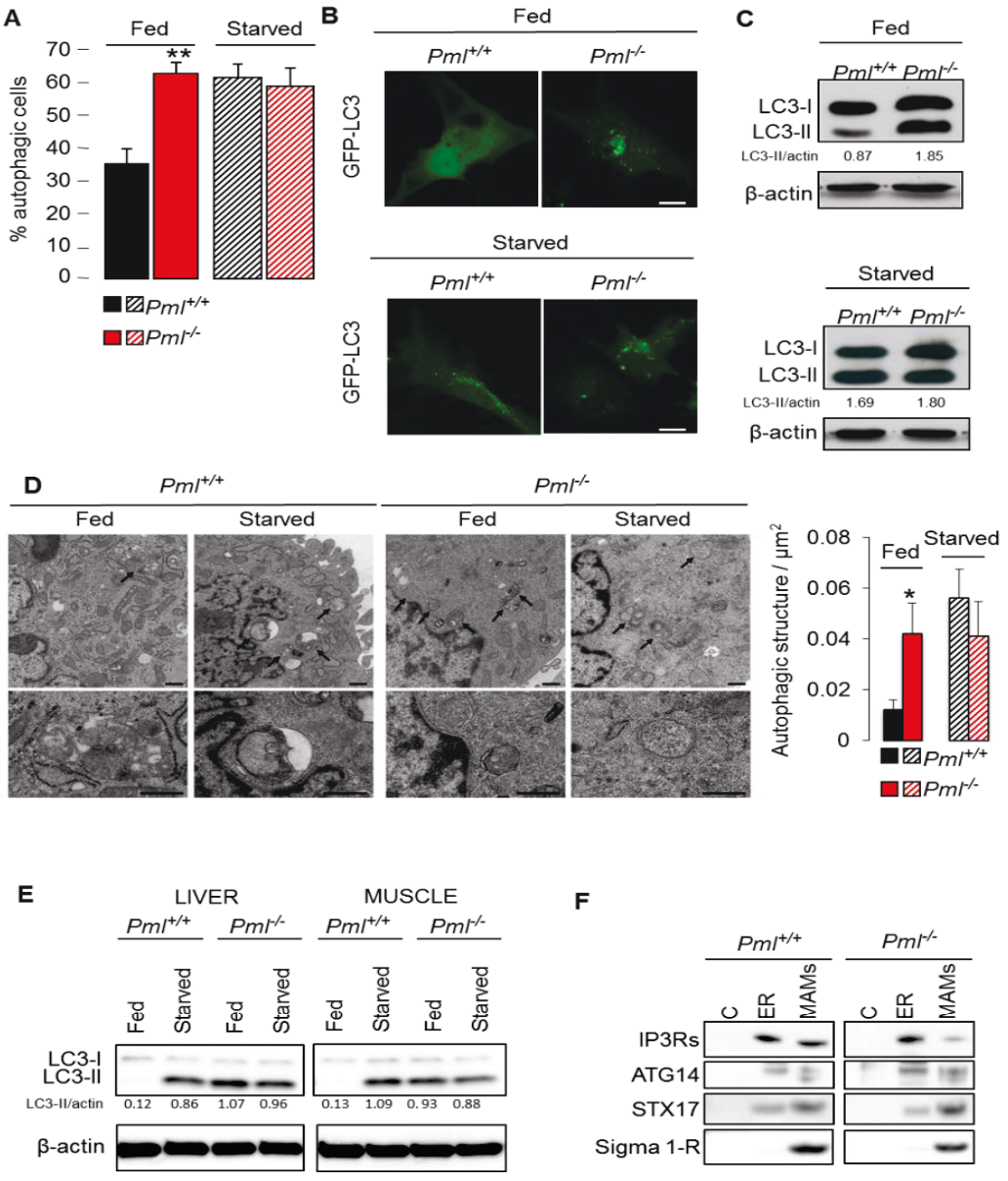

Figure 21. PML represses autophagic processes. *(A) Percentages of GFP-LC3 puncta-positive cells in Pml WT and KO MEFs transfected with the GFP-LC3 plasmidunder basal conditions (fed) and after starvation (starved: serum deprivation, 1 h). Bars: S.E.M. ** $p < 0.01$, n=4. (B) Representative images of GFP-LC3 puncta in MEFs. Scale bar, 10 µm. (C) Conversion of endogenous LC3-I to LC3-II, monitored via immunoblotting in Pml+/+ and Pml-/- MEFs cultured in regular medium (fed) or without nutrients (starved: serum deprivation, 1 h). (D) Ultrastructural evidence of higher autophagy levels in MEFs in the absence of Pml compared with WT conditions basal conditions (fed). (starved: serum deprivation, 1 h). Scale bar, 500 nm. Bars: S.E.M. * $p < 0.05$, n=3. (E) Immunoblotting of endogenous LC3 in the livers and skeletal muscle from fed or starved (24 h) Pml+/+ and Pml-/- mice.*
(F) Immunoblot of subcellular fractions isolated from Pml+/+ and Pml-/- MEFs, where IP3R is used as an ER marker, Sigma 1-R is used as a MAM marker, and ATG14/STX17 are used as autophagosome formation markers. C: cytosol; ER: endoplasmic reticulum; MAMs: mitochondria-associated membranes.

PML localization at endoplasmic reticulum (ER)/MAM contact sites is necessary for modulating autophagy

The localization of PML at ER/MAM contact sites is fundamental for its pro-apoptotic activity *via* a calcium (Ca^{2+})-mediated pathway [210]. Driven by this consideration, we determined whether PML also plays a role in the control of autophagy in these specialized domains. To address this question, we took advantage of an erPML chimeric protein, which contains the entire PML protein targeted to the outer surface of the ER and which is able to rescue sensitivity to apoptosis in *Pml*$^{-/-}$ MEFs [210]. erPML (but not a control construct targeted to nuclei, nuPML) localized at MAMs and suppressed the elevated levels of autophagy when re-introduced into *Pml*$^{-/-}$ MEFs (Figures 22A–22D) comparable to those measured in WT MEFs (Figure 21). *Pml*$^{-/-}$ MEFs retransfected with erPML (but not with nuPML) acquired the ability to increase autophagy in response to starvation (Figures 22A–22C). Hence, it appears that the presence of PML at MAMs may be important for the repression of autophagy.

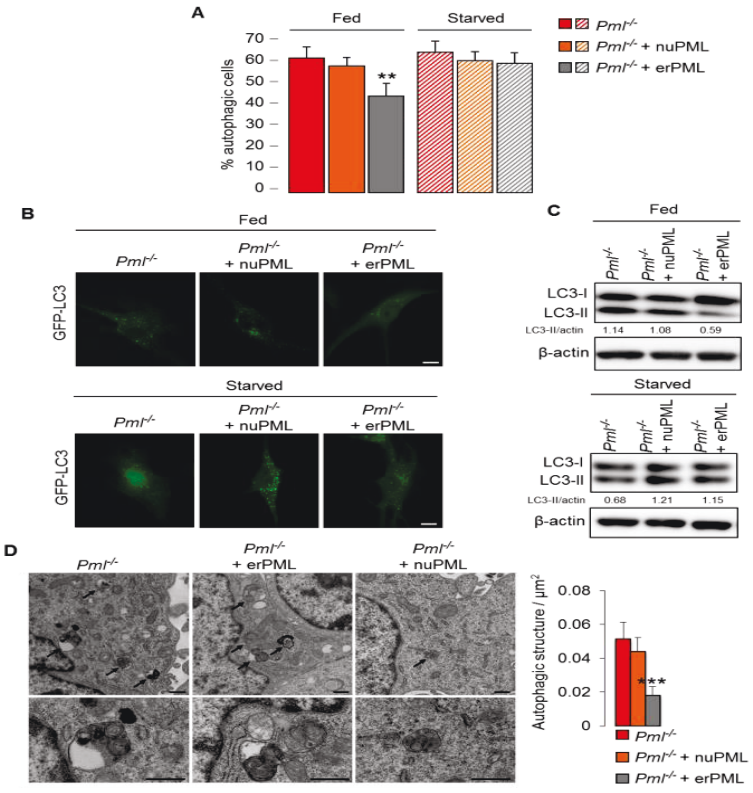

Figure 22. PML localization at ER/MAM domains controls the levels of autophagy*.(A) Percentages of GFP-LC3 puncta-positive cells induced by the transfection of erPML and nuPML chimeras into Pml*$^{-/-}$ *MEFs under resting conditions (fed) and after serum deprivation (starved: serum deprivation, 1 h). Bars: S.E.M. ** p < 0.01, n=4.*
(B) Representative images of GFP-LC3 puncta in Pml$^{-/-}$ *MEFs before and after re-introduction of the two chimeras, erPML and nuPML (fed: resting conditions; starved: serum deprivation, 1 h). Scale bar, 10 µm.*
(C) Immunoblotting to detect LC3 in PML KO MEFs after the re-introduction of erPML and nuPML chimeras, both under basal conditions (fed) and after serum starvation (starved: serum deprivation, 1 h).
(D) Images of autophagic ultrastructure in Pml$^{-/-}$ *MEFs following the transfection of erPML and nuPML chimeras. Scale bar, 500 nm. Bars: S.E.M. *** p < 0.005, n = 3.*

P53 drives PML localization at MAMs

Previously, the role of p53 in the regulation of autophagy was proposed to depend on its localization [282]. Cytoplasmic p53, particularly when associated with the ER membranes, represses basal pro-survival autophagy, whereas nuclear p53 fails to do so [283]. However, the precise molecular mechanism by which p53 suppresses autophagy remains elusive.

Because of the tight interaction between p53 and PML [284-289] we sought to investigate the possible effect of PML on autophagy in relation to p53. Therefore, we evaluated p53 and PML localization at points of close contact between the ER and mitochondria in *Pml*$^{-/-}$ and *p53*$^{-/-}$ backgrounds, respectively. Subcellular fractionation of MEFs with distinct genotypes revealed that p53 protein was associated with MAMs irrespective of the absence or presence of *Pml*. (data no shown), meaning that Pml does not control the subcellular localization of p53. In stark contrast, in the absence of p53, Pml delocalized from MAMs, as shown by comparative subcellular fractionation followed by immunoblots, immunogold detection by electron microscopy and immunofluorescence (IF) analyses of WT and *p53*$^{-/-}$ MEFs (Figures 23A–23C). These results suggested that PML might function as a master regulator of autophagy that acts downstream of p53.

This concept was confirmed by the introduction of the erPML chimera into *p53*$^{-/-}$ MEFs. Indeed, the forced localization of Pml at MAMs (Figure 23D) in *p53*$^{-/-}$ cells reduced GFP-LC3 puncta (Figures 23E–23G). Similarly, the re-introduction of p53^{wt}, which also localizes at the ER and MAMs [290], engaged Pml at those contact sites (Figures 23H and 23I) and suppressed signs of enhanced autophagy in *p53*$^{-/-}$ MEFs. Furthermore, a p53 mutant (p53^{K382R}) that is unable to inhibit autophagy when re-introduced into *p53*$^{-/-}$ cells [291] failed to localize at the ER/MAMs in *p53*$^{-/-}$ MEFs and, also failed to rescue Pml localization to MAMs (Figures 23J and 23K).

Overall, these results strongly suggest that proper Pml localization at MAM domains is fundamental for the repression of autophagy.

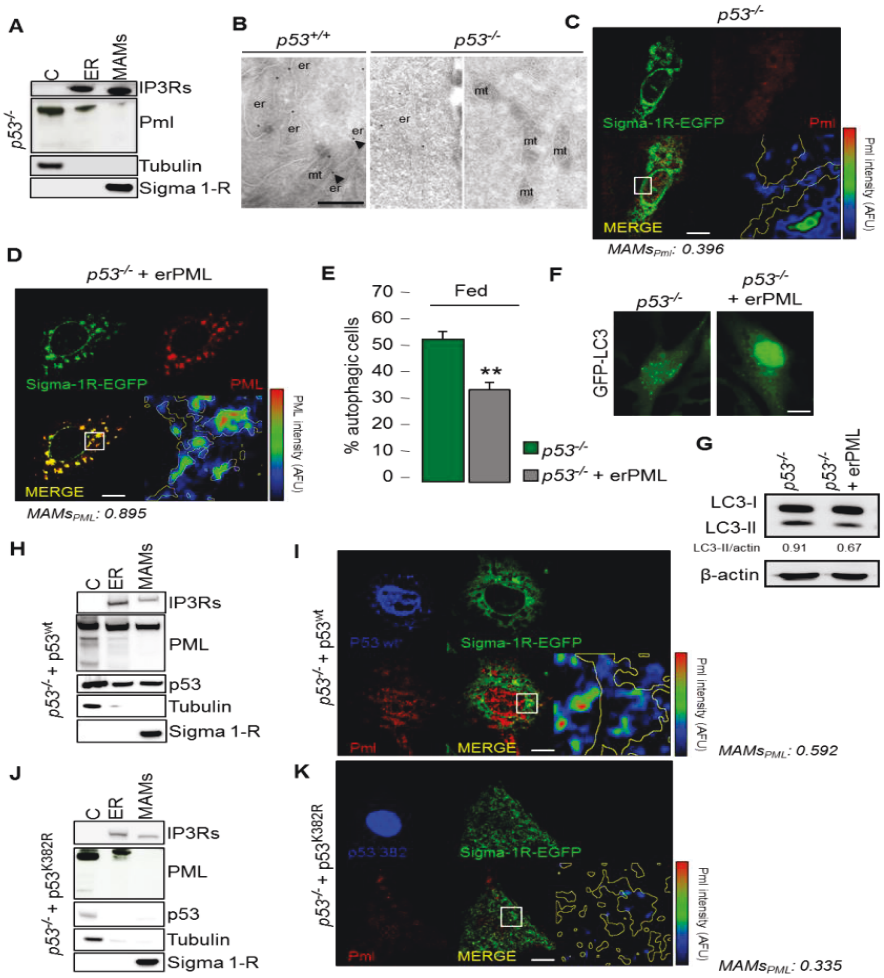

Figure 23. Delocalization of PML from the MAMs is a key feature associated with high levels of autophagy. *(A) Immunoblotting detection of Pml in p53$^{-/-}$ MEF fractions. C: cytosol; ER: endoplasmic reticulum; MAMs: mitochondria-associated membranes.(B) Immunogold labeling of Pml in p53$^{+/+}$ and p53$^{-/-}$ MEFs. In WT condition is indicated the presence of Pml at MAMs (arrowheads) and ER (er). In p53$^{-/-}$ background Pml labeling remains associated to the ER (er, center micrograph) but not to mitochondria or MAMs (mt, right micrograph). Scale bar, 500 nm.(C) The co-localization of Pml (red) and Sigma 1-R-EGFP (used as a MAM marker, green) in p53$^{-/-}$ MEFs and in (D) p53$^{-/-}$ MEFs following re-introduction of the erPML chimera was analyzed based on immunofluorescence using confocal images. The lower left panels display the merged image of the two stains. The lower right panels display the Pml signal overlaid with MAMs (MAM boundaries are highlighted in yellow) in a rainbow look-up table (LUT) (MAMs$_{PML}$: Manders coefficient for Pml staining was calculated according to Manders coefficient method as the proportion of Pml signal overlapping with the Sigma-1R marker). Scale bar, 10 µm.Reduced levels of autophagy were observed in p53$^{-/-}$ MEFs following erPML transfection as determined based (E)-(F) on the percentage of LC3-GFP puncta and on immunoblotting to detect LC3-I conversion into LC3-II (G). Bars: S.E.M. ** $p < 0.01$, n=4. Scale bar, 10 µm.(H) PML and p53 localization following the re-introduction of p53^{wt} as analyzed via immunoblotting in H1299 p53$^{-/-}$ cells fractions. (I) Immunofluorescence of Pml (red) and p53 (blue) in p53$^{-/-}$ MEFs after the re-introduction of p53^{wt}. Sigma 1-R-EGFP (green) was used as a MAM marker. The lower left panel displays the merged image of Pml and Sigma 1-R staining. The lower right panel displays the Pml signal overlaid with MAMs (MAM boundaries are highlighted in yellow) in a rainbow LUT (MAMs$_{PML}$: Manders coefficient for Pml staining was calculated according to Manders coefficient method as the proportion of Pml signal overlapping with the Sigma-1R marker). Scale bar, 10 µm.(J) PML and p53 localization following the re-introduction of mutant p53^{K382R} as analyzed via immunoblotting in H1299 p53$^{-/-}$ fractions where IP3R was used as an ER marker, Sigma 1-R was used as a MAM marker, and Tubulin was used as a cytosolic marker. C: cytosol; ER: endoplasmic reticulum; MAMs: mitochondria-associated membranes.*
(K) Immunofluorescence of Pml (red) and p53 (blue) in p53$^{-/-}$ MEFs after the re-introduction of mutant p53^{K382R}. Sigma 1-R-EGFP (green) was used as a MAM marker. The lower left panel displays the merged image of Pml and Sigma 1-R staining. The lower right panel displays the Pml signal overlaid with MAMs (MAM boundaries are highlighted in yellow) in a rainbow LUT (MAMs$_{PML}$: Manders coefficient for Pml staining was calculated according to Manders coefficient method as the proportion of Pml signal overlapping with the Sigma-1R marker). Scale bar, 10 µm.

Pml controls autophagy through the AMPK/mTOR/Ulk1 pathway

Autophagy is activated as a pro-survival mechanism in response to various cellular stresses associated with an insufficient energy supply [292,293]. The autophagy signaling network is controlled by a variety of kinases. In particular, a complex that includes AMP-activated protein kinase (AMPK), mammalian target of rapamycin (mTOR) and unc-51-like kinase 1 (Ulk1) has emerged as important for the regulation of autophagy [294-296]. Thus, we examined the relationship between PML-dependent autophagy and this multiprotein complex (Figure 24).

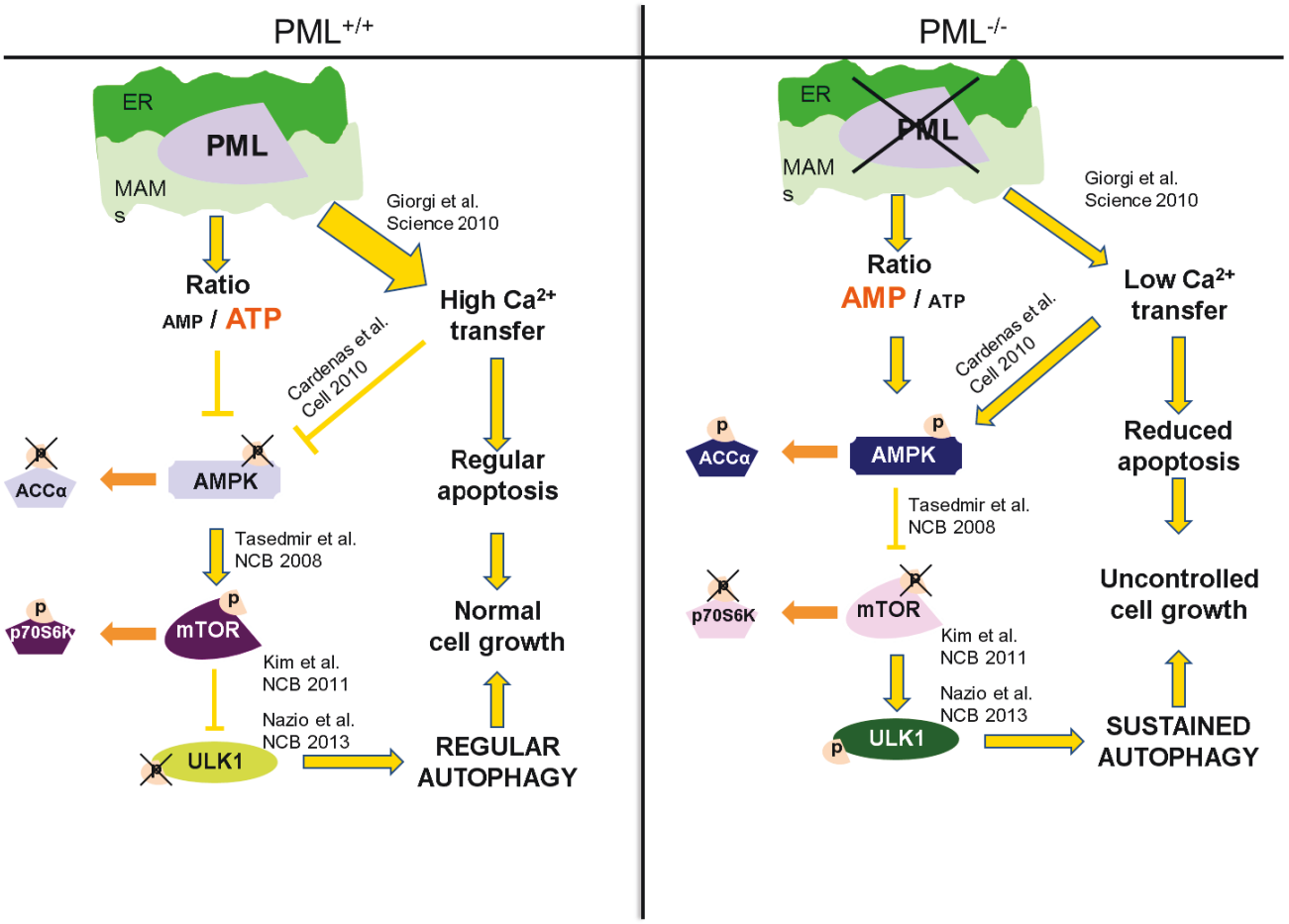

Figure 24, Schematic model of autophagy regulation by PML. *In the absence of Pml, the release of Ca^{2+} from the ER into the mitochondria and the production of ATP are reduced. This low energy status induces AMPK activation, mTOR inhibition and Ulk 1 phosphorylation, leading to an increased level of autophagy.*

AMPK is a conserved energy-sensing kinase that is activated by phosphorylation in response to low cellular energy levels [297]. Previously, we reported that in the absence of PML, cells produced less ATP after agonist stimulation [210]As the ratio of AMP to ATP represents an important means of regulating the activity of AMPK, we examined the role of AMPK by quantifying its phosphorylation. As expected, *Pml*$^{-/-}$ MEFs exhibited increased levels of phosphorylated AMPK

(Figure 25), which correlated with enhanced autophagy, compared with that of WT MEFs. Accordingly, the downstream AMPK substrate acetyl CoA carboxylase was hyper-phosphorylated (Figure 25A). Higher levels of AMPK phosphorylation, correlating with increased autophagy, were also observed in liver and skeletal muscles of adult *Pml*$^{-/-}$ mice compared to WT (Figure 25B).

In contrast to AMPK, mTOR activity reflects a higher energy status with the consequent inhibition of autophagy [294,295,298]. AMPK and mTOR have recently been proposed to regulate autophagy through the coordinated phosphorylation of Ulk1 [295,299]. To determine whether AMPK activation in the absence of Pml promotes autophagy by activating Ulk1, we examined the phosphorylation levels of both Ulk1 and mTOR. In agreement with the findings of Kim et al. [295], increased levels of LC3 lipidation in either *Pml*$^{-/-}$ cells or Pml KO mice tissues were associated with Ulk1 hyper-phosphorylation (which reflects Ulk1 activation), together with reduced phosphorylation of mTOR and its substrate p70^{S6K} (which reflects mTOR inhibition) (Figures 25A and 25B). These results are consistent with the possibility that PML controls autophagy through the AMPK/mTOR/Ulk1 pathway.

The critical role of Ca^{2+} in the formation of autophagosomes has recently been emphasized [300]. In addition to a high concentration of AMP, AMPK activity is upregulated through the inhibition of mitochondrial Ca^{2+} uptake due to reduced Ca^{2+} release *via* the inositol triphosphate receptor (IP3R) [300]. *Pml*$^{-/-}$ cells display a reduced Ca^{2+} transfer from the ER to mitochondria *via* IP3R, which protects cells from apoptosis [210]. To verify whether down-regulated ER-mitochondrial Ca^{2+} transfer is important for the induction of autophagy in *Pml*$^{-/-}$ cells, we increased mitochondrial Ca^{2+} uptake in *Pml*$^{-/-}$ cells by overexpressing the mitochondrial Ca^{2+} uniporter (MCU) [84,85]. MCU overexpression in *Pml*$^{-/-}$ MEFs increased the ability of mitochondria to accumulate Ca^{2+} (Figure 25C) and was sufficient to repress autophagy (Figures 25D-25F), suggesting that PML controls autophagy at ER-mitochondria contact sites by its effects on Ca^{2+} homeostasis.

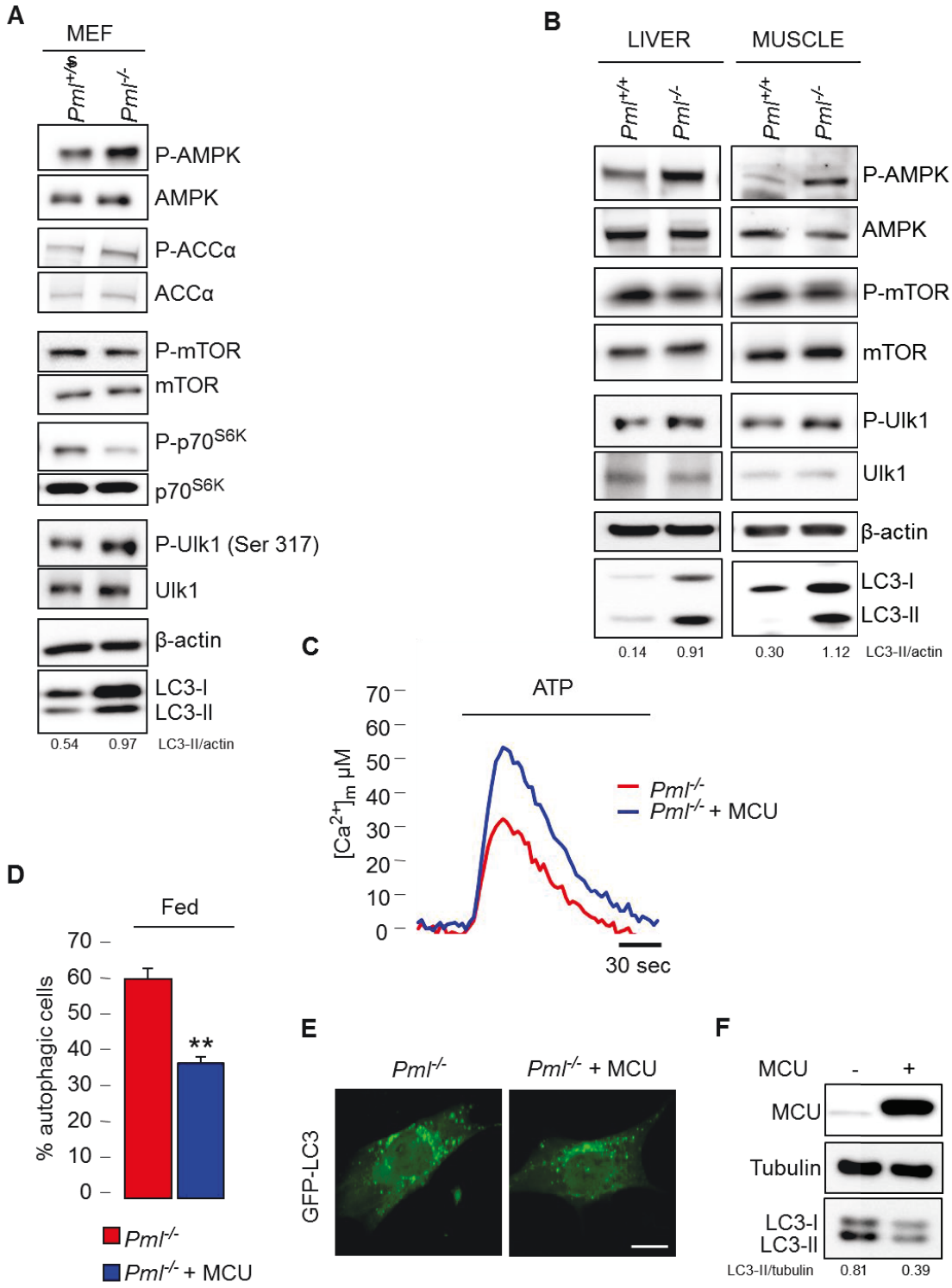

Figure 25. PML modulates autophagy through the AMPK/mTOR/Ulk1 pathway in a Ca^{2+}-dependent manner.
*(A) Immunoblot detection of the phosphorylation status of AMPK, ACCα, $p70^{S6K}$, mTOR and Ulk1 in $Pml^{+/+}$ and $Pml^{-/-}$ MEFs.(B) Detection of autophagy and AMPK-mTOR-Ulk1 phosphorylation levels in the liver and skeletal muscle of $Pml^{+/+}$ and $Pml^{-/-}$ mice.(C) Representative traces of increased mitochondrial Ca^{2+} levels in $Pml^{-/-}$ MEFs after MCU overexpression. $Pml^{-/-}$: $[Ca^{2+}]_m$ peak 33.7 ± 2.55; $Pml^{-/-}$ + MCU: $[Ca^{2+}]_m$ peak 59.2 ± 6.22) S.E.M. ** $p < 0.01$, n=3. Quantification of autophagy in $Pml^{-/-}$ MEFs following MCU overexpression via (D)-(E) analysis of GFP-LC3 puncta or (F) immunoblotting. Bars: S.E.M. ** $p < 0.01$, n=3. Scale bar, 10 µm.*

Loss of PML enhances resistance to metabolic stress

As a homeostatic process, autophagy plays a crucial role during metabolic stress in an attempt to maintain/restore cellular homeostasis [301,302]. Upon starvation, WT cells exhibited a rapid decrease in ATP production, as demonstrated previously [283], whereas cells lacking Pml maintained high ATP levels during stress (Figure 26A). Accordingly, *Pml*$^{-/-}$ cells maintained a higher mitochondrial membrane potential (Ψ_m) under stress conditions compared to WT controls (Figure 26B). This autophagy-dependent energized status of Pml KO cells conferred enhanced resistance to cell death (Figure 26C), favoring cell growth under unfavorable conditions (Figure 26D), such as those present in tumors.

We confirmed this energized status of Pml KO cells through analyzing mitochondrial function in cells responding to a metabolic stress. The oxygen consumption rate (OCR) was used as readout of mitochondrial basal respiration and ATP-linked respiration in *Pml*$^{+/+}$ and *Pml*$^{-/-}$ MEFs. As shown in Figure 26E, under basal conditions, the loss of PML induced only a minor reduction in basal and ATP-dependent OCRs. Interestingly, when MEFs were deprived from glucose, WT cells displayed a dramatic reduction in both basal and ATP-dependent OCRs, while in the *Pml*$^{-/-}$ cells, the OCR was only slightly affected. Accordingly, either genetic inhibition of autophagy (*Becn1* shRNA) or re-introduction of the erPML chimera into *Pml*$^{-/-}$ MEFs, prevented the protection of such cells from death in conditions of glucose depletion (data no shown). These results indicate that enhanced autophagy is responsible for the resistance of Pml-deficient cells from nutrient stress.

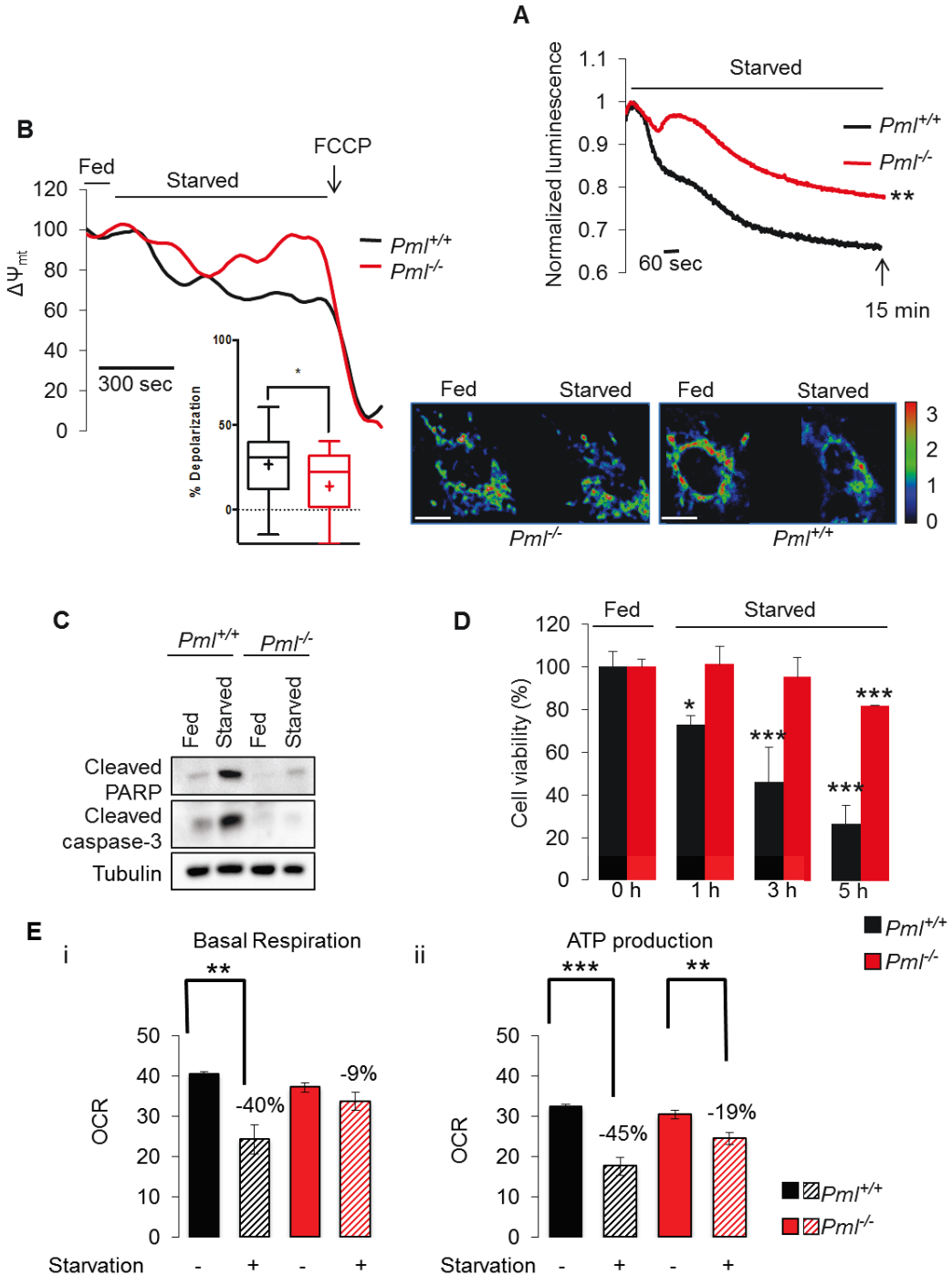

Figure 26. PML deletion favors cell survival under stress conditions due to autophagy activation.
*(A) Cytosolic ATP levels in Pml$^{+/+}$ and Pml$^{-/-}$ MEFs as measured by luciferase expression under starvation conditions (glucose deprivation for 15 min). ** $p < 0.01$, compared to WT condition, n=3.(B) Analysis of mitochondrial membrane potential (Ψ_m) as measured by TMRM intensity in Pml$^{+/+}$ and Pml$^{-/-}$ MEFs. Where indicated, cells were deprived of glucose or exposed to 1 μM carbonyl cyanide p-trifluoromethoxyphenylhydrazone (FCCP). On the right bottom side, representative images of the TMRM signal in the presence or absence of glucose are shown. Normalized TMRM intensity is displayed as a rainbow LUT. (statistical analysis cross: average, line: median, box: 25 and 75 percentile, bars: max and min value, * $p < 0.05$, $n = 3$). Scale bar, 10 μm. Pml KO cells are more resistant to metabolic stress-induced cell death than WT cells as confirmed by (C) immunoblot for two apoptotic markers, cleaved PARP and cleaved caspase 3, and by (D) cell viability assay. Metabolic stress is induced by glucose deprivation (3 h for western blot and the indicated hours for cell viability). Bars: S.E.M. * $p < 0.05$, *** $p < 0.005$, $n = 3$. (E) Basal-dependent (i) and ATP synthase-dependent (ii, + Oligomycin) mitochondrial O_2 consumption rates (OCR) in Pml$^{-/-}$ and Pml$^{+/+}$ MEFs under starvation conditions (glucose deprivation for 1 h). Bars: S.E.M. ** $p < 0.01$, *** $p < 0.005$, $n = 4$.*

Targeting autophagy in Pml null cells rescues chemotherapy-induced cell death

Accumulating evidence has indicated that malignant cells contained in established tumors utilize autophagy to resist chemotherapy-induced cell death. Indeed, solid tumors in particular develop regions of hypoxia and limited nutrient availability in their centers, creating a microenvironment of metabolic stress. Under these hostile conditions, autophagy activation promotes cell survival by providing missing nutrients [303,304]. Accordingly, the inhibition of autophagy augments the response of tumor cells to anticancer drugs [277,305-308]. Therefore, we comparatively determined the sensitivity of $Pml^{+/+}$ and $Pml^{-/-}$ MEFs to the chemotherapeutic agent 5-fluoracil (5-FU). As expected, $Pml^{-/-}$ cells were protected from apoptosis [210,253] compared to WT cells (Figures 27A and 27B). Pharmacological inhibition of autophagy by either 3-methyladenine (3-MA) or the antimalarial drug chloroquine (CQ) (data no shown) alone did not alter cell viability, yet markedly increased apoptosis when combined with 5-FU, and this effect was particular remarkable for $Pml^{-/-}$ MEFs (Figures 27A and 27B).

Next, we explored whether the synergistic effect of CQ and 5-FU was also applicable *in vivo*. Transformed $Pml^{+/+}$ and $Pml^{-/-}$ MEFs were injected subcutaneously into immunodeficient *nu/nu* mice, and the resultant tumor volumes were monitored (Figure 27C). $Pml^{-/-}$ cells exhibited a particularly high tumorigenic potential both *in vitro* and *in vivo* (Figures 27C and 27D), developing tumors that were 10-fold larger than those generated from WT cells.

Compared with the control conditions (PBS), 5-FU treatment slightly suppressed tumor growth, whereas 5-FU combined with CQ greatly reduced the sizes of $Pml^{-/-}$ tumors (Figures 27C and 27D). Genetic inhibition of autophagy (by means of *Becn1* shRNA) in $Pml^{-/-}$ cells reduced their tumorigenic potential and restored their sensitivity to chemotherapy as it reduced tumor development *in vivo* (data no shown).

Intravenous injection of a fluorescent probe (SR-FLIVO) was used for the direct detection of apoptosis-associated caspase activation within the tumors [309]. $Pml^{-/-}$ tumors were completely insensitive to 5-FU-induced apoptosis (Fig. 6E), correlating with elevated signs of autophagy (Figure 27F), yet responded to the combined treatment with 5-FU and CQ by vigorous apoptosis induction (Fig. 27E) and immunoblot-detectable caspase-3 maturation (Figure 27G). Hence elevated autophagy may be responsible for the growth advantage of $Pml^{-/-}$ cancers. Indeed, in colonic adenocarcinoma samples with reduced PML protein expression, levels of LC3 detectable by immunohistochemistry were relatively higher compared to those found in cancer tissues with PML protein abundance (Figure 27H).

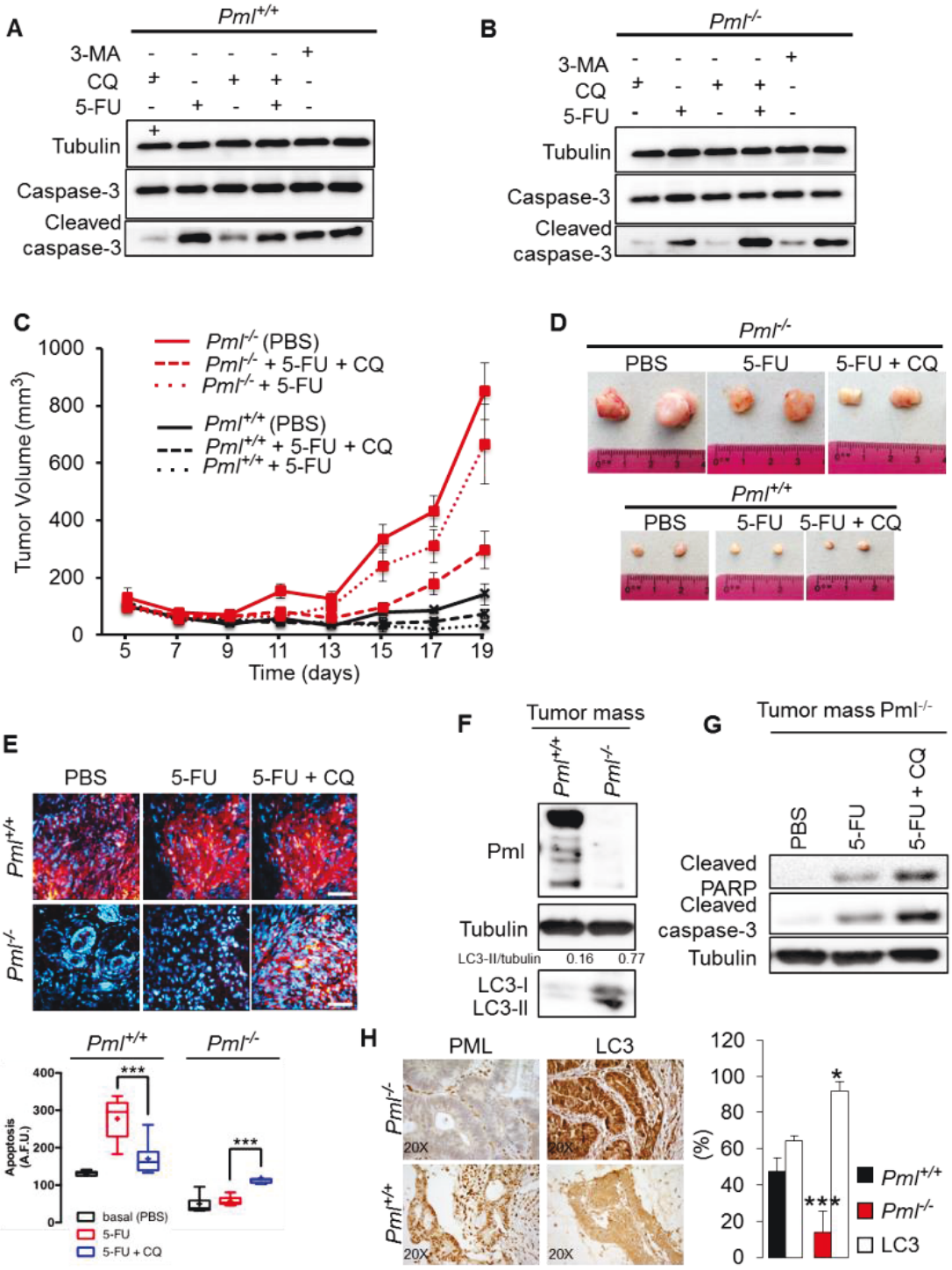

Figure 27 Inhibition of autophagy augments the cytotoxicity of chemotherapy treatment in Pml KO tumors.
*(A)-(B) $Pml^{+/+}$ MEFs are sensitive to 5-fluoracil-induced cell death (5-FU, 25 μM for 16 h), whereas Pml KO cells are resistant. Inhibition of autophagy by treatment with 3-MA (2.5 mM for 16 h) or CQ (5 μM for 16 h) increases apoptosis induced via chemotherapy treatment with 5-FU (25 μM for 16 h) in $Pml^{-/-}$ MEFs. (C) Tumor growth of $Pml^{-/-}$ and $Pml^{+/+}$ transformed MEF xenografts. (D) Representative images of mouse fibrosarcoma xenograft.(E) Analysis of apoptosis based on the intensity of fluorescence (SR-FLIVO) emitted in tumor tissue sections, accompanied by statistical analysis. (cross: average, line: median, box: 25 and 75 percentile, bars: max and min value, *** $p < 0.005$, $n = 3$). Scale bar, 50 μm.(F) Increased levels of autophagy in tumors derived from $Pml^{-/-}$-transformed MEFs as analyzed by immunoblotting. Tumors were excised on day 19 after inoculation. (G) Increased cytotoxicity-chemotherapy effects on $Pml^{-/-}$ tumors after autophagy inhibition.(H) Representative histological sections of human colon cancer immunostained for PML and LC3 accompanied by statistical analysis expressed as percentage of the staining intensity. Bars: S.E.M. * $p < 0.05$, *** $p < 0.005$, $n = 13$. Magnification 20X.*

Discussion

Loss of PML confers a metabolic advantage to cells under nutrient deprivation

Autophagy is an important homeostatic mechanism with a paradoxical dual role: it can function as a cell survival pathway, suppressing apoptosis, or it can lead to death. As a result, the connection between autophagy and apoptosis is complex and affects the treatment of diseases associated with cell death. Alteration of the autophagic machinery is associated with various human disorders, establishing autophagy as a novel therapeutic target (*i.e.*, a novel target for drug development). The connection of autophagy with the development of cancer has been well established, although the exact roles played by this process during various stages of tumor progression are not yet clear and, in some cases, are contradictory.

Here, we provide molecular insight into the acquisition of tumor-promoting behavior due to the loss of the PML protein. *PML* is a tumor suppressor gene that was originally related to the pathogenesis of acute promyelocytic leukemia (APL). However, the loss of PML was later found to be a critical event in various human cancers. We recently identified a new extra-nuclear transcription-independent function of PML in regulating cell survival through changes in Ca^{2+} signaling at ER/MAM contact sites [210]. Accumulating evidence has suggested that ER and MAM domains play a prominent role in autophagy [138,310] and emphasized the important role of IP3R and Ca^{2+} in autophagosome formation [300,311]; therefore, we sought to investigate the role of PML in these processes.

We clearly demonstrated that the localization of PML at the ER-mitochondria contact sites is fundamental not only for apoptosis control but also for autophagy regulation. At these sites, PML represses autophagosome formation and, thus, autophagy induction. We found that the mislocalization of Pml away from MAMs is necessary to activate autophagy in response to stress and that the same mechanism occurs in the absence of p53. Our data demonstrated that p53, which also localizes at ER/MAMs [290], indeed operates as a bridge to maintain the correct localization of Pml. p53 mutants, which are unable to localize to the ER/MAMs and are therefore unable to regulate Ca^{2+} transfer from the ER to the mitochondria [290], cannot preserve PML localization, making them incapable of suppressing autophagy. Restoration of the Ca^{2+} signal in the context of a $Pml^{-/-}$ or $p53^{-/-}$ background restores basal levels of autophagy and, in turn, apoptosis.

In this condition of PML loss, reduced IP3R-mediated Ca^{2+} transfer from the ER to mitochondria results in the activation of AMPK [312], which activates pro-survival autophagy [300] by a mechanism involving mTOR [282] and Ulk-1 pathways [294-296]. In our scenario, PML-deprived cells use enhanced

baseline levels of autophagy to obtain an advantage during metabolic stress conditions. However, what is the mechanism for this action?

Cell lacking Pml due to the inhibition of Ca^{2+} release activity have slightly diminished bioenergetics in terms of mitochondrial respiration and ATP production that are sensed by AMPK, which activates autophagy. Because oxygen and glucose supplies are often low in the tumor microenvironment, autophagy, as catabolic process, is necessary to obtain alternative carbons source to preserve normal cellular bioenergetics [300] and to confer resistance to cell death to Pml KO cells. Lipid or glutamine catabolism is considered the major alternative pathway to provide carbons for mitochondria [313]. PML promotes lipid utilization by fatty acid oxidation [314,315], excluding this pathway as a possible stimulated carbon source when PML is lost. Furthermore, autophagy can sustain mitochondrial respiration in a glutamine metabolism-dependent manner [316,317]. Thus, we could speculate that in the absence of Pml, stimulated glutamine catabolism by autophagy is used as an alternative pathway to sustain mitochondrial activity and, thus, cell survival during stress conditions.

As recent studies have suggested that autophagy represents an important mechanism of resistance to cancer treatments, we further investigated the cross-talk between autophagy and Pml-related cell death in *in vivo* models. We observed that the absence of Pml promotes tumor development associated with resistance to anticancer drugs due to increased autophagy levels in the tumor. Treatment with the autophagy inhibitors 3-MA and CQ restored chemotherapy-related apoptosis. Therefore, our findings hold therapeutic implications for the treatment of solid tumors associated with PML down-regulation.

Future perspectives

There is emerging evidence that autophagy is not only involved in the intracellular degradation of damaged proteins, but also plays an important role in nonclassical protein secretion. In particular, autophagy plays a critical role in the secretion of proinflammatory cytokines, such as the mammalian pro-inflammatory cytokines IL-1β and IL-18 [318,319]. IL1β is a cytokine that promotes inflammation, angiogenesis, and tissue remodeling [320]. Cleaved by CASP1 (caspase 1, apoptosis-related cysteine peptidase) to an active form by an NLRP3 (NLR family,pyrin domain containing 3) inflammasome complex, IL1β lacks a signal peptide and is released to the extracellular matrix via autophagosomes [318]. In particular it has been recently demonstrated that autophagy directly regulates IL-1β secretion and that mature IL-1β localized to the lumen of the membrane in early intermediates and mature autophagosomes [321]. The exact route by which the autophagosome delivers mature IL-1β to the cell surface as well as how it avoids fusion with degradative lysosome remains obscure, however fusion of the autophagosome directly with the plasma membrane would lead to the release of soluble IL-1β available to trigger an inflammatory response in the surrounding tissue.

Inflammasomes are molecular platforms activated upon cellular stress or infection that trigger the maturation of proinflammatory cytokines such as IL-1β to engage innate immune defenses.

The NLRP3 inflammasome is currently the most fully characterized inflammasome and consists of the NLRP3 scaffold, the ASC (PYCARD) adaptor and caspase-1[151]. NLRP3 is activated upon exposure to whole pathogens, as well as a number of structurally diverse PAMPs, DAMPs, and environmental irritants. Resting NLRP3 localizes to endoplasmic reticulum structures, whereas on inflammasome activation both NLRP3 and its adaptor ASC redistribute to the perinuclear space where they co-localize with ER and mitochondria organelle clusters [149].

These observations lead us to speculate about a possible role of PML protein in inflammatory process.

During my Phd we provide evidence that the localization of PML at the ER-mitochondria contact sites is fundamental not only for apoptosis control but also for autophagy regulation, repressing at these sites autophagosome formation and, thus, autophagy induction. We demonstrated that there is an increased autophagosome biogenesis in the absence of Pml (Figures 21F) and that the mislocalization of PML away from MAMs is necessary to activate autophagy in response to stress.

Given the interplay between autophagosome formation, IL-1β release and the NLRP3 inflammasome localization at the ER/MAMs, we wondering if PML could regulate NLRP3 inflammasome activation.

Although a role of PML in the regulation of inflammation has been recently suggested, the molecular pathway is far to be elucidated.

A recent study demonstrated that PML is a negative regulator of ASC protein, attenuating inflammasome activation by retaining ASC in the nucleus, acting to limit its function [322]. PML deficiency enhances the formation of ASC dimers in response to NLRP3 activation and also increases the cytoplasmic localization of ASC. The study confirms an interaction between PML and the NLRP3 inflammasome, however the precise role of PML in NLRP3 inflammasome formation and activation has not been identifyed yet.

Preliminary results obtained in the last part of my PhD show that in absence of PML, NLRP3 components redistribute at MAMs upon NLRP3 inflammasome activation (data not shown). This leads to enhanced levels of IL-1β in response to inflammasome activation in PML deficient macrophages, but no differences in IL-6 or TNF release (data not shown), suggesting a specific involvement of the NLRP3 inflammasome.

These preliminary data suggest a critical function of PML in the regulation of NLRP3 inflammasome and confirm the pivotal role played by MAMs in many cellular processes.

Because inflammatory cytokines such as IL-1β play an essential role in pathogenesis of cancers, the role of NLRP3 inflammasome in cancer and anti-tumor immune response is becoming a focus of investigations. We propose to study the critical function of PML in the tumor progression through an activation of NLRP3 inflammasome.

Materials and methods

Cell Culture, Transfection, and Detection of Cell Death.

Primary MEFs were prepared from embryos at day 13.5 of development (E13.5). Early passage (P2–P5) MEFs, grown in DMEM supplemented with 10% (vol/vol) FBS, were used in all experiments. MEFs were transfected with different constructs using the MicroPorator (Digital Bio). MEFs were transformed with SV40 large T antigen

HCT-116 cells were grown in McCoy's medium supplemented with 10% (vol/vol) FBS, 1% penicillin/streptomycin, and 1% (vol/vol) L-glutamine and transfected using a standard calcium phosphate procedure.

H1299 cells were grown in DMEM supplemented with 10% (vol/vol) FBS and transfected using a standard calcium phosphate procedure.

MDA-MD 468 cells were grown in DMEM supplemented with 10% (vol/vol) FBS and infected with adenovirus expressing a mitochondria-targeted aequorin chimera.

MEF, HCT-116, and MDA-MD 468 cells were treated with 1 μM ADRIA for 6 h, 10 μg/mL α-amanitin for 6 h, and 15 μM pifithrin α for 30 min.

Aequorin Measurements

Cells grown on 13-mm-round glass coverslips at 50% confluence were transfected with the appropriate cytosolic (cyt), mitochondrial (mt), or endoplasmic reticulum (er) targeted aequorin (Aeq) chimeras alone or together with expression constructs ER-p53, WT p53, or p53-ΔNLS. All aequorin measurements were performed in KRB. Agonists and other drugs were added to the medium as specified in the figure legends. The experiments were terminated by lysing the cells with 100 μM digitonin in a hypotonic Ca^{2+}-rich solution (10 mM CaCl2 in H2O), thus discharging the remaining aequorin pool. The light signal was collected and calibrated into [Ca^{2+}] values, as previously described [222]. In the experiments using permeabilized cells, a buffer mimicking the cytosolic ionic composition (intracellular buffer) was used: 130 mM KCl, 10 mM NaCl, 0.5 mM K2HPO4, 5 mM succinic acid, 1 mM MgSO4, 3 mM MgCl2, 20 mM Hepes, 1 mM pyruvate, 0.5 mM ATP, and 0.1 mM ADP (pH 7 at 37 °C). The intracellular buffer was supplemented with either 100 μM EGTA (intracellular buffer/EGTA) or 2 mM EGTA plus 2 mM Hydroxy-2-ethylenediaminetriacetic acid (HEEDTA)-buffered [Ca^{2+}] of 1 or 4 μM (intracellular buffer/Ca^{2+}), as calculated with Chelator software [323]. MEF cells were permeabilized by a 1-min perfusion with 50 μM digitonin (added to the intracellular buffer/EGTA) during the luminescence measurements.

The mitochondrial Ca^{2+} uptake rate was calculated as the first derivative by using OriginLab software. The higher value reached during Ca^{2+} addition represents the maximal Ca^{2+} uptake rate.

Fura-2 Measurements

The cytosolic Ca^{2+} response was evaluated using the fluorescent Ca^{2+} indicator Fura-2 AM (Life Technologies, Invitrogen). MEF cells were grown on 24-mm coverslips and incubated at 37 °C for 30 min in 1 mM Ca^{2+}/KRB supplemented with 2.5 mM Fura-2 AM, 0.02% Pluronic F-68 (SigmaAldrich), and 0.1 mM sulfinpyrazone (Sigma-Aldrich). The cells were then washed and supplemented with 1 mM Ca2+/KRB. To determine the cytosolic Ca^{2+} response, the cells were placed in an open Leyden chamber on a 37-°C thermostat-controlled stage and exposed to 340 nm/380 nm wavelength light using the Olympus xcellence multiple-wavelength high-resolution fluorescence microscopy system equipped with an ORCA ER CCD camera (Hamamatsu Photonics) and an Uplan FLN 40× oil objective (Olympus). The fluorescence data collected are expressed as emission ratios

FRET-Based Measurements of ER Ca^{2+}.

Single-cell measurements of ER luminal Ca^{2+} were performed in MEF cells transfected with D1ER-YC 4.3. After 36 h, the cells were imaged on an Axiovert 100TV microscope equipped with the Optosplit dual view system (Cairn Research) and the Evolve 512 EMCCD camera (Photometrics). D1ER-YC 4.3 was excited through an ET436/ 20× band-pass filter and emission was collected through a 63× plan apochromatic oil immersion, N.A. 1.4 (Zeiss). Emission light was split into two camera sensors through a T510 LPXR dichroic mirror and further separated through ET485/32 m and ET535/30 m band-pass filters for Cyan and FRET, respectively (filters and dichroic mirror were from Chroma). The fluorescence images were corrected for background and fluorescence bleed-through. The exposure time was typically 10 ms, and images were collected every 15 s. A ratiometric image was generated offline using the open-source software ImageJ (NIH), and the average ratio values were collected on an Excel spreadsheet. Ratiometric measurements were then normalized to the smallest value of the entire kinetic measurement

Subcellular Fractionation

Fractionations were performed as described [115,117]. IP3R, laminin, tubulin, and VDAC were used as markers. ER, endoplasmic reticulum; MAMs, mitochondria-associated membranes; C, cytosol.

Mitochondrial Morphology Analysis

Cells were seeded at 50,000 cells on 25-mm coverslips, allowed to grow for 24 h, and then infected with a GFP targeted to the mitochondria inserted in an adenoviral vector (Ad-mtGFP). After 36 h, the cells were treated as described and then imaged with a Nikon Swept Field confocal equipped with CFI Plan Apo VC60XH objective (N.A. 1.4) and an Andor DU885 EMCCD camera. Coverslips were placed in an incubated chamber with controlled temperature, CO2, and humidity, and then z stacks were acquired in 21 planes with a 0.6-mm distance to allow acquisition of the whole cell. Morphometric parameters were calculated on the best focused plane with NIS Elements (Nikon), and isosurface rendering and volume measurements were obtained with the 4D tools of MetaMorph (Universal Imaging)

Immunolocalization of p53 Protein

Cells (MEFs and HCT- 116) were fixed in 3.7% formaldehyde in PBS for 20 min, washed three times with PBS, and then incubated for 10 min in PBS supplemented with 50 mM NH4Cl. Permeabilization of cell membranes was accomplished with a 5-min incubation with 0.1% Triton X-100 in PBS, followed by a 1-h wash with 2% BSA in PBS. The cells were then incubated overnight at 37 °C in a wet chamber with a mouse anti-p53 antibody (1C12; Cell Signaling) diluted 1:50 with 2% BSA in PBS. Staining was then performed with Alexa 633 rabbit anti-mouse secondary antibodies. After each antibody incubation, the cells were washed four times with PBS. Images were acquired using an Axiovert 200M fluorescence microscope (Zeiss) equipped with 63× oil or 40× water immersion objectives (Zeiss) and a CoolSNAP HQ camera (Photometrics). Fifty-one planes along the z axis were acquired for each field, and the axial and lateral resolutions were established according to the Nyqist rate; then, 3D digital deconvolution was performed using the open-source software Fiji (fiji.sc/fiji). After deconvolution, colocalization between the Sec61-GFP and p53 signals was observed using the center-based object method in the JACoP plugin (rsb.info.nih.gov/ij/plugins/track/jacop.html).

Western blot

A total of 30 μg of protein was separated by SDS/PAGE, transferred onto a nitrocellulose membrane, and probed using the following antibodies: PML anti-mouse (1:1000) from Chemicon (Merck Millipore, Billerica, MA, USA); β-tubulin (1:3000), MCU (1:1000), p62 (1:3000), Sigma-1R (1:1000) and STX17 (1:1000) from Sigma-Aldrich (Saint Louis, MO, USA); Atg14 (1:500) from MBL (Woburn, MA); anti-cytochrome c (1:1,000) and IP3R3 (1:1000) from BD Biosciences (San Jose, CA, USA); ACC (1:1000), pACC (1:1000), AMPK (1:1000), pAMPK (1:1000), Beclin-

1 (1:1000), Caspase-3 (1:500), GAPDH (1:6000), LC3-B (1:1000), mTOR (1:1000), p-mTOR (1:1000), mouse-p53 (1:1000), p70S6 Kinase (1:1000), p-p70S6 kinase (1:1000), PARP (1:1000), ULK1 (1:1000) and pULK1Ser317 (1:1000) from Cell Signaling (Danvers, MA, USA); laminin (1:1,000), panVDAC (1:5,000) and SERCA 2b (1:500) from Abcam; p53 DO-1 (1:500) and PML anti-human (1:500) from Santa Cruz (Santa Cruz, CA, USA); H-Ras antiserum (1:1000) from Novus Biologicals (Littleton, CO, USA). Isotype-matched horseradish peroxidaseconjugated secondary antibodies were used, followed by detection using chemiluminescence (PerkinElmer).

Transformation assays and in vivo tumorigenicity

Low-passage MEF clones infected with H-RASV12 or H-RasV12 + p53 wt were resuspended in DMEM that was supplemented with 10% fetal bovine serum, penicillin (100 IU/ml) and streptomycin (100 IU/ml) and that contained 0.3% agarose. Then, the cells were plated on top of 1% agarose in the same medium at a cell density of 1 X 105 for each 60 mm plate. Colonies reaching at least 100 μm were scored after 14 days in culture. These experiments were performed in triplicate.

To assess the tumorigenicity of H-RASV12-infected MEFs, 1 X 10^6 cells were injected subcutaneously on both sides of athymic mice, and tumors were excised after 2 weeks.

Dorsal skinfold chamber and intravital microscopy

Dorsal skin-fold chambers were transplanted onto 7-week-old female athymic mice (Harlan). A cell pellet containing 10^6 tumor cells was placed onto the tissue surface (drop-on method) at three days post-surgery. Intravital microscopy analyses were performed two weeks after cell inoculation as follows: the mice were anesthetized by halothane and transferred to a custom-made warmed plate mounted on the stage of an upright spinning disk confocal system microscope (Olympus DSU) equipped with a water immersion objective (Fluor 40x, 1.0 N.A., Nikon) for observation.

Autophagy induction and inhibition

The autophagic process in vitro was triggered as follows: serum deprivation (EBSS, 1 h), glucose deprivation (1 h), rapamycin treatment (100 nM, 24 h in DMEM supplemented with 10% FBS), and lithium treatment (10 mM, 24 h in DMEM supplemented with FBS). The pharmacological inhibition of autophagic machinery was performed by treating cells with 2.5 mM 3-MA (16 h) or 5 μM CQ (16 h) in DMEM supplemented with 10% FBS. After treatment, the cells were fixed or lysed to detect the amount of autophagosome vesicles by fluorescence microscopy (with the

employment of the GFP-LC3 plasmid) or by immunoblot analysis (using LC3 antibody) (Klionsky et al., 2012; Mizushima et al., 2010).

Genetically inhibition of autophagy was performed using shRNA targeting Beclin1 (psirna42-mbeclin) (Invitrogen). We generated clones stably expressing shRNA beclin1 by culturing transfected cells in the presence of zeocin (500 ug/ml, added 48 h after transfection) for 3 weeks. Stable shRNABeclin1 clones were kept in the continuous presence of 50 ug/ml zeocin (Invitrogen).

For in vivo studies on the effects of starvation, mice were deprived of food for 24 h. The mice had free access to drinking water. After killing the mice, their tissues were processed and immunoblotted.

Analysis of autophagic flux

Primary $Pml^{+/+}$ and $Pml^{-/-}$ MEFs were treated either with autophagy inhibitor NH4Cl (20 μM) or bafilomycin A1 (BafA1, SIGMA) (100 nM) in complete DMEM medium (FBS 10%). After 2 h, the cells were collected, lysed and subjected to immunoblot [324]

For determination of autophagic flux lysosomal activity in vivo was blocked by intraperitoneal administration of 40 mg/kg body weight of leupeptin (Sigma) in saline solution. Control animals were injected with an equivalent volume of saline solution. Four hours after injection the animals were euthanized and the livers isolated.

Measurements of mitochondrial membrane potential (Ψm)

Ψm was assessed by loading cells with 10 nM tetramethyl rhodamine methyl ester (TMRM; Life Technologies, T-668) for 35 min at 37°C in KRB supplemented with 1 mM CaCl2. Images were acquired using an inverted microscope (Nikon LiveScan Swept Field Confocal Microscope Eclipse Ti equipped with NIS-Elements microscope imaging software and 40X oil immersion lens, Nikon Instruments). TMRM excitation was performed at 560 nm, and emission was collected through a 590 to 650 nm band-pass filter. After 2 min, KRB medium was exchanged with KRB without glucose. Images were acquired every 30 sec with a fixed 20 ms exposure time. FCCP (carbonyl cyanide p-trifluoromethoxyphenylhydrazone, 10 μM), an uncoupler of oxidative phosphorylation, was added after 30 acquisitions to completely collapse the electrical gradient established by the respiratory chain.

Cell proliferation and viability assay

Cells seeded in 6-well plates in triplicate and allowed to grow to 80% confluence were exposed to glucose deprivation for different time points (0, 1, 3 and 5h). Next, cells were centrifuged, washed

with PBS and the cell number was determined using a Tali™ image-based cytometer (Life Technologies). The data are presented as a histogram showing the percentage of the cell number referred to the control condition.

Cell survival assay

Cells seeded in 12-well plates in triplicate and allowed to grow to 80% confluence were treated with vehicle (positive control), 25 μM 5-FU, 5 μM CQ or 25 μM 5-FU and 5 μM CQ. After 48 h, the cells were washed with PBS, fixed in 4% paraformaldehyde and stained with 0.1% crystal violet. Crystal violet was dissolved with 1 mol/l acetic acid, and absorbance at 595 nm was measured.

Wound healing assay

$Pml^{+/+}$ and $Pml^{-/-}$ MEFs seeded in 6-well plates and grown to 90% confluence, 1 h before wounding, were treated with vehicle (positive control), 25 μM 5-FU, 5 μM CQ or 25 μM 5-FU and 5 μM CQ. The cell monolayer was wounded with a P200 pipette tip. Cells were monitored and captured by phase-contrast microscopy (a Leica phase-contrast microscope equipped with an ICC50 HD camera and a 4X objective). Then, the percentage of the open scratched area was measured using the Wound Healing Tool available in the software Fiji. Five replicates each of three independent experiments were performed.

Migration assay

In vitro cell migration assays were performed using Costar Transwell permeable polycarbonate supports (8.0 mm pores) in 24-well plates (Corning Inc.). Before seeding (1×10^5 $Pml^{+/+}$ and $Pml^{-/-}$ MEFs), the lower compartment was incubated with DMEM plus 10% FBS supplemented with vehicle (positive control), 25 μM 5-FU, 5 μM CQ or 25 μM 5-FU and 5 μM CQ. Non-migrated cells were removed using a cotton swab, and migrated cells were fixed and stained with crystal violet. The migratory cells of five fields were imaged under a Leica phase-contrast microscope equipped with an ICC50 HD camera and a 4X objective. The average number of migrating cells was calculated from the total number of cells counted per chamber using the Cell Counter plugin available in the software ImageJ.

Mouse treatment studies

Procedures involving animals and their care were in conformity with institutional guidelines, and all experimental protocols were approved by the Animal Ethics Committee. Mice were housed in a

temperature-controlled environment with 12 h light/dark cycles and received food and water *ad libitum*. Seven-week-old female athymic mice were housed and handled under aseptic conditions. Tumor xenografts were obtained by implanting female nude mice subcutaneously 5 x 10^6 transformed $Pml^{+/+}$ and $Pml^{-/-}$ MEFs in 50% of Matrigel (BD Biosciences). Tumor growth was monitored daily and tumor volumes were measured every other day with calipers using the following equation: Volume = π/6 x (a x b2), where a is the minor diameter and b is the major diameter. The mice were divided into the treatment groups and the control group, with 10 mice per group. After five days, the treatments were initiated as follows: (a) PBS group, animals received intraperitoneal (i.p.) injections of 100 µl PBS every day; (b) 5-FU group, animals received i.p. injections of 30 mg/kg 5FU in 100 µl PBS twice weekly; (c) 5-FU + chloroquine (CQ) group, animals received i.p. injections of 30 mg/kg 5-FU twice weekly and 60 mg/kg CQ in 100 µl PBS every day; and (d) CQ group, animals received i.p. injections of 60 mg/kg CQ in 100 µl PBS every day. After 2 weeks of treatment, all mice were sacrificed, and tumors were immunoblotted.

Detection of cell death in vivo

After an i.v. injection of 100 µl SR-FLIVO™ (Immunochemistry Technologies) via the lateral tail vein, the FLIVO reagent was allowed to circulate in the mouse for 30 min before the sacrifice. The tumors were excised, frozen, sectioned and stained for nuclei using DRAQ5 according to the manufacturer's protocol (Cell Signaling). After staining, the samples were mounted on coverslips and analyzed using a Zeiss LSM 510 confocal microscope equipped with an objective Fluor 40X/1.30 Oil. Images were background corrected, and signals were analyzed using open source Fiji software (available at http://fiji.sc/Fiji).

Tissue processing

$Pml^{+/+}$ and *$Pml^{-/-}$* mice were bred and maintained according to both the Federation for Laboratory Animal Science Associations and the Animal Experimental Ethics Committee guidelines. The mice were housed in a temperature-controlled environment with 12 h light/dark cycles and received food and water *ad libitum*. For studies on the effects of starvation, mice were deprived of food for 24 h. The mice had free access to drinking water. After killing the mice, their livers were homogenized in 20 mM Tris buffer (pH 7.4) containing 150 mM NaCl, 1% Triton X-100, 10 mM EDTA and protease inhibitor cocktail. Then, tissue extracts were centrifuged at 12,000 × g at 4°C for 10 min. Finally, protein extracts (20 µg each) were subjected to SDS-PAGE and immunoblotting. Mouse muscles were ground by mortar and pestle and lysed in a buffer containing 50 mM Tris (pH 7.5), 150 mM NaCl, 10 mM $MgCl_2$, 0.5 mM DTT, 1 mM EDTA, 10% glycerol, 2% SDS, 1% Triton X-

100, Roche Complete Protease Inhibitor Cocktail, 1 mM PMSF, 1 mM $NaVO_3$, 5 mM NaF and 3 mM β-glycerophosphate. Then, tissue extracts were centrifuged at 12,000 × g at 4°C for 10 min. Finally, protein extracts (20 μg each) were subjected to SDS-PAGE and immunoblotting. Mice tumors were excised and homogenized in lysis buffer (300 mM sucrose, 1 mM K_2HPO_4, 5.5 mM D-glucose, 20 mM Hepes, 1 mM phenylmethylsulfonylfluoride, and 0.5% IGEPAL) with a Potter pestle. Then, were centrifuged at 12,000 × g at 4°C for 15 min. Finally, protein extracts (20 μg each) were subjected to SDS-PAGE and immunoblotting.

XF bioenergetic analysis

OCRs in *Pml*$^{+/+}$ and *Pml*$^{-/-}$ MEFs were measured using a Seahorse XF96 instrument (Seahorse Biosciences, North Billerica, MA) according to the manufacturer's protocols. MEFs were seeded in a XF96 microplate at a density of 15,000 cells per well and allowed to attach. The following day, the medium was exchanged, where indicated, with 175 μl unbuffered XF assay media at pH 7.4 (Seahorse Biosciences) supplemented with 5.5 mM glucose (Sigma), 1 mM sodium pyruvate and 1 mM glutamine or with 175 μl unbuffered XF assay media at pH 7.4 (Seahorse Biosciences) without glucose, sodium pyruvate or glutamine. Then, the microplate was placed in a 37°C non-CO_2 incubator for 60 min. Respiration was measured in four blocks of three for 3 min each. The first block measured the basal respiration rate. Next, 1 μm oligomycin (Seahorse Biosciences, North Billerica, MA) was added to inhibit complex V, and the second block was measured. Then, 1 μm FCCP (Seahorse Biosciences, North Billerica, MA) was added to uncouple respiration, and the third block was measured. Finally, 1 μm antimycin A (Seahorse Biosciences, North Billerica, MA) and 1 μm rotenone (Seahorse Biosciences, North Billerica, MA) were added to inhibit complex III, and the last measurements were performed. Immediately after finishing the measurements, the cells were washed with PBS, fixed in 4% paraformaldehyde and stained with 0.1% crystal violet. Crystal violet was dissolved with 1 mol/l acetic acid, and absorbance at 595 nm was measured as an index of cell amount.

References

1. Berridge, M.J., Lipp, P. & Bootman, M.D. The versatility and universality of calcium signalling. *Nature reviews. Molecular cell biology* **1**, 11-21 (2000).
2. Rizzuto, R. & Pozzan, T. When calcium goes wrong: genetic alterations of a ubiquitous signaling route. *Nature genetics* **34**, 135-141 (2003).
3. Roderick, H.L. & Cook, S.J. Ca2+ signalling checkpoints in cancer: remodelling Ca2+ for cancer cell proliferation and survival. *Nature reviews. Cancer* **8**, 361-375 (2008).
4. Berridge, M.J., Bootman, M.D. & Roderick, H.L. Calcium signalling: dynamics, homeostasis and remodelling. *Nature reviews. Molecular cell biology* **4**, 517-529 (2003).
5. Rizzuto, R.*, et al.* Ca(2+) transfer from the ER to mitochondria: when, how and why. *Biochimica et biophysica acta* **1787**, 1342-1351 (2009).
6. Brini, M. & Carafoli, E. Calcium pumps in health and disease. *Physiological reviews* **89**, 1341-1378 (2009).
7. Blaustein, M.P. & Lederer, W.J. Sodium/calcium exchange: its physiological implications. *Physiological reviews* **79**, 763-854 (1999).
8. Bertolino, M. & Llinas, R.R. The central role of voltage-activated and receptor-operated calcium channels in neuronal cells. *Annual review of pharmacology and toxicology* **32**, 399-421 (1992).
9. McFadzean, I. & Gibson, A. The developing relationship between receptor-operated and store-operated calcium channels in smooth muscle. *British journal of pharmacology* **135**, 1-13 (2002).
10. Meldolesi, J. & Pozzan, T. Pathways of Ca2+ influx at the plasma membrane: voltage-, receptor-, and second messenger-operated channels. *Experimental cell research* **171**, 271-283 (1987).
11. Foskett, J.K., White, C., Cheung, K.H. & Mak, D.O. Inositol trisphosphate receptor Ca2+ release channels. *Physiological reviews* **87**, 593-658 (2007).
12. Sutko, J.L. & Airey, J.A. Ryanodine receptor Ca2+ release channels: does diversity in form equal diversity in function? *Physiological reviews* **76**, 1027-1071 (1996).
13. Patel, S., Joseph, S.K. & Thomas, A.P. Molecular properties of inositol 1,4,5-trisphosphate receptors. *Cell calcium* **25**, 247-264 (1999).
14. Patterson, R.L., Boehning, D. & Snyder, S.H. Inositol 1,4,5-trisphosphate receptors as signal integrators. *Annual review of biochemistry* **73**, 437-465 (2004).
15. Berridge, M.J. Calcium microdomains: organization and function. *Cell calcium* **40**, 405-412 (2006).
16. Berridge, M.J. Inositol trisphosphate and calcium signalling mechanisms. *Biochimica et biophysica acta* **1793**, 933-940 (2009).
17. John, L.M., Lechleiter, J.D. & Camacho, P. Differential modulation of SERCA2 isoforms by calreticulin. *The Journal of cell biology* **142**, 963-973 (1998).
18. Varnai, P., Hunyady, L. & Balla, T. STIM and Orai: the long-awaited constituents of store-operated calcium entry. *Trends in pharmacological sciences* **30**, 118-128 (2009).
19. Saris, N.E. & Carafoli, E. A historical review of cellular calcium handling, with emphasis on mitochondria. *Biochemistry. Biokhimiia* **70**, 187-194 (2005).
20. Pinton, P., Pozzan, T. & Rizzuto, R. The Golgi apparatus is an inositol 1,4,5-trisphosphate-sensitive Ca2+ store, with functional properties distinct from those of the endoplasmic reticulum. *The EMBO journal* **17**, 5298-5308 (1998).
21. Mitchell, K.J.*, et al.* Dense core secretory vesicles revealed as a dynamic Ca(2+) store in neuroendocrine cells with a vesicle-associated membrane protein aequorin chimaera. *The Journal of cell biology* **155**, 41-51 (2001).

22. Rodriguez, A., Webster, P., Ortego, J. & Andrews, N.W. Lysosomes behave as Ca2+-regulated exocytic vesicles in fibroblasts and epithelial cells. *The Journal of cell biology* **137**, 93-104 (1997).
23. Gerasimenko, J.V., Tepikin, A.V., Petersen, O.H. & Gerasimenko, O.V. Calcium uptake via endocytosis with rapid release from acidifying endosomes. *Current biology : CB* **8**, 1335-1338 (1998).
24. Drago, I., Giacomello, M., Pizzo, P. & Pozzan, T. Calcium dynamics in the peroxisomal lumen of living cells. *The Journal of biological chemistry* **283**, 14384-14390 (2008).
25. Lasorsa, F.M.*, et al.* Peroxisomes as novel players in cell calcium homeostasis. *The Journal of biological chemistry* **283**, 15300-15308 (2008).
26. Rizzuto, R. & Pozzan, T. Microdomains of intracellular Ca2+: molecular determinants and functional consequences. *Physiological reviews* **86**, 369-408 (2006).
27. Carafoli, E. Historical review: mitochondria and calcium: ups and downs of an unusual relationship. *Trends in biochemical sciences* **28**, 175-181 (2003).
28. Mitchell, P. Chemiosmotic coupling in oxidative and photosynthetic phosphorylation. *Biol Rev Camb Philos Soc* **41**, 445-502 (1966).
29. Rizzuto, R., Simpson, A.W., Brini, M. & Pozzan, T. Rapid changes of mitochondrial Ca2+ revealed by specifically targeted recombinant aequorin. *Nature* **358**, 325-327 (1992).
30. Rizzuto, R., Brini, M., Murgia, M. & Pozzan, T. Microdomains with high Ca2+ close to IP3-sensitive channels that are sensed by neighboring mitochondria. *Science* **262**, 744-747 (1993).
31. Csordas, G., Thomas, A.P. & Hajnoczky, G. Quasi-synaptic calcium signal transmission between endoplasmic reticulum and mitochondria. *EMBO J* **18**, 96-108 (1999).
32. Palmer, A.E. & Tsien, R.Y. Measuring calcium signaling using genetically targetable fluorescent indicators. *Nat Protoc* **1**, 1057-1065 (2006).
33. Rizzuto, R.*, et al.* Close contacts with the endoplasmic reticulum as determinants of mitochondrial Ca2+ responses. *Science* **280**, 1763-1766 (1998).
34. Giacomello, M.*, et al.* Ca2+ hot spots on the mitochondrial surface are generated by Ca2+ mobilization from stores, but not by activation of store-operated Ca2+ channels. *Mol Cell* **38**, 280-290 (2010).
35. Palmer, A.E.*, et al.* Ca2+ indicators based on computationally redesigned calmodulin-peptide pairs. *Chemistry & biology* **13**, 521-530 (2006).
36. Csordas, G.*, et al.* Imaging interorganelle contacts and local calcium dynamics at the ER-mitochondrial interface. *Mol Cell* **39**, 121-132 (2010).
37. Inoue, T., Heo, W.D., Grimley, J.S., Wandless, T.J. & Meyer, T. An inducible translocation strategy to rapidly activate and inhibit small GTPase signaling pathways. *Nat Methods* **2**, 415-418 (2005).
38. Patergnani, S.*, et al.* Calcium signaling around Mitochondria Associated Membranes (MAMs). *Cell communication and signaling : CCS* **9**, 19 (2011).
39. Voeltz, G.K., Prinz, W.A., Shibata, Y., Rist, J.M. & Rapoport, T.A. A class of membrane proteins shaping the tubular endoplasmic reticulum. *Cell* **124**, 573-586 (2006).
40. Shibata, Y., Voeltz, G.K. & Rapoport, T.A. Rough sheets and smooth tubules. *Cell* **126**, 435-439 (2006).
41. English, A.R., Zurek, N. & Voeltz, G.K. Peripheral ER structure and function. *Curr Opin Cell Biol* **21**, 596-602 (2009).
42. Shibata, Y.*, et al.* Mechanisms determining the morphology of the peripheral ER. *Cell* **143**, 774-788 (2010).
43. Chevet, E., Cameron, P.H., Pelletier, M.F., Thomas, D.Y. & Bergeron, J.J. The endoplasmic reticulum: integration of protein folding, quality control, signaling and degradation. *Curr Opin Struct Biol* **11**, 120-124 (2001).

44. Palade, G. Intracellular aspects of the process of protein synthesis. *Science* **189**, 347-358 (1975).
45. Bootman, M.D., Petersen, O.H. & Verkhratsky, A. The endoplasmic reticulum is a focal point for co-ordination of cellular activity. *Cell Calcium* **32**, 231-234 (2002).
46. Verkhratsky, A. & Petersen, O.H. The endoplasmic reticulum as an integrating signalling organelle: from neuronal signalling to neuronal death. *Eur J Pharmacol* **447**, 141-154 (2002).
47. Jobsis, F.F. & O'Connor, M.J. Calcium release and reabsorption in the sartorius muscle of the toad. *Biochem Biophys Res Commun* **25**, 246-252 (1966).
48. Ridgway, E.B. & Ashley, C.C. Calcium transients in single muscle fibers. *Biochem Biophys Res Commun* **29**, 229-234 (1967).
49. Ashley, C.C. & Ridgway, E.B. On the relationships between membrane potential, calcium transient and tension in single barnacle muscle fibres. *J Physiol* **209**, 105-130 (1970).
50. MacKrill, J.J. Protein-protein interactions in intracellular Ca2+-release channel function. *Biochem J* **337 (Pt 3)**, 345-361 (1999).
51. Rebecchi, M.J. & Pentyala, S.N. Structure, function, and control of phosphoinositide-specific phospholipase C. *Physiol Rev* **80**, 1291-1335 (2000).
52. Litjens, T.*, et al.* Phospholipase C-gamma1 is required for the activation of store-operated Ca2+ channels in liver cells. *Biochem J* **405**, 269-276 (2007).
53. Iwai, M.*, et al.* Molecular cloning of mouse type 2 and type 3 inositol 1,4,5-trisphosphate receptors and identification of a novel type 2 receptor splice variant. *J Biol Chem* **280**, 10305-10317 (2005).
54. Mikoshiba, K. IP3 receptor/Ca2+ channel: from discovery to new signaling concepts. *J Neurochem* **102**, 1426-1446 (2007).
55. Iwai, M., Michikawa, T., Bosanac, I., Ikura, M. & Mikoshiba, K. Molecular basis of the isoform-specific ligand-binding affinity of inositol 1,4,5-trisphosphate receptors. *J Biol Chem* **282**, 12755-12764 (2007).
56. Parker, I., Choi, J. & Yao, Y. Elementary events of InsP3-induced Ca2+ liberation in Xenopus oocytes: hot spots, puffs and blips. *Cell Calcium* **20**, 105-121 (1996).
57. Rooney, T.A. & Thomas, A.P. Intracellular calcium waves generated by Ins(1,4,5)P3-dependent mechanisms. *Cell Calcium* **14**, 674-690 (1993).
58. Allbritton, N.L. & Meyer, T. Localized calcium spikes and propagating calcium waves. *Cell Calcium* **14**, 691-697 (1993).
59. Hirata, M., Suematsu, E., Hashimoto, T., Hamachi, T. & Koga, T. Release of Ca2+ from a non-mitochondrial store site in peritoneal macrophages treated with saponin by inositol 1,4,5-trisphosphate. *Biochem J* **223**, 229-236 (1984).
60. Iino, M. Biphasic Ca2+ dependence of inositol 1,4,5-trisphosphate-induced Ca release in smooth muscle cells of the guinea pig taenia caeci. *J Gen Physiol* **95**, 1103-1122 (1990).
61. Missiaen, L., Taylor, C.W. & Berridge, M.J. Luminal Ca2+ promoting spontaneous Ca2+ release from inositol trisphosphate-sensitive stores in rat hepatocytes. *J Physiol* **455**, 623-640 (1992).
62. Hajnoczky, G., Hager, R. & Thomas, A.P. Mitochondria suppress local feedback activation of inositol 1,4, 5-trisphosphate receptors by Ca2+. *J Biol Chem* **274**, 14157-14162 (1999).
63. Smith, J.B., Smith, L. & Higgins, B.L. Temperature and nucleotide dependence of calcium release by myo-inositol 1,4,5-trisphosphate in cultured vascular smooth muscle cells. *J Biol Chem* **260**, 14413-14416 (1985).
64. Bezprozvanny, I. & Ehrlich, B.E. ATP modulates the function of inositol 1,4,5-trisphosphate-gated channels at two sites. *Neuron* **10**, 1175-1184 (1993).
65. Iino, M. Effects of adenine nucleotides on inositol 1,4,5-trisphosphate-induced calcium release in vascular smooth muscle cells. *J Gen Physiol* **98**, 681-698 (1991).

66. Vanderheyden, V.*, et al.* Regulation of inositol 1,4,5-trisphosphate-induced Ca2+ release by reversible phosphorylation and dephosphorylation. *Biochim Biophys Acta* **1793**, 959-970 (2009).
67. Khan, M.T., Wagner, L., 2nd, Yule, D.I., Bhanumathy, C. & Joseph, S.K. Akt kinase phosphorylation of inositol 1,4,5-trisphosphate receptors. *J Biol Chem* **281**, 3731-3737 (2006).
68. Bugrim, A.E. Regulation of Ca2+ release by cAMP-dependent protein kinase. A mechanism for agonist-specific calcium signaling? *Cell Calcium* **25**, 219-226 (1999).
69. Murthy, K.S. & Zhou, H. Selective phosphorylation of the IP3R-I in vivo by cGMP-dependent protein kinase in smooth muscle. *Am J Physiol Gastrointest Liver Physiol* **284**, G221-230 (2003).
70. Bagni, C., Mannucci, L., Dotti, C.G. & Amaldi, F. Chemical stimulation of synaptosomes modulates alpha -Ca2+/calmodulin-dependent protein kinase II mRNA association to polysomes. *J Neurosci* **20**, RC76 (2000).
71. Vermassen, E.*, et al.* Regulation of the phosphorylation of the inositol 1,4,5-trisphosphate receptor by protein kinase C. *Biochem Biophys Res Commun* **319**, 888-893 (2004).
72. Jayaraman, T., Ondrias, K., Ondriasova, E. & Marks, A.R. Regulation of the inositol 1,4,5-trisphosphate receptor by tyrosine phosphorylation. *Science* **272**, 1492-1494 (1996).
73. Dyall, S.D., Brown, M.T. & Johnson, P.J. Ancient invasions: from endosymbionts to organelles. *Science* **304**, 253-257 (2004).
74. Mokranjac, D. & Neupert, W. Protein import into mitochondria. *Biochem Soc Trans* **33**, 1019-1023 (2005).
75. Mannella, C.A. Structure and dynamics of the mitochondrial inner membrane cristae. *Biochim Biophys Acta* **1763**, 542-548 (2006).
76. Mitchell, P. & Moyle, J. Chemiosmotic hypothesis of oxidative phosphorylation. *Nature* **213**, 137-139 (1967).
77. Rimessi, A., Giorgi, C., Pinton, P. & Rizzuto, R. The versatility of mitochondrial calcium signals: from stimulation of cell metabolism to induction of cell death. *Biochim Biophys Acta* **1777**, 808-816 (2008).
78. Marchi, S. & Pinton, P. The mitochondrial calcium uniporter complex: molecular components, structure and physiopathological implications. *The Journal of physiology* **592**, 829-839 (2014).
79. Bragadin, M., Pozzan, T. & Azzone, G.F. Kinetics of Ca2+ carrier in rat liver mitochondria. *Biochemistry* **18**, 5972-5978 (1979).
80. Moreau, B., Nelson, C. & Parekh, A.B. Biphasic regulation of mitochondrial Ca2+ uptake by cytosolic Ca2+ concentration. *Current biology : CB* **16**, 1672-1677 (2006).
81. Trenker, M., Malli, R., Fertschai, I., Levak-Frank, S. & Graier, W.F. Uncoupling proteins 2 and 3 are fundamental for mitochondrial Ca2+ uniport. *Nature cell biology* **9**, 445-452 (2007).
82. Brookes, P.S.*, et al.* UCPs--unlikely calcium porters. *Nature cell biology* **10**, 1235-1237; author reply 1237-1240 (2008).
83. Perocchi, F.*, et al.* MICU1 encodes a mitochondrial EF hand protein required for Ca(2+) uptake. *Nature* **467**, 291-296 (2010).
84. De Stefani, D., Raffaello, A., Teardo, E., Szabo, I. & Rizzuto, R. A forty-kilodalton protein of the inner membrane is the mitochondrial calcium uniporter. *Nature* **476**, 336-340 (2011).
85. Baughman, J.M.*, et al.* Integrative genomics identifies MCU as an essential component of the mitochondrial calcium uniporter. *Nature* **476**, 341-345 (2011).
86. Kirichok, Y., Krapivinsky, G. & Clapham, D.E. The mitochondrial calcium uniporter is a highly selective ion channel. *Nature* **427**, 360-364 (2004).
87. Mallilankaraman, K.*, et al.* MCUR1 is an essential component of mitochondrial Ca2+ uptake that regulates cellular metabolism. *Nature cell biology* **14**, 1336-1343 (2012).

88. Jiang, D., Zhao, L. & Clapham, D.E. Genome-wide RNAi screen identifies Letm1 as a mitochondrial Ca2+/H+ antiporter. *Science* **326**, 144-147 (2009).
89. Nowikovsky, K.*, et al.* The LETM1/YOL027 gene family encodes a factor of the mitochondrial K+ homeostasis with a potential role in the Wolf-Hirschhorn syndrome. *The Journal of biological chemistry* **279**, 30307-30315 (2004).
90. Palty, R.*, et al.* NCLX is an essential component of mitochondrial Na+/Ca2+ exchange. *Proceedings of the National Academy of Sciences of the United States of America* **107**, 436-441 (2010).
91. Joseph, S.K. & Hajnoczky, G. IP3 receptors in cell survival and apoptosis: Ca2+ release and beyond. *Apoptosis* **12**, 951-968 (2007).
92. Pinton, P., Giorgi, C., Siviero, R., Zecchini, E. & Rizzuto, R. Calcium and apoptosis: ER-mitochondria Ca2+ transfer in the control of apoptosis. *Oncogene* **27**, 6407-6418 (2008).
93. Sugawara, H., Kurosaki, M., Takata, M. & Kurosaki, T. Genetic evidence for involvement of type 1, type 2 and type 3 inositol 1,4,5-trisphosphate receptors in signal transduction through the B-cell antigen receptor. *EMBO J* **16**, 3078-3088 (1997).
94. Jayaraman, T. & Marks, A.R. T cells deficient in inositol 1,4,5-trisphosphate receptor are resistant to apoptosis. *Mol Cell Biol* **17**, 3005-3012 (1997).
95. Hayashi, T. & Su, T.P. Sigma-1 receptor chaperones at the ER-mitochondrion interface regulate Ca(2+) signaling and cell survival. *Cell* **131**, 596-610 (2007).
96. Mendes, C.C.*, et al.* The type III inositol 1,4,5-trisphosphate receptor preferentially transmits apoptotic Ca2+ signals into mitochondria. *J Biol Chem* **280**, 40892-40900 (2005).
97. Khan, A.A.*, et al.* Lymphocyte apoptosis: mediation by increased type 3 inositol 1,4,5-trisphosphate receptor. *Science* **273**, 503-507 (1996).
98. Boehning, D.*, et al.* Cytochrome c binds to inositol (1,4,5) trisphosphate receptors, amplifying calcium-dependent apoptosis. *Nat Cell Biol* **5**, 1051-1061 (2003).
99. Pinton, P.*, et al.* The Ca2+ concentration of the endoplasmic reticulum is a key determinant of ceramide-induced apoptosis: significance for the molecular mechanism of Bcl-2 action. *The EMBO journal* **20**, 2690-2701 (2001).
100. Scorrano, L.*, et al.* BAX and BAK regulation of endoplasmic reticulum Ca2+: a control point for apoptosis. *Science* **300**, 135-139 (2003).
101. Pinton, P.*, et al.* Reduced loading of intracellular Ca(2+) stores and downregulation of capacitative Ca(2+) influx in Bcl-2-overexpressing cells. *J Cell Biol* **148**, 857-862 (2000).
102. Oakes, S.A.*, et al.* Proapoptotic BAX and BAK regulate the type 1 inositol trisphosphate receptor and calcium leak from the endoplasmic reticulum. *Proceedings of the National Academy of Sciences of the United States of America* **102**, 105-110 (2005).
103. Szado, T.*, et al.* Phosphorylation of inositol 1,4,5-trisphosphate receptors by protein kinase B/Akt inhibits Ca2+ release and apoptosis. *Proc Natl Acad Sci U S A* **105**, 2427-2432 (2008).
104. Marchi, S.*, et al.* Akt kinase reducing endoplasmic reticulum Ca2+ release protects cells from Ca2+-dependent apoptotic stimuli. *Biochemical and biophysical research communications* **375**, 501-505 (2008).
105. Copeland, D.E. & Dalton, A.J. An association between mitochondria and the endoplasmic reticulum in cells of the pseudobranch gland of a teleost. *The Journal of biophysical and biochemical cytology* **5**, 393-396 (1959).
106. Lewis, J.A. & Tata, J.R. A rapidly sedimenting fraction of rat liver endoplasmic reticulum. *J Cell Sci* **13**, 447-459 (1973).
107. Morre, D.J., Merritt, W.D. & Lembi, C.A. Connections between mitochondria and endoplasmic reticulum in rat liver and onion stem. *Protoplasma* **73**, 43-49 (1971).
108. Mannella, C.A., Buttle, K., Rath, B.K. & Marko, M. Electron microscopic tomography of rat-liver mitochondria and their interaction with the endoplasmic reticulum. *Biofactors* **8**, 225-228 (1998).

109. Soltys, B.J. & Gupta, R.S. Interrelationships of endoplasmic reticulum, mitochondria, intermediate filaments, and microtubules--a quadruple fluorescence labeling study. *Biochem Cell Biol* **70**, 1174-1186 (1992).
110. Mannella, C.A., Marko, M., Penczek, P., Barnard, D. & Frank, J. The internal compartmentation of rat-liver mitochondria: tomographic study using the high-voltage transmission electron microscope. *Microsc Res Tech* **27**, 278-283 (1994).
111. Achleitner, G.*, et al.* Association between the endoplasmic reticulum and mitochondria of yeast facilitates interorganelle transport of phospholipids through membrane contact. *Eur J Biochem* **264**, 545-553 (1999).
112. Csordas, G.*, et al.* Structural and functional features and significance of the physical linkage between ER and mitochondria. *The Journal of cell biology* **174**, 915-921 (2006).
113. de Brito, O.M. & Scorrano, L. Mitofusin 2 tethers endoplasmic reticulum to mitochondria. *Nature* **456**, 605-610 (2008).
114. Dennis, E.A. & Kennedy, E.P. Intracellular sites of lipid synthesis and the biogenesis of mitochondria. *J Lipid Res* **13**, 263-267 (1972).
115. Vance, J.E. Phospholipid synthesis in a membrane fraction associated with mitochondria. *The Journal of biological chemistry* **265**, 7248-7256 (1990).
116. Vance, J.E., Stone, S.J. & Faust, J.R. Abnormalities in mitochondria-associated membranes and phospholipid biosynthetic enzymes in the mnd/mnd mouse model of neuronal ceroid lipofuscinosis. *Biochim Biophys Acta* **1344**, 286-299 (1997).
117. Wieckowski, M.R., Giorgi, C., Lebiedzinska, M., Duszynski, J. & Pinton, P. Isolation of mitochondria-associated membranes and mitochondria from animal tissues and cells. *Nature protocols* **4**, 1582-1590 (2009).
118. Pichler, H.*, et al.* A subfraction of the yeast endoplasmic reticulum associates with the plasma membrane and has a high capacity to synthesize lipids. *Eur J Biochem* **268**, 2351-2361 (2001).
119. Wu, M.M., Buchanan, J., Luik, R.M. & Lewis, R.S. Ca2+ store depletion causes STIM1 to accumulate in ER regions closely associated with the plasma membrane. *J Cell Biol* **174**, 803-813 (2006).
120. Frieden, M., Arnaudeau, S., Castelbou, C. & Demaurex, N. Subplasmalemmal mitochondria modulate the activity of plasma membrane Ca2+-ATPases. *J Biol Chem* **280**, 43198-43208 (2005).
121. Koziel, K.*, et al.* Plasma membrane associated membranes (PAM) from Jurkat cells contain STIM1 protein is PAM involved in the capacitative calcium entry? *Int J Biochem Cell Biol* **41**, 2440-2449 (2009).
122. Piccini, M.*, et al.* FACL4, a new gene encoding long-chain acyl-CoA synthetase 4, is deleted in a family with Alport syndrome, elliptocytosis, and mental retardation. *Genomics* **47**, 350-358 (1998).
123. Stone, S.J. & Vance, J.E. Phosphatidylserine synthase-1 and -2 are localized to mitochondria-associated membranes. *J Biol Chem* **275**, 34534-34540 (2000).
124. Lebiedzinska, M., Szabadkai, G., Jones, A.W., Duszynski, J. & Wieckowski, M.R. Interactions between the endoplasmic reticulum, mitochondria, plasma membrane and other subcellular organelles. *The international journal of biochemistry & cell biology* **41**, 1805-1816 (2009).
125. Hayashi, T., Rizzuto, R., Hajnoczky, G. & Su, T.P. MAM: more than just a housekeeper. *Trends in cell biology* **19**, 81-88 (2009).
126. Giorgi, C., De Stefani, D., Bononi, A., Rizzuto, R. & Pinton, P. Structural and functional link between the mitochondrial network and the endoplasmic reticulum. *The international journal of biochemistry & cell biology* **41**, 1817-1827 (2009).
127. Decuypere, J.P.*, et al.* The IP(3) receptor-mitochondria connection in apoptosis and autophagy. *Biochim Biophys Acta* **1813**, 1003-1013 (2011).

128. Szabadkai, G., *et al.* Chaperone-mediated coupling of endoplasmic reticulum and mitochondrial Ca2+ channels. *The Journal of cell biology* **175**, 901-911 (2006).
129. Sanjuan, M.A. & Green, D.R. Eating for good health: linking autophagy and phagocytosis in host defense. *Autophagy* **4**, 607-611 (2008).
130. Pareja, M.E. & Colombo, M.I. Autophagic clearance of bacterial pathogens: molecular recognition of intracellular microorganisms. *Frontiers in cellular and infection microbiology* **3**, 54 (2013).
131. Lin, X., *et al.* Interaction domains of p62: a bridge between p62 and selective autophagy. *DNA and cell biology* **32**, 220-227 (2013).
132. Rimessi, A., *et al.* Perturbed mitochondrial Ca2+ signals as causes or consequences of mitophagy induction. *Autophagy* **9**, 1677-1686 (2013).
133. Cebollero, E., Reggiori, F. & Kraft, C. Reticulophagy and ribophagy: regulated degradation of protein production factories. *International journal of cell biology* **2012**, 182834 (2012).
134. He, C. & Klionsky, D.J. Regulation mechanisms and signaling pathways of autophagy. *Annual review of genetics* **43**, 67-93 (2009).
135. Klionsky, D.J., *et al.* A unified nomenclature for yeast autophagy-related genes. *Developmental cell* **5**, 539-545 (2003).
136. Klionsky, D.J. Autophagy: from phenomenology to molecular understanding in less than a decade. *Nature reviews. Molecular cell biology* **8**, 931-937 (2007).
137. Hailey, D.W., *et al.* Mitochondria supply membranes for autophagosome biogenesis during starvation. *Cell* **141**, 656-667 (2010).
138. Hamasaki, M., *et al.* Autophagosomes form at ER-mitochondria contact sites. *Nature* **495**, 389-393 (2013).
139. Jewell, J.L., Russell, R.C. & Guan, K.L. Amino acid signalling upstream of mTOR. *Nature reviews. Molecular cell biology* **14**, 133-139 (2013).
140. Jung, C.H., Ro, S.H., Cao, J., Otto, N.M. & Kim, D.H. mTOR regulation of autophagy. *FEBS letters* **584**, 1287-1295 (2010).
141. Wullschleger, S., Loewith, R. & Hall, M.N. TOR signaling in growth and metabolism. *Cell* **124**, 471-484 (2006).
142. Betz, C., *et al.* Feature Article: mTOR complex 2-Akt signaling at mitochondria-associated endoplasmic reticulum membranes (MAM) regulates mitochondrial physiology. *Proceedings of the National Academy of Sciences of the United States of America* **110**, 12526-12534 (2013).
143. Bui, M., *et al.* Rab32 modulates apoptosis onset and mitochondria-associated membrane (MAM) properties. *The Journal of biological chemistry* **285**, 31590-31602 (2010).
144. Colombi, M., *et al.* Genome-wide shRNA screen reveals increased mitochondrial dependence upon mTORC2 addiction. *Oncogene* **30**, 1551-1565 (2011).
145. Pinton, P., *et al.* Protein kinase C beta and prolyl isomerase 1 regulate mitochondrial effects of the life-span determinant p66Shc. *Science* **315**, 659-663 (2007).
146. Hattori, N., Saiki, S. & Imai, Y. Regulation by mitophagy. *The international journal of biochemistry & cell biology* **53**, 147-150 (2014).
147. Redmann, M., Dodson, M., Boyer-Guittaut, M., Darley-Usmar, V. & Zhang, J. Mitophagy mechanisms and role in human diseases. *The international journal of biochemistry & cell biology* **53**, 127-133 (2014).
148. Cook, K.L., *et al.* Mitochondria directly donate their membrane to form autophagosomes during a novel mechanism of parkin-associated mitophagy. *Cell & bioscience* **4**, 16 (2014).
149. Zhou, R., Yazdi, A.S., Menu, P. & Tschopp, J. A role for mitochondria in NLRP3 inflammasome activation. *Nature* **469**, 221-225 (2011).
150. Tschopp, J. Mitochondria: Sovereign of inflammation? *European journal of immunology* **41**, 1196-1202 (2011).
151. Schroder, K. & Tschopp, J. The inflammasomes. *Cell* **140**, 821-832 (2010).

152. Brown, G.C. & Borutaite, V. There is no evidence that mitochondria are the main source of reactive oxygen species in mammalian cells. *Mitochondrion* **12**, 1-4 (2012).
153. Saxena, G., Chen, J. & Shalev, A. Intracellular shuttling and mitochondrial function of thioredoxin-interacting protein. *The Journal of biological chemistry* **285**, 3997-4005 (2010).
154. Zhou, R., Tardivel, A., Thorens, B., Choi, I. & Tschopp, J. Thioredoxin-interacting protein links oxidative stress to inflammasome activation. *Nature immunology* **11**, 136-140 (2010).
155. Oslowski, C.M.*, et al.* Thioredoxin-interacting protein mediates ER stress-induced beta cell death through initiation of the inflammasome. *Cell metabolism* **16**, 265-273 (2012).
156. Subramanian, N., Natarajan, K., Clatworthy, M.R., Wang, Z. & Germain, R.N. The adaptor MAVS promotes NLRP3 mitochondrial localization and inflammasome activation. *Cell* **153**, 348-361 (2013).
157. Arnoult, D., Soares, F., Tattoli, I. & Girardin, S.E. Mitochondria in innate immunity. *EMBO reports* **12**, 901-910 (2011).
158. Ishikawa, H. & Barber, G.N. STING is an endoplasmic reticulum adaptor that facilitates innate immune signalling. *Nature* **455**, 674-678 (2008).
159. Park, S.*, et al.* The mitochondrial antiviral protein MAVS associates with NLRP3 and regulates its inflammasome activity. *J Immunol* **191**, 4358-4366 (2013).
160. Lane, D.P. & Crawford, L.V. T antigen is bound to a host protein in SV40-transformed cells. *Nature* **278**, 261-263 (1979).
161. Chang, C., Simmons, D.T., Martin, M.A. & Mora, P.T. Identification and partial characterization of new antigens from simian virus 40-transformed mouse cells. *Journal of virology* **31**, 463-471 (1979).
162. Kress, M., May, E., Cassingena, R. & May, P. Simian virus 40-transformed cells express new species of proteins precipitable by anti-simian virus 40 tumor serum. *Journal of virology* **31**, 472-483 (1979).
163. Linzer, D.I. & Levine, A.J. Characterization of a 54K dalton cellular SV40 tumor antigen present in SV40-transformed cells and uninfected embryonal carcinoma cells. *Cell* **17**, 43-52 (1979).
164. Melero, J.A., Stitt, D.T., Mangel, W.F. & Carroll, R.B. Identification of new polypeptide species (48-55K) immunoprecipitable by antiserum to purified large T antigen and present in SV40-infected and -transformed cells. *Virology* **93**, 466-480 (1979).
165. Baker, S.J.*, et al.* Chromosome 17 deletions and p53 gene mutations in colorectal carcinomas. *Science* **244**, 217-221 (1989).
166. Haupt, Y., Maya, R., Kazaz, A. & Oren, M. Mdm2 promotes the rapid degradation of p53. *Nature* **387**, 296-299 (1997).
167. Kamijo, T., Bodner, S., van de Kamp, E., Randle, D.H. & Sherr, C.J. Tumor spectrum in ARF-deficient mice. *Cancer research* **59**, 2217-2222 (1999).
168. Lohrum, M.A., Ludwig, R.L., Kubbutat, M.H., Hanlon, M. & Vousden, K.H. Regulation of HDM2 activity by the ribosomal protein L11. *Cancer cell* **3**, 577-587 (2003).
169. Christophorou, M.A., Ringshausen, I., Finch, A.J., Swigart, L.B. & Evan, G.I. The pathological response to DNA damage does not contribute to p53-mediated tumour suppression. *Nature* **443**, 214-217 (2006).
170. Efeyan, A., Collado, M., Velasco-Miguel, S. & Serrano, M. Genetic dissection of the role of p21Cip1/Waf1 in p53-mediated tumour suppression. *Oncogene* **26**, 1645-1649 (2007).
171. Jones, R.G.*, et al.* AMP-activated protein kinase induces a p53-dependent metabolic checkpoint. *Molecular cell* **18**, 283-293 (2005).
172. Matoba, S.*, et al.* p53 regulates mitochondrial respiration. *Science* **312**, 1650-1653 (2006).
173. Polyak, K., Xia, Y., Zweier, J.L., Kinzler, K.W. & Vogelstein, B. A model for p53-induced apoptosis. *Nature* **389**, 300-305 (1997).

174. Rivera, A. & Maxwell, S.A. The p53-induced gene-6 (proline oxidase) mediates apoptosis through a calcineurin-dependent pathway. *The Journal of biological chemistry* **280**, 29346-29354 (2005).
175. Faraonio, R.*, et al.* p53 suppresses the Nrf2-dependent transcription of antioxidant response genes. *The Journal of biological chemistry* **281**, 39776-39784 (2006).
176. Budanov, A.V., Sablina, A.A., Feinstein, E., Koonin, E.V. & Chumakov, P.M. Regeneration of peroxiredoxins by p53-regulated sestrins, homologs of bacterial AhpD. *Science* **304**, 596-600 (2004).
177. Hussain, S.P.*, et al.* p53-induced up-regulation of MnSOD and GPx but not catalase increases oxidative stress and apoptosis. *Cancer research* **64**, 2350-2356 (2004).
178. Yoon, K.A., Nakamura, Y. & Arakawa, H. Identification of ALDH4 as a p53-inducible gene and its protective role in cellular stresses. *Journal of human genetics* **49**, 134-140 (2004).
179. Caelles, C., Helmberg, A. & Karin, M. p53-dependent apoptosis in the absence of transcriptional activation of p53-target genes. *Nature* **370**, 220-223 (1994).
180. Haupt, Y., Rowan, S., Shaulian, E., Vousden, K.H. & Oren, M. Induction of apoptosis in HeLa cells by trans-activation-deficient p53. *Genes & development* **9**, 2170-2183 (1995).
181. Gottlieb, E. & Oren, M. p53 facilitates pRb cleavage in IL-3-deprived cells: novel pro-apoptotic activity of p53. *The EMBO journal* **17**, 3587-3596 (1998).
182. Ding, H.F.*, et al.* Oncogene-dependent regulation of caspase activation by p53 protein in a cell-free system. *The Journal of biological chemistry* **273**, 28378-28383 (1998).
183. Marchenko, N.D., Zaika, A. & Moll, U.M. Death signal-induced localization of p53 protein to mitochondria. A potential role in apoptotic signaling. *The Journal of biological chemistry* **275**, 16202-16212 (2000).
184. Mihara, M.*, et al.* p53 has a direct apoptogenic role at the mitochondria. *Molecular cell* **11**, 577-590 (2003).
185. Arima, Y.*, et al.* Transcriptional blockade induces p53-dependent apoptosis associated with translocation of p53 to mitochondria. *The Journal of biological chemistry* **280**, 19166-19176 (2005).
186. Moll, U.M., Marchenko, N. & Zhang, X.K. p53 and Nur77/TR3 - transcription factors that directly target mitochondria for cell death induction. *Oncogene* **25**, 4725-4743 (2006).
187. Sansome, C., Zaika, A., Marchenko, N.D. & Moll, U.M. Hypoxia death stimulus induces translocation of p53 protein to mitochondria. Detection by immunofluorescence on whole cells. *FEBS letters* **488**, 110-115 (2001).
188. Tomita, Y.*, et al.* WT p53, but not tumor-derived mutants, bind to Bcl2 via the DNA binding domain and induce mitochondrial permeabilization. *The Journal of biological chemistry* **281**, 8600-8606 (2006).
189. Sot, B., Freund, S.M. & Fersht, A.R. Comparative biophysical characterization of p53 with the pro-apoptotic BAK and the anti-apoptotic BCL-xL. *The Journal of biological chemistry* **282**, 29193-29200 (2007).
190. Leu, J.I., Dumont, P., Hafey, M., Murphy, M.E. & George, D.L. Mitochondrial p53 activates Bak and causes disruption of a Bak-Mcl1 complex. *Nature cell biology* **6**, 443-450 (2004).
191. Pietsch, E.C.*, et al.* Oligomerization of BAK by p53 utilizes conserved residues of the p53 DNA binding domain. *The Journal of biological chemistry* **283**, 21294-21304 (2008).
192. Wolff, S., Erster, S., Palacios, G. & Moll, U.M. p53's mitochondrial translocation and MOMP action is independent of Puma and Bax and severely disrupts mitochondrial membrane integrity. *Cell research* **18**, 733-744 (2008).
193. Chipuk, J.E., Bouchier-Hayes, L., Kuwana, T., Newmeyer, D.D. & Green, D.R. PUMA couples the nuclear and cytoplasmic proapoptotic function of p53. *Science* **309**, 1732-1735 (2005).

194. Soussi, T. & Lozano, G. p53 mutation heterogeneity in cancer. *Biochemical and biophysical research communications* **331**, 834-842 (2005).
195. Mancini, F.*, et al.* MDM4 (MDMX) localizes at the mitochondria and facilitates the p53-mediated intrinsic-apoptotic pathway. *The EMBO journal* **28**, 1926-1939 (2009).
196. Parant, J.*, et al.* Rescue of embryonic lethality in Mdm4-null mice by loss of Trp53 suggests a nonoverlapping pathway with MDM2 to regulate p53. *Nature genetics* **29**, 92-95 (2001).
197. Migliorini, D.*, et al.* Mdm4 (Mdmx) regulates p53-induced growth arrest and neuronal cell death during early embryonic mouse development. *Molecular and cellular biology* **22**, 5527-5538 (2002).
198. Marchenko, N.D., Wolff, S., Erster, S., Becker, K. & Moll, U.M. Monoubiquitylation promotes mitochondrial p53 translocation. *The EMBO journal* **26**, 923-934 (2007).
199. Haglund, K.*, et al.* Multiple monoubiquitination of RTKs is sufficient for their endocytosis and degradation. *Nature cell biology* **5**, 461-466 (2003).
200. Sigismund, S., Polo, S. & Di Fiore, P.P. Signaling through monoubiquitination. *Current topics in microbiology and immunology* **286**, 149-185 (2004).
201. Thrower, J.S., Hoffman, L., Rechsteiner, M. & Pickart, C.M. Recognition of the polyubiquitin proteolytic signal. *The EMBO journal* **19**, 94-102 (2000).
202. Endo, H., Kamada, H., Nito, C., Nishi, T. & Chan, P.H. Mitochondrial translocation of p53 mediates release of cytochrome c and hippocampal CA1 neuronal death after transient global cerebral ischemia in rats. *The Journal of neuroscience : the official journal of the Society for Neuroscience* **26**, 7974-7983 (2006).
203. Kelly, K.J., Plotkin, Z., Vulgamott, S.L. & Dagher, P.C. P53 mediates the apoptotic response to GTP depletion after renal ischemia-reperfusion: protective role of a p53 inhibitor. *Journal of the American Society of Nephrology : JASN* **14**, 128-138 (2003).
204. Green, D.R. & Kroemer, G. Cytoplasmic functions of the tumour suppressor p53. *Nature* **458**, 1127-1130 (2009).
205. Vousden, K.H. & Lane, D.P. p53 in health and disease. *Nature reviews. Molecular cell biology* **8**, 275-283 (2007).
206. Vogelstein, B., Lane, D. & Levine, A.J. Surfing the p53 network. *Nature* **408**, 307-310 (2000).
207. Haupt, S., Berger, M., Goldberg, Z. & Haupt, Y. Apoptosis - the p53 network. *Journal of cell science* **116**, 4077-4085 (2003).
208. Moll, U.M., Wolff, S., Speidel, D. & Deppert, W. Transcription-independent pro-apoptotic functions of p53. *Current opinion in cell biology* **17**, 631-636 (2005).
209. Sorrentino, G.*, et al.* The prolyl-isomerase Pin1 activates the mitochondrial death program of p53. *Cell death and differentiation* **20**, 198-208 (2013).
210. Giorgi, C.*, et al.* PML regulates apoptosis at endoplasmic reticulum by modulating calcium release. *Science* **330**, 1247-1251 (2010).
211. Bernardi, R., Papa, A. & Pandolfi, P.P. Regulation of apoptosis by PML and the PML-NBs. *Oncogene* **27**, 6299-6312 (2008).
212. Rowland, A.A. & Voeltz, G.K. Endoplasmic reticulum-mitochondria contacts: function of the junction. *Nature reviews. Molecular cell biology* **13**, 607-625 (2012).
213. Sano, R.*, et al.* GM1-ganglioside accumulation at the mitochondria-associated ER membranes links ER stress to Ca(2+)-dependent mitochondrial apoptosis. *Molecular cell* **36**, 500-511 (2009).
214. Pinton, P., Giorgi, C. & Pandolfi, P.P. The role of PML in the control of apoptotic cell fate: a new key player at ER-mitochondria sites. *Cell death and differentiation* **18**, 1450-1456 (2011).
215. Costes, S.V.*, et al.* Automatic and quantitative measurement of protein-protein colocalization in live cells. *Biophysical journal* **86**, 3993-4003 (2004).

216. Li, J., Lee, B. & Lee, A.S. Endoplasmic reticulum stress-induced apoptosis: multiple pathways and activation of p53-up-regulated modulator of apoptosis (PUMA) and NOXA by p53. *The Journal of biological chemistry* **281**, 7260-7270 (2006).
217. Giorgi, C.*, et al.* Mitochondrial Ca(2+) and apoptosis. *Cell calcium* **52**, 36-43 (2012).
218. Mattson, M.P. & Chan, S.L. Calcium orchestrates apoptosis. *Nature cell biology* **5**, 1041-1043 (2003).
219. Orrenius, S., Zhivotovsky, B. & Nicotera, P. Regulation of cell death: the calcium-apoptosis link. *Nature reviews. Molecular cell biology* **4**, 552-565 (2003).
220. Akl, H. & Bultynck, G. Altered Ca(2+) signaling in cancer cells: proto-oncogenes and tumor suppressors targeting IP3 receptors. *Biochimica et biophysica acta* **1835**, 180-193 (2013).
221. Clapham, D.E. Calcium signaling. *Cell* **131**, 1047-1058 (2007).
222. Bonora, M.*, et al.* Subcellular calcium measurements in mammalian cells using jellyfish photoprotein aequorin-based probes. *Nature protocols* **8**, 2105-2118 (2013).
223. Yang, M., Ellenberg, J., Bonifacino, J.S. & Weissman, A.M. The transmembrane domain of a carboxyl-terminal anchored protein determines localization to the endoplasmic reticulum. *The Journal of biological chemistry* **272**, 1970-1975 (1997).
224. Vaseva, A.V. & Moll, U.M. The mitochondrial p53 pathway. *Biochimica et biophysica acta* **1787**, 414-420 (2009).
225. Knyushko, T.V., Sharov, V.S., Williams, T.D., Schoneich, C. & Bigelow, D.J. 3-Nitrotyrosine modification of SERCA2a in the aging heart: a distinct signature of the cellular redox environment. *Biochemistry* **44**, 13071-13081 (2005).
226. Seo, Y.H. & Carroll, K.S. Profiling protein thiol oxidation in tumor cells using sulfenic acid-specific antibodies. *Proceedings of the National Academy of Sciences of the United States of America* **106**, 16163-16168 (2009).
227. Raturi, A. & Simmen, T. Where the endoplasmic reticulum and the mitochondrion tie the knot: the mitochondria-associated membrane (MAM). *Biochimica et biophysica acta* **1833**, 213-224 (2013).
228. Bononi, A.*, et al.* Identification of PTEN at the ER and MAMs and its regulation of Ca(2+) signaling and apoptosis in a protein phosphatase-dependent manner. *Cell death and differentiation* **20**, 1631-1643 (2013).
229. Bonora, M.*, et al.* Role of the c subunit of the FO ATP synthase in mitochondrial permeability transition. *Cell Cycle* **12**, 674-683 (2013).
230. Brini, M., Bano, D., Manni, S., Rizzuto, R. & Carafoli, E. Effects of PMCA and SERCA pump overexpression on the kinetics of cell Ca(2+) signalling. *The EMBO journal* **19**, 4926-4935 (2000).
231. Qin, F.*, et al.* Hydrogen peroxide-mediated SERCA cysteine 674 oxidation contributes to impaired cardiac myocyte relaxation in senescent mouse heart. *Journal of the American Heart Association* **2**, e000184 (2013).
232. Bishop, J.E., Squier, T.C., Bigelow, D.J. & Inesi, G. (Iodoacetamido)fluorescein labels a pair of proximal cysteines on the Ca2+-ATPase of sarcoplasmic reticulum. *Biochemistry* **27**, 5233-5240 (1988).
233. Miliani de Marval, P.L. & Zhang, Y. The RP-Mdm2-p53 pathway and tumorigenesis. *Oncotarget* **2**, 234-238 (2011).
234. Rudolf, R., Mongillo, M., Magalhaes, P.J. & Pozzan, T. In vivo monitoring of Ca(2+) uptake into mitochondria of mouse skeletal muscle during contraction. *The Journal of cell biology* **166**, 527-536 (2004).
235. Zilfou, J.T. & Lowe, S.W. Tumor suppressive functions of p53. *Cold Spring Harbor perspectives in biology* **1**, a001883 (2009).
236. Marouco, D., Garabadgiu, A.V., Melino, G. & Barlev, N.A. Lysine-specific modifications of p53: a matter of life and death? *Oncotarget* **4**, 1556-1571 (2013).

237. Agostinis, P.*, et al.* Photodynamic therapy of cancer: an update. *CA: a cancer journal for clinicians* **61**, 250-281 (2011).
238. Dolmans, D.E., Fukumura, D. & Jain, R.K. Photodynamic therapy for cancer. *Nature reviews. Cancer* **3**, 380-387 (2003).
239. Shahzidi, S.*, et al.* Simultaneously targeting mitochondria and endoplasmic reticulum by photodynamic therapy induces apoptosis in human lymphoma cells. *Photochemical & photobiological sciences : Official journal of the European Photochemistry Association and the European Society for Photobiology* **10**, 1773-1782 (2011).
240. Sckell, A. & Leunig, M. The dorsal skinfold chamber: studying angiogenesis by intravital microscopy. *Methods Mol Biol* **467**, 305-317 (2009).
241. Bublitz, M.*, et al.* Ion pathways in the sarcoplasmic reticulum Ca2+-ATPase. *The Journal of biological chemistry* **288**, 10759-10765 (2013).
242. Hajnoczky, G.*, et al.* Mitochondrial calcium signalling and cell death: approaches for assessing the role of mitochondrial Ca2+ uptake in apoptosis. *Cell calcium* **40**, 553-560 (2006).
243. Lehr, H.A., Leunig, M., Menger, M.D., Nolte, D. & Messmer, K. Dorsal skinfold chamber technique for intravital microscopy in nude mice. *The American journal of pathology* **143**, 1055-1062 (1993).
244. Salomoni, P. & Pandolfi, P.P. The role of PML in tumor suppression. *Cell* **108**, 165-170 (2002).
245. Gurrieri, C.*, et al.* Loss of the tumor suppressor PML in human cancers of multiple histologic origins. *Journal of the National Cancer Institute* **96**, 269-279 (2004).
246. Pandolfi, P.P.*, et al.* Structure and origin of the acute promyelocytic leukemia myl/RAR alpha cDNA and characterization of its retinoid-binding and transactivation properties. *Oncogene* **6**, 1285-1292 (1991).
247. Salomoni, P., Ferguson, B.J., Wyllie, A.H. & Rich, T. New insights into the role of PML in tumour suppression. *Cell research* **18**, 622-640 (2008).
248. Jensen, K., Shiels, C. & Freemont, P.S. PML protein isoforms and the RBCC/TRIM motif. *Oncogene* **20**, 7223-7233 (2001).
249. Bernardi, R. & Pandolfi, P.P. Structure, dynamics and functions of promyelocytic leukaemia nuclear bodies. *Nature reviews. Molecular cell biology* **8**, 1006-1016 (2007).
250. Nisole, S., Maroui, M.A., Mascle, X.H., Aubry, M. & Chelbi-Alix, M.K. Differential Roles of PML Isoforms. *Frontiers in oncology* **3**, 125 (2013).
251. Lallemand-Breitenbach, V. & de The, H. PML nuclear bodies. *Cold Spring Harbor perspectives in biology* **2**, a000661 (2010).
252. Shen, T.H., Lin, H.K., Scaglioni, P.P., Yung, T.M. & Pandolfi, P.P. The mechanisms of PML-nuclear body formation. *Molecular cell* **24**, 331-339 (2006).
253. Wang, Z.G.*, et al.* PML is essential for multiple apoptotic pathways. *Nature genetics* **20**, 266-272 (1998).
254. Trotman, L.C.*, et al.* Identification of a tumour suppressor network opposing nuclear Akt function. *Nature* **441**, 523-527 (2006).
255. Boe, S.O. & Simonsen, A. Autophagic degradation of an oncoprotein. *Autophagy* **6**, 964-965 (2010).
256. Mizushima, N., Levine, B., Cuervo, A.M. & Klionsky, D.J. Autophagy fights disease through cellular self-digestion. *Nature* **451**, 1069-1075 (2008).
257. Meijer, A.J. & Codogno, P. Regulation and role of autophagy in mammalian cells. *The international journal of biochemistry & cell biology* **36**, 2445-2462 (2004).
258. Laane, E.*, et al.* Cell death induced by dexamethasone in lymphoid leukemia is mediated through initiation of autophagy. *Cell death and differentiation* **16**, 1018-1029 (2009).
259. Isakson, P., Bjoras, M., Boe, S.O. & Simonsen, A. Autophagy contributes to therapy-induced degradation of the PML/RARA oncoprotein. *Blood* **116**, 2324-2331 (2010).

260. Wang, Z.*, et al.* Autophagy regulates myeloid cell differentiation by p62/SQSTM1-mediated degradation of PML-RARalpha oncoprotein. *Autophagy* **7**, 401-411 (2011).
261. Occhionorelli, M.*, et al.* The self-association coiled-coil domain of PML is sufficient for the oncogenic conversion of the retinoic acid receptor (RAR) alpha. *Leukemia* **25**, 814-820 (2011).
262. Sternsdorf, T.*, et al.* Forced retinoic acid receptor alpha homodimers prime mice for APL-like leukemia. *Cancer cell* **9**, 81-94 (2006).
263. Rego, E.M.*, et al.* Role of promyelocytic leukemia (PML) protein in tumor suppression. *The Journal of experimental medicine* **193**, 521-529 (2001).
264. Lim, J.H., Liu, Y., Reineke, E. & Kao, H.Y. Mitogen-activated protein kinase extracellular signal-regulated kinase 2 phosphorylates and promotes Pin1 protein-dependent promyelocytic leukemia protein turnover. *The Journal of biological chemistry* **286**, 44403-44411 (2011).
265. Reineke, E.L.*, et al.* Degradation of the tumor suppressor PML by Pin1 contributes to the cancer phenotype of breast cancer MDA-MB-231 cells. *Molecular and cellular biology* **28**, 997-1006 (2008).
266. Huber, K.E., Carey, L.A. & Wazer, D.E. Breast cancer molecular subtypes in patients with locally advanced disease: impact on prognosis, patterns of recurrence, and response to therapy. *Seminars in radiation oncology* **19**, 204-210 (2009).
267. Carracedo, A.*, et al.* A metabolic prosurvival role for PML in breast cancer. *The Journal of clinical investigation* **122**, 3088-3100 (2012).
268. Ito, K.*, et al.* PML targeting eradicates quiescent leukaemia-initiating cells. *Nature* **453**, 1072-1078 (2008).
269. Regad, T., Bellodi, C., Nicotera, P. & Salomoni, P. The tumor suppressor Pml regulates cell fate in the developing neocortex. *Nature neuroscience* **12**, 132-140 (2009).
270. Hanahan, D. & Weinberg, R.A. Hallmarks of cancer: the next generation. *Cell* **144**, 646-674 (2011).
271. Booth, L.A., Tavallai, S., Hamed, H.A., Cruickshanks, N. & Dent, P. The role of cell signalling in the crosstalk between autophagy and apoptosis. *Cellular signalling* **26**, 549-555 (2014).
272. Eisenberg-Lerner, A., Bialik, S., Simon, H.U. & Kimchi, A. Life and death partners: apoptosis, autophagy and the cross-talk between them. *Cell death and differentiation* **16**, 966-975 (2009).
273. Galluzzi, L.*, et al.* Autophagy in malignant transformation and cancer progression. *The EMBO journal* **34**, 856-880 (2015).
274. Marino, G., Niso-Santano, M., Baehrecke, E.H. & Kroemer, G. Self-consumption: the interplay of autophagy and apoptosis. *Nature reviews. Molecular cell biology* **15**, 81-94 (2014).
275. Su, Z., Yang, Z., Xu, Y., Chen, Y. & Yu, Q. Apoptosis, autophagy, necroptosis, and cancer metastasis. *Molecular cancer* **14**, 48 (2015).
276. Huang, Y.*, et al.* PML-RARalpha enhances constitutive autophagic activity through inhibiting the Akt/mTOR pathway. *Autophagy* **7**, 1132-1144 (2011).
277. Sehgal, A.R.*, et al.* You eat what you are: autophagy inhibition as a therapeutic strategy in leukemia. *Leukemia* **29**, 517-525 (2015).
278. Sui, X.*, et al.* Autophagy and chemotherapy resistance: a promising therapeutic target for cancer treatment. *Cell death & disease* **4**, e838 (2013).
279. Piazza, F., Gurrieri, C. & Pandolfi, P.P. The theory of APL. *Oncogene* **20**, 7216-7222 (2001).
280. Klionsky, D.J.*, et al.* Guidelines for the use and interpretation of assays for monitoring autophagy. *Autophagy* **8**, 445-544 (2012).

281. Esteban-Martinez, L. & Boya, P. Autophagic flux determination in vivo and ex vivo. *Methods* **75**, 79-86 (2015).
282. Tasdemir, E.*, et al.* Regulation of autophagy by cytoplasmic p53. *Nat.Cell Biol.* **10**, 676-687 (2008).
283. Tasdemir, E.*, et al.* Regulation of autophagy by cytoplasmic p53. *Nature cell biology* **10**, 676-687 (2008).
284. Alsheich-Bartok, O.*, et al.* PML enhances the regulation of p53 by CK1 in response to DNA damage. *Oncogene* **27**, 3653-3661 (2008).
285. Ablain, J.*, et al.* Activation of a promyelocytic leukemia-tumor protein 53 axis underlies acute promyelocytic leukemia cure. *Nature medicine* **20**, 167-174 (2014).
286. Bellodi, C.*, et al.* A cytoplasmic PML mutant inhibits p53 function. *Cell Cycle* **5**, 2688-2692 (2006).
287. Guo, A.*, et al.* The function of PML in p53-dependent apoptosis. *Nature cell biology* **2**, 730-736 (2000).
288. Haupt, S.*, et al.* Loss of PML cooperates with mutant p53 to drive more aggressive cancers in a gender-dependent manner. *Cell Cycle* **12**, 1722-1731 (2013).
289. Papa, A., Cordon-Cardo, C., Bernardi, R. & Pandolfi, P.P. Compound In Vivo Inactivation of Pml and p53 Uncovers a Functional Interaction in Angiosarcoma Suppression. *Genes & cancer* **3**, 599-603 (2012).
290. Giorgi, C.*, et al.* p53 at the endoplasmic reticulum regulates apoptosis in a Ca2+-dependent manner. *Proceedings of the National Academy of Sciences of the United States of America* **112**, 1779-1784 (2015).
291. Morselli, E.*, et al.* p53 inhibits autophagy by interacting with the human ortholog of yeast Atg17, RB1CC1/FIP200. *Cell Cycle* **10**, 2763-2769 (2011).
292. Amaravadi, R.K.*, et al.* Principles and current strategies for targeting autophagy for cancer treatment. *Clinical cancer research : an official journal of the American Association for Cancer Research* **17**, 654-666 (2011).
293. Galluzzi, L., Pietrocola, F., Levine, B. & Kroemer, G. Metabolic control of autophagy. *Cell* **159**, 1263-1276 (2014).
294. Alers, S., Loffler, A.S., Wesselborg, S. & Stork, B. Role of AMPK-mTOR-Ulk1/2 in the regulation of autophagy: cross talk, shortcuts, and feedbacks. *Molecular and cellular biology* **32**, 2-11 (2012).
295. Kim, J., Kundu, M., Viollet, B. & Guan, K.L. AMPK and mTOR regulate autophagy through direct phosphorylation of Ulk1. *Nature cell biology* **13**, 132-141 (2011).
296. Nazio, F.*, et al.* mTOR inhibits autophagy by controlling ULK1 ubiquitylation, self-association and function through AMBRA1 and TRAF6. *Nat Cell Biol* **15**, 406-416 (2013).
297. Mihaylova, M.M. & Shaw, R.J. The AMPK signalling pathway coordinates cell growth, autophagy and metabolism. *Nat Cell Biol* **13**, 1016-1023 (2011).
298. Faivre, S., Kroemer, G. & Raymond, E. Current development of mTOR inhibitors as anticancer agents. *Nature reviews. Drug discovery* **5**, 671-688 (2006).
299. Egan, D.F.*, et al.* Phosphorylation of ULK1 (hATG1) by AMP-activated protein kinase connects energy sensing to mitophagy. *Science* **331**, 456-461 (2011).
300. Cardenas, C.*, et al.* Essential regulation of cell bioenergetics by constitutive InsP3 receptor Ca2+ transfer to mitochondria. *Cell* **142**, 270-283 (2010).
301. Degenhardt, K.*, et al.* Autophagy promotes tumor cell survival and restricts necrosis, inflammation, and tumorigenesis. *Cancer cell* **10**, 51-64 (2006).
302. Rabinowitz, J.D. & White, E. Autophagy and metabolism. *Science* **330**, 1344-1348 (2010).
303. Maes, H., Rubio, N., Garg, A.D. & Agostinis, P. Autophagy: shaping the tumor microenvironment and therapeutic response. *Trends in molecular medicine* **19**, 428-446 (2013).

304. Xu, Y., Xia, X. & Pan, H. Active autophagy in the tumor microenvironment: A novel mechanism for cancer metastasis. *Oncology letters* **5**, 411-416 (2013).
305. Amaravadi, R.K.*, et al.* Autophagy inhibition enhances therapy-induced apoptosis in a Myc-induced model of lymphoma. *The Journal of clinical investigation* **117**, 326-336 (2007).
306. Chittaranjan, S.*, et al.* Autophagy inhibition augments the anticancer effects of epirubicin treatment in anthracycline-sensitive and -resistant triple-negative breast cancer. *Clinical cancer research : an official journal of the American Association for Cancer Research* **20**, 3159-3173 (2014).
307. Li, J., Hou, N., Faried, A., Tsutsumi, S. & Kuwano, H. Inhibition of autophagy augments 5-fluorouracil chemotherapy in human colon cancer in vitro and in vivo model. *Eur J Cancer* **46**, 1900-1909 (2010).
308. Selvakumaran, M., Amaravadi, R.K., Vasilevskaya, I.A. & O'Dwyer, P.J. Autophagy inhibition sensitizes colon cancer cells to antiangiogenic and cytotoxic therapy. *Clinical cancer research : an official journal of the American Association for Cancer Research* **19**, 2995-3007 (2013).
309. Giorgi, C.*, et al.* Intravital imaging reveals p53-dependent cancer cell death induced by phototherapy via calcium signaling. *Oncotarget* **6**, 1435-1445 (2015).
310. Heath-Engel, H.M., Chang, N.C. & Shore, G.C. The endoplasmic reticulum in apoptosis and autophagy: role of the BCL-2 protein family. *Oncogene* **27**, 6419-6433 (2008).
311. Criollo, A.*, et al.* Regulation of autophagy by the inositol trisphosphate receptor. *Cell death and differentiation* **14**, 1029-1039 (2007).
312. Cheng, X.*, et al.* Ablation of promyelocytic leukemia protein (PML) re-patterns energy balance and protects mice from obesity induced by a Western diet. *The Journal of biological chemistry* **288**, 29746-29759 (2013).
313. Boroughs, L.K. & DeBerardinis, R.J. Metabolic pathways promoting cancer cell survival and growth. *Nat Cell Biol* **17**, 351-359 (2015).
314. Carracedo, A., Cantley, L.C. & Pandolfi, P.P. Cancer metabolism: fatty acid oxidation in the limelight. *Nat Rev Cancer* **13**, 227-232 (2013).
315. Ito, K.*, et al.* A PML-PPAR-delta pathway for fatty acid oxidation regulates hematopoietic stem cell maintenance. *Nat Med* **18**, 1350-1358 (2012).
316. Strohecker, A.M.*, et al.* Autophagy sustains mitochondrial glutamine metabolism and growth of BrafV600E-driven lung tumors. *Cancer discovery* **3**, 1272-1285 (2013).
317. Lin, T.C.*, et al.* Autophagy: resetting glutamine-dependent metabolism and oxygen consumption. *Autophagy* **8**, 1477-1493 (2012).
318. Dupont, N.*, et al.* Autophagy-based unconventional secretory pathway for extracellular delivery of IL-1beta. *The EMBO journal* **30**, 4701-4711 (2011).
319. Bruns, C., McCaffery, J.M., Curwin, A.J., Duran, J.M. & Malhotra, V. Biogenesis of a novel compartment for autophagosome-mediated unconventional protein secretion. *The Journal of cell biology* **195**, 979-992 (2011).
320. Okamoto, M.*, et al.* Constitutively active inflammasome in human melanoma cells mediating autoinflammation via caspase-1 processing and secretion of interleukin-1beta. *The Journal of biological chemistry* **285**, 6477-6488 (2010).
321. Zhang, M., Kenny, S.J., Ge, L., Xu, K. & Schekman, R. Translocation of interleukin-1beta into a vesicle intermediate in autophagy-mediated secretion. *eLife* **4**(2015).
322. Dowling, J.K.*, et al.* Promyelocytic leukemia protein interacts with the apoptosis-associated speck-like protein to limit inflammasome activation. *The Journal of biological chemistry* **289**, 6429-6437 (2014).
323. Schoenmakers, T.J., Visser, G.J., Flik, G. & Theuvenet, A.P. CHELATOR: an improved method for computing metal ion concentrations in physiological solutions. *BioTechniques* **12**, 870-874, 876-879 (1992).

324. Klionsky, D.J., *et al.* Guidelines for the use and interpretation of assays for monitoring autophagy. *Autophagy* **8**, 445-544 (2012).